ROLE OF GLUTATHIONE IN OZONE-INDUCED EPITHELIAL HYPERPLASIA IN THE NASAL AIRWAYS OF INFANT MONKEYS AND RATS

By

STEPHAN A. CAREY

A DISSERTATION

Submitted to
Michigan State University
in partial fulfillment of the requirements
for the degree of

DOCTOR OF PHILOSOPHY

Comparative Medicine and Integrative Biology

2009

ABSTRACT

ROLE OF GLUTATHIONE IN OZONE-INDUCED EPITHELIAL HYPERPLASIA IN THE NASAL AIRWAYS OF INFANT MONKEYS AND RATS

By

Stephan A. Carey

Ozone, the major oxidant pollutant in photochemical smog, causes toxic epithelial injury in the nasal and tracheobronchial airways of laboratory animals and people. Epidemiologic studies suggest that children may be more susceptible to the respiratory health effects of ozone exposure than adults. The majority of children in the United States live in areas in which the atmospheric ozone concentration exceeds the current National Ambient Air Quality Standard for this pollutant. Repeated exposure to high ambient levels of ozone induces site-specific rhinitis, mucous cell metaplasia, and epithelial hyperplasia in the nasal airways of adult, laboratory monkeys and rats. These remodeling events in the nasal airways of adult monkeys and rats are associated with an altered response to subsequent ozone challenge, and thus may serve as a protective adaptation. Low molecular weight antioxidants, such as the tripeptide glutathione (GSH), in the nasal epithelium and the overlying epithelial lining fluid (ELF) are regarded as the first line of defense against these and other inhaled oxidant pollutants. Recent studies have also implicated GSH in the development of pulmonary tolerance to ozone-induced injury, and in the pathogenesis of oxidant-mediated cell proliferation. Few studies have examined the effects of ozone exposure on the developing nasal airways of immature animal models. The overall goal of these experiments was to demonstrate that the site-specificity and temporal pattern of ozone-induced nasal epithelial remodeling in immature rats and infant monkeys is related to the local regulation of intracellular GSH.

Infant, male rhesus macaques were exposed episodically to repeated cycles of ozone (0.5 ppm) and filtered air (0 ppm) for two or five months. The time-course of morphologic and immunohistochemical events comprising this ozone-induced nasal epithelial injury and repair were determined, and these were compared to site-matched changes in the steady-state levels of GSH in the nasal mucosa. In addition, a whole-animal inhalation study was conducted using an immature rodent model to determine the role of GSH in ozone-induced epithelial hyperplasia in the developing nasal airways of rats. Immature male F344 rats were exposed to three consecutive days of ozone (0.8 ppm) or filtered air. Infant monkeys episodically exposed to ozone for 5 months developed acute rhinitis, epithelial hyperplasia, and squamous metaplasia in the anterior nasal cavity. These animals also exhibited a significant increase in intracellular GSH concentration in the nasal mucosa corresponding to the site of remodeling. GSH concentration was positively correlated with the epithelial numeric cell density following filtered air or ozone exposure. In immature rats, ozone-induced epithelial hyperplasia was also associated with a local increase in GSH concentration. However, GSH depletion had no effect on ozone-induced cell proliferation. In conclusion, ozone-induced epithelial hyperplasia in the nasal airways is temporally correlated with local increases in mucosal GSH concentrations. However, ozone-induced hyperplasia in the nasal airways of rats is not a GSH-dependent phenomenon. Furthermore, since GSH upregulation is not unique to sites of injury in the nasal airways, other factors (e.g., interactions with other nasal antioxidants) must also contribute to the site-specificity of ozone-related nasal injury and repair.

To my bride, Regina.

Your love, your sacrifice, and your smile

make this and all things possible.

ACKNOWLEDGEMENTS

I would like to thank the many people whose time, wisdom, and encouragement contributed to my personal and professional development during this process. I will be forever indebted to my mentor, Dr. Jack Harkema. His guidance, generosity with his knowledge and resources, experience, trust, and patience provided me with the opportunity to develop a relevant research project of which I am truly proud. His enthusiasm for teaching and passion for research provided a nurturing, welcoming environment for my graduate training. I am very grateful to my committee members, Dr. James Wagner, Dr. Susan Ewart, and Dr. Ed Robinson, for their guidance, advice, and willingness to invest their time and effort into my graduate program and my professional development. I have great respect for each of them, and it gives me great honor to now be considered their colleagues. I am also grateful for the guidance, wisdom, and support of Dr. Vilma Yuzbasiyan-Gurkan, who, despite her many responsibilities, always made me feel as if I was her first priority.

Through my work with Dr. Harkema, I have also had the unique privilege of learning from expert collaborators across the country. I owe many thanks to Dr. Charles Plopper, Dr. Julia Kimbell, Dr. Richard Corley, Dr. Carol Ballinger, and Dr. Kevin Minard, for sharing their knowledge and expertise. I would especially like to thank Dr. Edward Postlethwait for being so generously giving of his time, resources, and expertise, for the benefit of my training. My research project would not have been possible without their effort and generosity.

My research was made both possible and enjoyable through the efforts of the members of our lab, Lori Bramble, Ryan Lewandowski, Dr. Daher Ibrahim-Aibo, Dr. Daven Jackson, Kara Corps, and Dr. Neil Birmingham. My research efforts were also made possible by the invaluable contributions of Amy Porter, Kathy Joseph, and Rick Rosebury in the Clinical Center Histology Lab, Ralph Common in the Electron Microscopy Lab, and Sarah Davis, Brian Tarkington, Louise Olsen, Dr. Ruth McDonald, Dr. Lisa Miller, Dr. Kristina Abel, and Dr. Veronique de Silva from the California National Primate Research Center.

None of this would have been possible without generous financial support from Pfizer Animal Health. I would particularly like to thank Dr. Michael Spensley and Dr. Michael Kennedy of Pfizer for their support of my work and development. I would also like to thank Dr. Robert Roth, Dr. Norbert Kaminski, the Center for Integrative Toxicology, and NIH (NIEHS) P01 ES011617 for funding my research program.

Finally, I need to thank my parents for their unconditional love and support, and for instilling in me the work ethic necessary to complete this milestone. I would like to thank my precious children, Daria, Sophia, and Harrison, for their resilience during my long hours away, and for being such wonderful inspirations for me. It is with the deepest gratitude that I thank my bride, Regina, whose sacrifice was the greatest during this process. She is the most important and most difficult to thank, as my words fail to fully express how essential her effort was to the achievement of this and all of my goals. With her love, support, care, patience, I have become the husband, father, and scientist that I am today.

TABLE OF CONTENTS

LIST OF TABLES

LIST OF FIGURES

Images in this dissertation are presented in color.

LIST OF ABBREVIATIONS

3D	three-dimensional
AB/PAS	alcian blue/periodic acid Schiff
AH_2	ascorbate
ANOVA	analysis of variance
AP-1	activator protein-1
BALF	bronchoalveolar lavage fluid
BALT	bronchus-associated lymphoid tissue
BrdU	bromo-deoxyuridine
BSO	L-buthionine-[S,R]-sulfoximine
CAD	computer aided design
cDNA	copy deoxyribonucleic acid
CFD	computational fluid dynamics
CINC	cytokine-induced neutrophil chemoattractant
CSC	cigarette smoke condensate
C_T	cycle threshold
DDV	digital data viewer
DNA	deoxyribonucleic acid
EH	epithelial hyperplasia
ELF	epithelial lining fluid
ET	ethmoturbinate
F344	Fischer 344 rat

FA	filtered air
FI	fold-increase
GALT	gut-associated lymphoid tissue
GAPDH	glyceraldehyde-3-phosphate dehydrogenase
GCL	glutamate cysteine ligase
GCL-C	glutamate cysteine ligase, catalytic subunit
GCL-M	glutamate cysteine ligase, modulatory subunit
GGT	γ-glutamyltranspeptidase
GPx	glutathione peroxidase
GR	glutathione reductase
GS·	glutathionyl radical
GSH	glutathione
GSSG	glutathione disulfide
G6PDH	glucose-6-phosphate dehydrogenase
H&E	hematoxylin and eosin
HO-1	heme oxygenase-1
HP	hard palate
HPLC	high performance liquid chromatography
IL	interleukin
iNOS	inducible nitric oxide synthase
LE	lymphoepithelium
MCM	mucous cell metaplasia
MIP-2	macrophage inflammatory protein-2

MPO	myeloperoxidase
MR	magnetic resonance
mRNA	messenger ribonucleic acid
MT	maxilloturbinate
NAAQS	national ambient air quality standard
NAC	N-acetylcysteine
NADH	nicotinamide adenine dinucleotide
NADPH	nicotinamide adenine dinucleotide phosphate
NALT	nasal-associated lymphoid tissue
NP	nasopharynx
NQO1	NADPH:Quinone oxidoreductase
Nrf2	nuclear factor-erythroid 2 related factor
NTE	non-ciliated transitional epithelium
O_3	ozone
OE	olfactory epithelium
PCNA	proliferating cell nuclear antigen
PCR	polymerase chain reaction
PMN	polymorphonuclear leukocyte
ppm	parts per million
RE	respiratory epithelium
RNA	ribonucleic acid
RNS	reactive nitrogen species
ROS	reactive oxygen species

RT	reverse transcriptase
SE	squamous epithelium
SEM	standard error of the mean
SOD	superoxide dismutase
STL	stereolithography
TNF	tumor necrosis factor
UA	uric acid
VOC	volatile organic compound

CHAPTER 1

INTRODUCTION

Tropospheric ozone, the principal oxidant pollutant in photochemical smog, is recognized as one of the most important environmental pollutants due largely to its adverse health effects on the respiratory system. The nasal cavity is an important target of inhaled airborne pollutants such as ozone, due in part to its proximal location in the respiratory tract. Specialized epithelial functions including absorption of reactive gases (Brain 1970), filtration and removal of particulates and gases (Proctor and Anderson 1982), and metabolism of inhaled xenobiotics (Dahl and Hadley 1991), equip the nasal cavity to serve a protective role as a "scrubbing tower," limiting access of inhaled chemical agents to the more delicate pulmonary parenchyma and conducting airways (Brain 1970). These same functions also expose the mucosa of the nasal airways to higher concentrations of these inhaled xenobiotics, making the nose more susceptible to injury from certain highly reactive inhaled oxidant pollutants, including ozone.

Ozone-Induced Nasal Airway Injury—Human Health Significance. Residents of Mexico City, a population chronically exposed to high ambient levels of ozone, experienced loss of cilia, basal cell hyperplasia, and squamous metaplasia in the nasal airways (Calderon-Garciduenas et al. 1992). Controlled ozone experiments using human subjects indicated that ozone induces similar profiles of nasal and pulmonary airway inflammation (Graham and Koren 1990; Koren et al. 1990). Inflammatory markers (percent neutrophils, IL-6, fibronectin) in bronchoalveolar lavage fluid (BALF) were decreased in subjects exposed daily to ozone (0.2 ppm) for four consecutive days, compared to subjects exposed for a single day (Devlin 1993). A similar attenuation of BALF inflammation was observed, despite evidence of ongoing airway epithelial injury,

in response to repeated ozone exposures in human volunteers (Christian et al. 1998). These experiments, which characterize the responses to repeated exposures, are of particular human health importance, as repeated or episodic exposure likely mimics the pattern of exposure experienced by most people (Sram et al. 1996).

Children may be at increased risk of airway injury induced by oxidant pollutants (Kim 2004). Factors supporting this age-related heterogeneity in airway injury include differences in airway geometry and delivered ozone dose, differences in the distribution of susceptible epithelial populations; and differences in intrinsic epithelial defenses against oxidative stress (antioxidants, mucus, epithelial repair capacity) in the respiratory tract between children and adults. The respiratory tract undergoes significant post-natal development in children. Ozone exposures early in life are associated with long-term consequences in the pulmonary airways. Pollutant exposure during the critical period of post-natal lung growth in children impairs lung development, which results in lung function deficits in adulthood (Gauderman et al. 2004). Childhood ozone exposure also causes inflammation, epithelial necrosis, ciliary loss, and epithelial hyperplasia in the nasal airways (Koltai 1994; Calderon-Garciduenas et al. 1995; Kopp et al. 1999). However, the long-term ramifications of this early exposure have not been investigated.

Ozone-Induced Nasal Airway Injury—Non-Human Primate Models. Short- and long-term (daily) ozone exposures cause significant nasal airway injury in experimental animal models. Most of these studies during the past 20 years were conducted in adult rodent and macaque monkey models, and have been the subject of a recent review

(Nikasinovic et al. 2003). The macaque monkey serves as an important animal model of upper airway toxicology because their nasal airways resemble, at a gross and microscopic level, the nasal airways of humans (Harkema 1991; Yeh et al. 1997). The first of these studies used an adult bonnet monkey (*Macaca radiata*) model exposed to 0.15 or 0.30 ppm ozone for 6 or 90 days. In these studies, ozone-induced lesions were confined to the anterior nasal airways (Harkema et al. 1987; Harkema et al. 1987). The principal lesions observed in this model included neutrophilic rhinitis at 6 days, and ciliated cell necrosis with loss of cilia, epithelial hyperplasia, and mucous cell metaplasia (MCM) at both 6 and 90 days. The epithelial remodeling events identified at 90 days were associated with attenuation of the inflammatory cell infiltration compared to 6-day exposure. These lesions specifically involved the non-ciliated transitional epithelium (NTE) and the adjacent ciliated respiratory epithelium (RE). Similar hyperplastic lesions (cuboidal bronchiolar cell hyperplasia) were also identified in the terminal bronchiolar epithelium of the lungs in ozone-exposed monkeys (Harkema et al. 1993). Thus, assessment of nasal airway injury in monkeys may also serve as a sentinel for injury to the more delicate pulmonary airways. Furthermore, these reports document that the nasal airways of monkeys, which are morphologically similar to human nasal airways, are susceptible to injury at levels near the National Ambient Air Quality Standard ozone concentration of 0.075 ppm.

Ozone-Induced Nasal Airway Injury—Fischer 344 Rat Model. Rats exposed to 0.8 ppm ozone, 6h/day for 7 days develop MCM and epithelial hyperplasia in the non-

ciliated transitional epithelium lining the maxilloturbinates, nasoturbinates, and lateral wall of the proximal aspect of the nasal airways (Harkema et al. 1989). Ozone-induced MCM persists, and in some regions progresses, for at least seven days post-exposure (Harkema et al. 1989). The ozone-induced lesions in Fischer 344 (F344) rats exposed to 0.8 ppm for 7 days histologically resemble those induced in macaque monkeys exposed to 0.3 ppm ozone for 6 days (Harkema et al. 1987). No nasal lesions were identified in rats exposed to 0.12 ppm ozone for 7 days. This is in contrast to the MCM induced in the nasal airways of macaque monkeys exposed to 0.15 ppm ozone, 8h/day for 6 days (Harkema et al. 1987). This differential, species-dependent response suggests that the rat NTE may be more resistant to ozone-induced injury than the NTE in the monkey, and supports the use of higher ozone concentrations for comparative toxicology studies in rat models.

The temporal relationships among neutrophil influx, epithelial necrosis, and epithelial DNA synthesis, following a single exposure to 0.5 ppm ozone in rats are well characterized (Hotchkiss et al. 1997). Epithelial cell loss (due to necrosis) appears within 8 hours after the end of the exposure, and DNA synthesis begins within 12 hours, and peaks within 24 hours, after the end of a single 8-hour ozone exposure. Cho et al. (Cho et al. 1999) investigated the time course of cellular events preceding epithelial hyperplasia and MCM during the course of a three-day ozone exposure in rats (8h/day, 0.5ppm). During a three-day exposure, DNA synthesis peaked on day two of exposure, three days prior to the peak of the epithelial hyperplastic response (Cho et al. 1999). These findings indicate that the cellular events underlying the ozone-induced phenotypic alterations in

the nasal epithelium begin within the first eight hours of exposure, and that the cellular commitment to cell proliferation occurs within the first two days of ozone exposure.

***Site*-Specificity of Ozone-Induced Injury in the Respiratory Tract.** The epithelial responses to ozone exposure vary markedly by site within the respiratory tract. In rhesus monkeys, the nature and magnitude of ozone-induced cellular injury vary significantly by location in both the nasal and pulmonary airways. In the lungs, ozone exposure targets the ciliated respiratory epithelium of the trachea and type I pneumocytes lining the terminal bronchioles (Castleman et al. 1980; Wilson et al. 1984; Nikula et al. 1988). In the nasal airways, ozone-induced injury is confined to the anterior nasal cavity, specifically targeting the NTE and ciliated RE (Harkema et al. 1987; Harkema et al. 1987; Carey et al. 2007). The location of ozone-induced injury in the respiratory tract is due to a combination of the local site-specific dose of ozone and tissue susceptibility (Morgan and Monticello 1990). In the nasal airways, regional differences in ozone dose are related to the ambient concentration of ozone, physicochemical properties of the inhaled gas mixture, and nasal airflow patterns. The intranasal differences in susceptibility to ozone-induced injury can be due to many factors, including structural differences in epithelial populations (e.g. ciliated, keratinized), local metabolic capacity, or local differences in innervation or vasculature. The basis for the variations in tissue susceptibility may also be related to the nature and magnitude of the tissue response to oxidant challenge.

Airway Antioxidants and Ozone Interactions. Antioxidant molecules in the epithelial lining fluid (ELF) of the respiratory system are considered to provide the first line of defense against cellular stress from inhaled oxidant pollutants (Cross et al. 1994). Intracellular antioxidant molecules also play a role in the cellular defense against inhaled oxidants, both within the intracellular compartment as well as in the maintenance of ELF levels. These include low molecular weight antioxidants such as ascorbate (AH_2), uric acid (UA), α-tocopherol, and glutathione (GSH), and larger protein complex enzymes, including superoxide dismutase (Stenfors et al.), glutathione peroxidase (GPx), and glutathione reductase (GR). The low molecular weight antioxidants are of particular interest, since recent evidence suggests that the tissue concentrations of these substances decrease with age (Lenton et al. 2000), and in certain disease states (Dibbert et al. 1999). Several studies have correlated fluctuations in the levels of these low molecular weight antioxidants with the onset of airway cellular damage *in vivo* (Guidot and Roman 2002), or with the appearance of indicators of cellular damage *in vitro* (Ballinger et al. 2005). Furthermore, recent reports also support associations between oxidant-mediated respiratory tract injury and changes in the levels or activity of cellular antioxidants (Kirschvink et al. 2002; Comhair et al. 2005).

Interactions between ozone and respiratory tract epithelial cells are governed in large part by ELF and intracellular antioxidants (Figure 1-1). Inhaled ozone may be effectively removed, or quenched, in the presence of protective levels of antioxidants. Without adequate antioxidant protection, however, the respiratory airways become susceptible to oxidant-mediated damage. Ozone is an extremely reactive oxidant gas, and is relatively

insoluble in aqueous solutions. For these reason, it is unlikely that ozone itself is capable of penetrating the ELF layer and oxidizing epithelial cell membranes (Cross et al. 1998). A growing body of evidence suggests that ozone itself does not produce cytotoxicity to airway epithelial cells, but rather does so by generating reactive secondary products within the epithelial lining fluid (ELF), which subsequently induce cellular damage to the underlying epithelium (Postlethwait et al. 1998). While antioxidants are largely considered to confer protection to the airway epithelium during oxidant pollutant exposure, results from several recent investigations support the concept that the presence of ELF antioxidants may facilitate oxidant damage by mediating this

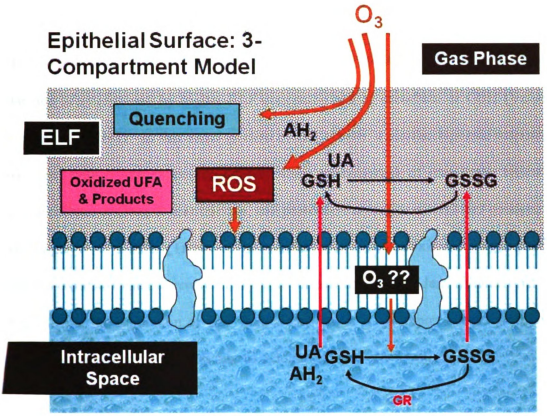

Figure 1-1. Potential fates of inhaled ozone in the nasal cavity. Diagrammatic representation of the epithelial surface lining the anterior nasal cavity. Prior to initiating reactions with cell surface and intracellular targets, gas-phase ozone (O_3) in the airway lumen must penetrate the epithelial lining fluid (ELF) layer. Reactions with ELF antioxidants, including ascorbate (AH), uric acid (UA), and glutathione (GSH) may completely quench inhaled ozone, conferring complete protection. It is also possible that ozone itself may completely penetrate the ELF intact and directly react with membrane and intracellular lipids and proteins. However, reactions with ELF antioxidants can also generate reactive oxygen species (ROS), which may mediate ozone-induced cell membrane protein oxidation and lipid peroxidation via "reactive absorption." ELF antioxidant levels are maintained in part by the regulation of intracellular antioxidant concentrations. In the case of GSH, this balance is maintained through a combination of *de novo* synthesis, redox recycling of oxidized glutathione (GSSG) via glutathione reductase (GR), and scavenging of extracellular GSH and GSSG.

"reactive absorption," and thereby yielding toxic reaction products. It has been shown *in vitro*, that the presence of low concentrations of ascorbate or glutathione (GSH) within the ELF augments membrane oxidation during NO_2 exposure. NO_2-induced membrane damage is ameliorated by higher ELF concentrations of ascorbate or GSH (Velsor and Postlethwait 1997). In this same *in vitro* model system, a similar biphasic response was observed with ozone exposure, demonstrating enhancement of membrane oxidation at low ascorbate or GSH concentrations, and protection at higher antioxidant concentrations (Ballinger et al. 2005). These results indicate that ELF antioxidants confer protection against oxidant-induced airway injury in a concentration-dependent manner, and further suggest that the regulation of ELF antioxidant levels is an important factor in both the mediation of and epithelial response to oxidant-induced airway injury.

Potential Role of Glutathione in Epithelial Adaptation and Remodeling. The concept of pulmonary tolerance to ozone exposure has been well described in both human volunteers and experimental animal models. Prolonged exposure to ozone and other inhaled pollutants results in biochemical changes that render the epithelium resistant to further oxidant injury. Among these are increases in the activity of several antioxidants, including glutathione (GSH), within the airway epithelium (Plopper et al. 1994; Duan et al. 1996). Daily ozone exposure (0.75 ppm, 12h/day for 7 days) results in a sustained increase in BALF levels of uric acid and glutathione in calves. BALF antioxidant levels increase by day 3 of exposure, remain elevated through day 7, and are accompanied by a corresponding decrease in the number of neutrophils in BALF (Kirschvink et al. 2002). While these mechanisms have not been extensively investigated in the nasal epithelium,

the similarity in epithelial types between the nasal and pulmonary airways suggests that similar adaptation could occur within the nasal cavity.

Injury to nasal and pulmonary epithelial cells exposed to ozone is highly focal and site-specific *in vivo*. Several factors may contribute to this site specificity, including local ozone dose, susceptibility of the local epithelium, and capacity for antioxidant protection. Significant variability exists across different subcompartments of the monkey and mouse lung in both the rates of consumption and resynthesis of GSH during ozone challenge *in vitro* (Duan et al. 1996). In all regions of mouse lung examined (trachea, minor daughter, and parenchyma), tissue GSH levels were initially depleted by ozone exposure, and returned to baseline levels within 2 hours of the end of exposure. Tissue GSH levels in comparable regions of monkey lung were also similarly depleted by ozone exposure, and required up to 4 hours for re-synthesis or redox recycling to return GSH to baseline levels. There are also variations in the activities of glutathione-S-transferase and glutathione peroxidase, enzymes that require GSH as a substrate, across different regions of monkey lung (Duan et al. 1993). In young adult monkeys, the sites of ozone-induced GSH depletion correspond with sites of exposure-related injury in the pulmonary airways (Plopper et al. 1998). These results suggest that site- and species-dependent susceptibility to ozone-induced lower airway injury may be in part mediated by the capacity of the local epithelium to regulate or replace consumed antioxidants. The relationship between local GSH regulation and susceptibility to oxidant-mediated injury in the upper airways has not been extensively investigated.

Investigators in several previous reports have suggested that the degree of epithelial injury may play a role in the progression of epithelial remodeling. Reports of ozone and formaldehyde inhalation studies indicate that *sublethal* cellular injury is sufficient, and perhaps necessary, to trigger toxicant-induced cell proliferation (Monticello et al. 1991; Henderson et al. 1993). Exposure to low concentrations of cigarette smoke condensate (CSC), a mixture of toxic compounds including particulate matter, endotoxin, and oxidant pollutant gases (Stockley et al. 2008), triggers cell proliferation in two lines of bronchial epithelial cells *in vitro*. Exposure to high concentrations of CSC inhibits cell proliferation in these same cell lines. This inhibitory effect of the high concentrations is due in part to higher levels of cytotoxicity. Administration of the cysteine donor compound, N-acetylcysteine (NAC) ameliorated the inhibitory effect on cell proliferation, indicating that this effect is mediated in part by CSC-induced depletion of non-protein thiol levels (e.g. GSH), and that restoration of non-protein thiol levels via NAC also restores proliferative capacity in these cells (Luppi et al. 2005). This also indicates that the magnitude of cellular injury plays a role in the subsequent epithelial remodeling process; and that glutathione, which exhibits site- and species-dependent kinetics in response to oxidant challenge, may be an integral factor in site- and species-dependent, oxidant-induced epithelial remodeling in the nasal airways.

Several studies implicate glutathione upregulation as a necessary precursor to the stimulation of cell proliferation, specifically to entry into S-phase of the cell cycle. Increased intracellular GSH concentration is a precursor to G_1/S transition following mitogenic stimulation in quiescent (G_0) fibroblasts. Furthermore, inhibition of GSH

synthesis inhibits DNA synthesis and reduces the percentage of cells capable of entering S-phase (Shaw and Chou 1986; Kavanagh et al. 1990). The molecular mechanisms underlying this regulation remain unclear. Previous studies have indicated that intracellular redox balance is an important regulator of cell cycle progression (Menon et al. 2003)(Lu et al. 2007). Thus, it is possible that intracellular GSH regulates cell cycle progression, and ultimately, cell proliferation, via its role in the maintenance of intracellular redox balance.

Overall Goal: The overall goal of my thesis experiments was to determine the relationship between the regulation of nasal antioxidants and susceptibility to ozone-induced nasal airway injury and repair. Specifically, my studies were designed to determine the association between the local regulation of GSH and the site-specificity of ozone-induced injury and repair in the nasal airways of infant monkeys and rats, and to determine the role of GSH in the pathogenesis of nasal epithelial hyperplasia following ozone exposure in infant monkeys and immature rats. Based on previous studies demonstrating correlations between local GSH regulation and ozone-induced injury in the pulmonary airways, we anticipated that GSH would be a determinant in the susceptibility to ozone injury in the nasal airways, and that changes in GSH regulation would parallel the onset of epithelial hyperplasia.

Governing Hypothesis: The spatial distribution and temporal pattern of ozone-induced epithelial hyperplasia in the nasal airways are dependent on the local regulation of GSH.

Specific Aims:

I: To describe the temporal relationships between ozone exposure and the development of epithelial hyperplasia in the nasal airways of infant monkeys and rats. These studies were specifically designed to determine the temporal association between the ozone exposure and the process of epithelial hyperplasia in the anterior nasal airways of infant rats and monkeys acutely or episodically exposed to high ambient levels of ozone. Infant monkeys and immature rats were exposed episodically (monkeys) or daily (rats) to ozone or filtered air. The morphologic responses of the nasal epithelium were extensively characterized and quantified during the course of daily and episodic ozone exposures using standard histopathologic and morphometric techniques.

II: To test the hypothesis that GSH upregulation is spatially and temporally correlated with sites of ozone-induced injury and repair in the nasal airways of infant monkeys. These studies were designed to test the hypothesis that the site-specificity of ozone-induced epithelial hyperplasia in the nasal airways of infant monkeys and rats is due, in part, to the local regulation of GSH following ozone exposure. The location and severity of ozone-induced injury (including epithelial hyperplasia) in the left nasal passages (described in **Specific Aim I**) was documented using morphometric techniques, and mapped on three-dimensional models of the left nasal airways of infant monkeys. The biochemical responses to daily and episodic ozone exposure (changes in antioxidant concentrations, determination of antioxidant and pro-inflammatory gene expression) were determined in site-matched mucosal samples from the contralateral nasal passage. Morphologic and biochemical responses were also evaluated in regions

that did not exhibit ozone-induced injury. The relationship between ozone-induced epithelial hyperplasia and steady-state GSH concentrations was described using correlation analysis.

***III*: To test the hypothesis that ozone-induced epithelial hyperplasia in the nasal airways of immature rats is a GSH-dependent event.** These studies were designed to determine the effect of *in vivo* GSH depletion, during early ozone exposure, on the initiation of cell proliferation and the subsequent development of epithelial hyperplasia. Immature male F344 rats were exposed daily to ozone or filtered air. Half of the rats were treated with L-buthionine-[S,R]-sulfoximine (BSO), to cause depletion of intracellular GSH. BSO is an irreversible inhibitor of glutamate cysteine ligase (GCL), the rate-limiting enzyme in *de novo* GSH synthesis. These experiments served to determine the role of GSH and GSH regulation, during early ozone exposures, in the development of ozone-induced nasal epithelial hyperplasia in immature rats (Figure 1-2).

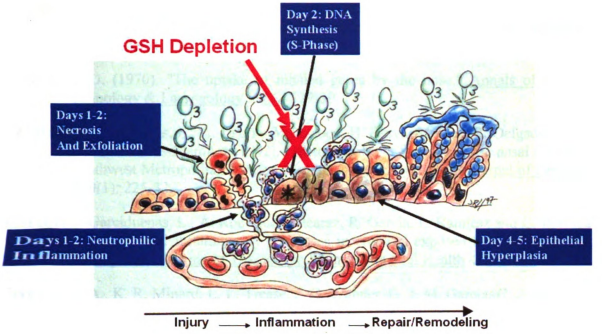

Figure 1-2. Potential role of GSH in ozone-induced epithelial hyperplasia in the nasal airways of rats. Daily exposures to ozone cause neutrophilic inflammation, epithelial necrosis and exfoliation on Day 1, followed by the initiation of DNA synthesis and cell proliferation on Day 2. These early cellular events precede the development of ozone-induced epithelial hyperplasia on Days 4-5. We hypothesize that ozone-induced GSH upregulation maintains intracellular redox balance, facilitating cell cycle progression and epithelial hyperplasia, and that GSH depletion will prevent this cytoprotection, and inhibit the development of epithelial hyperplasia.

REFERENCES

Ballinger, C. A., R. Cueto, G. Squadrito, J. F. Coffin, L. W. Velsor, W. A. Pryor and E. M. Postlethwait (2005). "Antioxidant-mediated augmentation of ozone-induced membrane oxidation." Free radical biology & medicine. **38**(4): 515-26.

Brain, J. D. (1970). "The uptake of inhaled gases by the nose." Annals of Otology, Rhinology & Laryngology **79**(3): 529-39.

Calderon-Garciduenas, L., A. Osorno-Velazquez, H. Bravo-Alvarez, R. Delgado-Chavez and R. Barrios-Marquez (1992). "Histopathologic changes of the nasal mucosa in southwest Metropolitan Mexico City inhabitants." American Journal of Pathology **140**(1): 225-32.

Calderon-Garciduenas, L., A. Rodriguez-Alcaraz, R. Garcia, L. Ramirez and G. Barragan (1995). "Nasal inflammatory responses in children exposed to a polluted urban atmosphere." Journal of Toxicology & Environmental Health **45**(4): 427-37.

Carey, S. A., K. R. Minard, L. L. Trease, J. G. Wagner, G. J. M. Garcia, C. A. Ballinger, J. S. Kimbell, C. Plopper, R. A. Corley, E. M. Postlethwait and J. R. Harkema (2007). "Three-Dimensional Mapping of Ozone-Induced Injury in the Nasal Airways of Monkeys Using Magnetic Resonance Imaging and Morphometric Techniques." Toxicologic Pathology **35**(1): 27-40.

Castleman, W. L., D. L. Dungworth, L. W. Schwartz and W. S. Tyler (1980). "Acute respiratory bronchiolitis: an ultrastructural and autoradiographic study of epithelial cell injury and renewal in rhesus monkeys exposed to ozone." Am J Pathol **98**(3): 811-40.

Cho, H. Y., J. A. Hotchkiss, C. B. Bennett and J. R. Harkema (1999). "Effects of pre-existing rhinitis on ozone-induced mucous cell metaplasia in rat nasal epithelium." Toxicology & Applied Pharmacology **158**(2): 92-102.

Cho, H. Y., J. A. Hotchkiss and J. R. Harkema (1999). "Inflammatory and epithelial responses during the development of ozone-induced mucous cell metaplasia in the nasal epithelium of rats." Toxicological Sciences **51**(1): 135-45.

Christian, D. L., L. L. Chen, C. H. Scannell, R. E. Ferrando, B. S. Welch and J. R. Balmes (1998). "Ozone-induced inflammation is attenuated with multiday exposure." American Journal of Respiratory & Critical Care Medicine **158**(2): 532-7.

Comhair, S. A., W. Xu, S. Ghosh, F. B. Thunnissen, A. Almasan, W. J. Calhoun, A. J. Janocha, L. Zheng, S. L. Hazen and S. C. Erzurum (2005). "Superoxide dismutase inactivation in pathophysiology of asthmatic airway remodeling and reactivity.[see comment]." American Journal of Pathology **166**(3): 663-74.

Cross, C. E., A. van der Vliet, S. Louie, J. J. Thiele and B. Halliwell (1998). "Oxidative stress and antioxidants at biosurfaces: plants, skin, and respiratory tract surfaces." Environ Health Perspect **106 Suppl 5**: 1241-51.

Cross, C. E., A. van der Vliet, C. A. O'Neill, S. Louie and B. Halliwell (1994). "Oxidants, antioxidants, and respiratory tract lining fluids." Environ Health Perspect **102 Suppl 10**: 185-91.

Dahl, A. R. and W. M. Hadley (1991). "Nasal cavity enzymes involved in xenobiotic metabolism: effects on the toxicity of inhalants." Critical Reviews in Toxicology **21**(5): 345-72.

Devlin, R. B. (1993). "Identification of subpopulations that are sensitive to ozone exposure: use of end points currently available and potential use of laboratory-based end points under development." Environmental Health Perspectives **101 Suppl 4**: 225-30.

Dibbert, B., M. Weber, W. H. Nikolaizik, P. Vogt, M. H. Schoni, K. Blaser and H. U. Simon (1999). "Cytokine-mediated Bax deficiency and consequent delayed neutrophil apoptosis: a general mechanism to accumulate effector cells in inflammation." Proc Natl Acad Sci U S A **96**(23): 13330-5.

Duan, X., A. R. Buckpitt and C. G. Plopper (1993). "Variation in antioxidant enzyme activities in anatomic subcompartments within rat and rhesus monkey lung." Toxicol Appl Pharmacol **123**(1): 73-82.

Duan, X., C. Plopper, P. Brennan and A. Buckpitt (1996). "Rates of glutathione synthesis in lung subcompartments of mice and monkeys: possible role in species and site selective injury." Journal of Pharmacology & Experimental Therapeutics **277**(3): 1402-9.

Gauderman, W. J., E. Avol, F. Gilliland, H. Vora, D. Thomas, K. Berhane, R. McConnell, N. Kuenzli, F. Lurmann, E. Rappaport, H. Margolis, D. Bates and J. Peters (2004). "The effect of air pollution on lung development from 10 to 18 years of age.[see comment][erratum appears in N Engl J Med. 2005 Mar 24;352(12):1276]." New England Journal of Medicine **351**(11): 1057-67.

Graham, D. E. and H. S. Koren (1990). "Biomarkers of inflammation in ozone-exposed humans. Comparison of the nasal and bronchoalveolar lavage." American Review of Respiratory Disease **142**(1): 152-6.

Guidot, D. M. and J. Roman (2002). "Chronic ethanol ingestion increases susceptibility to acute lung injury: role of oxidative stress and tissue remodeling." Chest **122**(6 Suppl): 309S-314S.

Harkema, J. R. (1991). "Comparative aspects of nasal airway anatomy: relevance to inhalation toxicology." Toxicologic Pathology **19**(4 Pt 1): 321-36.

Harkema, J. R., J. A. Hotchkiss and R. F. Henderson (1989). "Effects of 0.12 and 0.80 ppm ozone on rat nasal and nasopharyngeal epithelial mucosubstances: quantitative histochemistry." Toxicologic Pathology **17**(3): 525-35.

Harkema, J. R., C. G. Plopper, D. M. Hyde and J. A. St George (1987). "Regional differences in quantities of histochemically detectable mucosubstances in nasal, paranasal, and nasopharyngeal epithelium of the bonnet monkey." Journal of Histochemistry & Cytochemistry **35**(3): 279-86.

Harkema, J. R., C. G. Plopper, D. M. Hyde, J. A. St George and D. L. Dungworth (1987). "Effects of an ambient level of ozone on primate nasal epithelial mucosubstances. Quantitative histochemistry." American Journal of Pathology **127**(1): 90-6.

Harkema, J. R., C. G. Plopper, D. M. Hyde, J. A. St George, D. W. Wilson and D. L. Dungworth (1987). "Response of the macaque nasal epithelium to ambient levels of ozone. A morphologic and morphometric study of the transitional and respiratory epithelium." American Journal of Pathology **128**(1): 29-44.

Harkema, J. R., C. G. Plopper, D. M. Hyde, J. A. St George, D. W. Wilson and D. L. Dungworth (1993). "Response of macaque bronchiolar epithelium to ambient concentrations of ozone." Am J Pathol **143**(3): 857-66.

Henderson, R. F., J. A. Hotchkiss, I. Y. Chang, B. R. Scott and J. R. Harkema (1993). "Effect of cumulative exposure on nasal response to ozone." Toxicology & Applied Pharmacology **119**(1): 59-65.

Hotchkiss, J. A., J. R. Harkema and N. F. Johnson (1997). "Kinetics of nasal epithelial cell loss and proliferation in F344 rats following a single exposure to 0.5 ppm ozone." Toxicology & Applied Pharmacology **143**(1): 75-82.

Kavanagh, T. J., A. Grossmann, E. P. Jaecks, J. C. Jinneman, D. L. Eaton, G. M. Martin and P. S. Rabinovitch (1990). "Proliferative capacity of human peripheral blood lymphocytes sorted on the basis of glutathione content." J Cell Physiol **145**(3): 472-80.

Kim, J. J. (2004). "Ambient air pollution: health hazards to children." Pediatrics **114**(6): 1699-707.

Kirschvink, N., L. Fievez, F. Bureau, G. Degand, G. Maghuin-Rogister, N. Smith, T. Art and P. Lekeux (2002). "Adaptation to multiday ozone exposure is associated with a sustained increase of bronchoalveolar uric acid." Free Radical Research **36**(1): 23-32.

Koltai, P. J. (1994). "Effects of air pollution on the upper respiratory tract of children." Otolaryngology - Head & Neck Surgery **111**(1): 9-11.

Kopp, M. V., C. Ulmer, G. Ihorst, H. H. Seydewitz, T. Frischer, J. Forster and J. Kuehr (1999). "Upper airway inflammation in children exposed to ambient ozone and potential signs of adaptation." European Respiratory Journal **14**(4): 854-61.

Koren, H. S., G. E. Hatch and D. E. Graham (1990). "Nasal lavage as a tool in assessing acute inflammation in response to inhaled pollutants." Toxicology **60**(1-2): 15-25.

Lenton, K. J., H. Therriault, A. M. Cantin, T. Fèulèop, H. Payette and J. R. Wagner (2000). "Direct correlation of glutathione and ascorbate and their dependence on age and season in human lymphocytes." The American journal of clinical nutrition. **71**(5): 1194-200.

Lu, Q., F. L. Jourd'Heuil and D. Jourd'Heuil (2007). "Redox control of G(1)/S cell cycle regulators during nitric oxide-mediated cell cycle arrest." J Cell Physiol **212**(3): 827-39.

Luppi, F., J. Aarbiou, S. van Wetering, I. Rahman, W. I. de Boer, K. F. Rabe and P. S. Hiemstra (2005). "Effects of cigarette smoke condensate on proliferation and wound closure of bronchial epithelial cells in vitro: role of glutathione." Respiratory Research **6**: 140.

Menon, S. G., E. H. Sarsour, D. R. Spitz, R. Higashikubo, M. Sturm, H. Zhang and P. C. Goswami (2003). "Redox Regulation of the G1 to S Phase Transition in the Mouse Embryo Fibroblast Cell Cycle." Cancer Res **63**(9): 2109-2117.

Monticello, T. M., R. Renne and K. T. Morgan (1991). "Chemically induced cell proliferation in upper respiratory tract carcinogenesis." Progress in Clinical & Biological Research **369**: 323-35.

Morgan, K. T. and T. M. Monticello (1990). "Airflow, gas deposition, and lesion distribution in the nasal passages." Environmental Health Perspectives **85**: 209-18.

Nikasinovic, L., I. Momas and N. Seta (2003). "Nasal Epithelial and Inflammatory Response to Ozone Exposure: A Review of Laboratory-Based Studies Published Since 1985." Journal of Toxicology and Environmental Health, Part B **6**(5): 521 - 568.

Nikula, K. J., D. W. Wilson, S. N. Giri, C. G. Plopper and D. L. Dungworth (1988). "The response of the rat tracheal epithelium to ozone exposure. Injury, adaptation, and repair." Am J Pathol **131**(2): 373-84.

Plopper, C. G., X. Duan, A. R. Buckpitt and K. E. Pinkerton (1994). "Dose-dependent tolerance to ozone. IV. Site-specific elevation in antioxidant enzymes in the lungs of rats exposed for 90 days or 20 months." Toxicology & Applied Pharmacology **127**(1): 124-31.

Plopper, C. G., G. E. Hatch, V. Wong, X. Duan, A. J. Weir, B. K. Tarkington, R. B. Devlin, S. Becker and A. R. Buckpitt (1998). "Relationship of inhaled ozone concentration to acute tracheobronchial epithelial injury, site-specific ozone dose, and glutathione depletion in rhesus monkeys." Am J Respir Cell Mol Biol **19**(3): 387-99.

Postlethwait, E. M., R. Cueto, L. W. Velsor and W. A. Pryor (1998). "O3-induced formation of bioactive lipids: estimated surface concentrations and lining layer effects." The American journal of physiology. **274**(6): L1006-16.

Proctor, D. and I. Anderson (1982). The Nose: Upper Airway Physiology and the Atmospheric Environment. Amsterdam, Elsevier Biomedical Press.

Shaw, J. P. and I. N. Chou (1986). "Elevation of intracellular glutathione content associated with mitogenic stimulation of quiescent fibroblasts." J Cell Physiol **129**(2): 193-8.

Sram, R. J., I. Benes, B. Binkova, J. Dejmek, D. Horstman, F. Kotesovec, D. Otto, S. D. Perreault, J. Rubes, S. G. Selevan, I. Skalik, R. K. Stevens and J. Lewtas (1996). "Teplice program--the impact of air pollution on human health." Environ Health Perspect **104 Suppl 4**: 699-714.

Stenfors, N., C. Nordenhall, S. S. Salvi, I. Mudway, M. Soderberg, A. Blomberg, R. Helleday, J. O. Levin, S. T. Holgate, F. J. Kelly, A. J. Frew and T. Sandstrom (2004). "Different airway inflammatory responses in asthmatic and healthy humans exposed to diesel." European Respiratory Journal **23**(1): 82-6.

Stockley, R. A., S. I. Rennard, K. Rabe, B. Celli and L. M. Hepp (2008). Cigarette Smoke-Induced Disease. Chronic Obstructive Pulmonary Disease: 385-396.

Velsor, L. W. and E. M. Postlethwait (1997). "NO2-induced generation of extracellular reactive oxygen is mediated by epithelial lining layer antioxidants." The American journal of physiology. **273**(6): L1265-75.

Wilson, D. W., C. G. Plopper and D. L. Dungworth (1984). "The response of the macaque tracheobronchial epithelium to acute ozone injury. A quantitative ultrastructural and autoradiographic study." Am J Pathol **116**(2): 193-206.

Yeh, H. C., R. M. Brinker, J. R. Harkema and B. A. Muggenburg (1997). "A comparative analysis of primate nasal airways using magnetic resonance imaging and nasal casts." J Aerosol Med **10**(4): 319-29.

CHAPTER 2

LOCAL ANTIOXIDANT PROFILE OF THE RAT NASAL CAVITY: A REVIEW OF THE EXPERIMENTAL LITERATURE

ABSTRACT

Environmental pollutants are a known cause of lung pathology. Inhaled oxidants such as ozone, nitrogen oxides, and tobacco smoke are important environmental causes of pulmonary epithelial damage. Antioxidants in the epithelium lining the respiratory tract, and those in the overlying epithelial lining fluid (ELF), constitute the initial lines of defense against these airborne toxicants (Cross et al. 1994). The nasal cavity is an important target for inhaled oxidant toxicants, and also may serve as a sentinel for potential lower airway toxicity. The rat is an important animal model for inhalation toxicologic risk assessment studies, and recent studies have begun to evaluate the antioxidant profiles of the rat nasal cavity as a potential factor in the susceptibility to oxidant pollutant-mediated airway injury. Assessment of the levels of constitutive and inducible antioxidants in this model species, as well as comparisons between animal models and humans, will aid in the understanding of the mechanisms of oxidant damage by inhaled toxicants, and may reveal important pathways for intervention.

INTRODUCTION

The tissues of the respiratory tract are first-line targets of the effects of environmental pollutants. Several of these pollutants exert their toxic effects on the respiratory system by directly inducing oxidative damage to the epithelium or to components of the epithelial lining fluid (ELF). Ozone, the major oxidant pollutant in photochemical smog, causes peroxidation of cell membrane fatty acids in pulmonary epithelial cells of humans (Baskin and Salem 1997; Cross et al. 1998). These peroxides can trigger chain reactions in adjacent molecules, and initiate a cascade of reactions yielding equally reactive by-products (Sandstrom 1995). The oxides of nitrogen, primarily generated during high temperature combustion, are capable of causing similar epithelial cell membrane damage in the respiratory tract. In addition to directly causing epithelial damage, inhaled oxidants can also damage membrane and surface fluid proteins, and the products of this molecular damage, including free radicals, can generate further epithelial damage and perpetuate membrane chain reactions (Maples et al. 1993). Constituents of tobacco smoke, diesel exhaust, and other pollutant gaseous and particulate mixtures possess oxidant properties capable of inducing cellular damage to the respiratory system, alone and in combination with other pollutants (Sandstrom 1995).

The epithelium of the respiratory system possesses an intrinsic antioxidant system that serves as the initial line of defense against these environmental toxicants (Cross et al. 1994). This system is comprised of two major classes of antioxidant compounds. The first class, the antioxidant protein enzymes, including superoxide dismutase (Stenfors et al. 2004), catalase (Harkema et al.), glutathione peroxidase (GPx), and glutathione reductase (GR), primarily provide intracellular defense against endogenous oxidants and

the secondary effects of exogenous oxidant pollutants. Some membrane-bound and extracellular forms of these enzymes also exist (e.g. extracellular SOD). The second class, low molecular weight antioxidant molecules, including glutathione, α-tocopherol, ascorbic acid (AH_2), and uric acid (UA), can be located within epithelial cells as well as within the ELF. These intrinsic antioxidants, primarily synthesized to neutralize endogenously generated oxidants during cellular respiration, also provide an important source of initial protection from inhaled oxidants.

The pulmonary effects of inhaled xenobiotic oxidants, including ozone, as well as the role of lung tissue antioxidants, have been extensively investigated and well characterized in humans (Barr et al. 1990; Devlin et al. 1991; Frischer et al. 1993; Cross et al. 1994; Sandstrom 1995; Calderon-Garciduenas et al. 2000; Calderon-Garciduenas et al. 2000; Mudway et al. 2004) and in experimental animal models (Castleman et al. 1973; Dungworth et al. 1975; Frank et al. 1978; Castleman et al. 1980; Slade et al. 1985; Harkema et al. 1999). People demonstrate significant differences in susceptibility to the harmful effects of ozone, with certain subsets of the population exhibiting heightened sensitivity to ozone exposure (Devlin 1993). Susceptibility of the lung to the effects of inhaled oxidants is determined in part by the antioxidant capacity, both constitutive and inducible, of the pulmonary epithelium (Plopper et al. 1998). The importance of this intrinsic antioxidant system in the lung is illustrated by the heterogeneity among species and ages in susceptibility to hyperoxia. Adult rabbits, rats, and mice exhibit higher sensitivity to hyperoxia-induced lung injury than neonates of these species, which can more readily upregulate tissue levels of antioxidant enzymes, and are therefore resistant to lung injury from similar insult (Frank et al. 1978).

Historically, the nasal cavity has been considered primarily for its role as a "scrubbing tower" for the pulmonary airways in inhalation toxicological studies. Functions of the nasal cavity relevant to this purpose include warming and humidifying inspired air, trapping respirable particles and antigens in its mucus layer, and phase I xenobiotic metabolism (Thornton Manning and Dahl 1997). Recently, the nasal cavity has received attention as an important primary target for inhaled oxidants, including ozone. The nasal epithelial and inflammatory responses to ozone exposure have been the subject of a recent literature review (Nikasinovic et al. 2003). Nasal injury associated with ozone exposure has been described in humans (Koltai 1994; Calderon Garciduenas et al. 1996; Calderon Garciduenas et al. 1997; Kopp et al. 1999; Sienra Monge et al. 2004), non-human primates (Harkema et al. 1987; Harkema et al. 1993), and experimental rodent models (Hotchkiss et al. 1989; Cho et al. 1999; Wagner et al. 2003), and significant heterogeneity exists among the location, character, and severity of the lesions among the different experimental animal models. Several factors may play a role in the variability observed in ozone susceptibility across species, including differences in airway geometry and airflow, and the resultant variations in local ozone dose, specific epithelial type susceptibility, and differences in the distribution of susceptible epithelial populations. As with the pulmonary airways, site-dependent differences also exist in the responses to inhaled ozone challenge among different regions of the nasal airways. It also follows that susceptibility to airway damage by ozone exposure in the nasal airways may also be due in part to local antioxidant capacity.

As in the pulmonary airways, the epithelium of the nasal cavity provides an intrinsic antioxidant array, consisting of antioxidant enzymes and low molecular weight antioxidant molecules. Each of these compounds possesses different substrate specificity and tissue activity, and thus, the level of protection provided to the epithelium may vary according to the type of oxidant challenging the epithelium. The antioxidant array in the nasal cavity of humans has been characterized in previous investigations (Peden et al. 1993; Mudway et al. 1999; van der Vliet et al. 1999). Several studies have suggested that low molecular weight antioxidant uric acid is the major antioxidant in the human upper respiratory tract (Peden et al. 1990; Peden et al. 1993; van der Vliet et al. 1999), with reduced glutathione, ascorbic acid, SOD species, and catalase also conferring protection to the nasal cavity in humans.

The rat is an important experimental animal model for inhalation toxicological studies. Many of these investigations in rats have focused on the effects of oxidant xenobiotics or pollutants, such as chlorine (Barrow et al. 1979; Hester et al. 2002), ozone (Hotchkiss et al. 1989; Cho et al. 1999; Harkema et al. 1999), and nitrogen dioxide (Mautz et al. 2001) (Ichinose et al. 1991) on the nasal epithelium. Despite the fact that the upper airways are susceptible to injury from inhaled oxidants, investigation of the antioxidant profile of the rat nasal cavity has only recently garnered scientific attention. The local nasal biochemical and metabolic differences between humans and experimental animal models must be considered during interspecies extrapolation of the toxic effects of inhaled oxidant gases. In light of the heterogeneity demonstrated among different ages and species in the pulmonary response to oxidant challenge (Slade et al. 1985; Hatch et al. 1994), it seems logical that characterization of the susceptibility profile of the nasal

cavity of the relevant animal models to oxidant challenge would aid in the selection of appropriate models for human risk assessment, and facilitate extrapolation of toxicology data from animal models to humans.

The purposes of this review are to provide a brief review of the major environmental oxidant pollutants (ozone and nitrogen oxides) and the biochemistry of the major antioxidant substances in rat nasal epithelium and nasal ELF, to review the experimental data regarding nasal antioxidant profiles in rat models, and to discuss the potential implications of these findings with regard to extrapolation from rat models of *in*halation toxicology for human risk assessment.

SOURCES OF BIOLOGICALLY RELEVANT ENVIRONMENTAL OXIDANTS

Ozone and Reactive Oxygen Species

Ozone (O_3), the principal oxidant pollutant in photochemical smog, is a highly potent oxidant, capable of inducing nasal and pulmonary epithelial damage in rats at ambient concentrations (Hotchkiss et al. 1989). In the stratosphere (the atmosphere 10-20 miles above the earth's surface), ultraviolet radiation splits molecular oxygen (O_2) into atomic oxygen ($O\cdot$), which rapidly reacts with O_2 to produce O_3. This reaction yields ozone at concentrations of up to 10 ppm. Stratospheric ozone, often referred to as "good" ozone, or the "ozone layer," serves to limit the amount of damaging ultraviolet light that reaches the earth's surface. In the troposphere (the atmosphere within 5 miles of the earth's surface), ozone is primarily produced through actions of ultraviolet radiation on polluted air. Tropospheric ozone, also called "ground level" ozone, is generated predominantly through the reaction of nitrogen oxides with oxygen in the

presence of sunlight. Ultraviolet radiation reacts with nitrogen dioxide (NO_2), which results in the generation of nitric oxide radical (NO·) and O·, the latter of which combines with O_2 to form ground level ozone. In clean air, the NO· quickly reacts with O· (see "**Nitrogen Oxides**" below) to regenerate NO_2, and thus prevents ozone accumulation. In urban centers, the high motor vehicle use results in the emission of volatile organic compounds (VOCs) into the atmosphere. These VOCs serve as a source of hydrocarbons, which can react with O· to yield hydrocarbon radicals. These reactive hydrocarbon radicals can subsequently oxidize NO· to form NO_2 (Peden et al. 1995). As a consequence, ozone is no longer consumed in the scavenging of NO·, and is subsequently allowed to accumulate in the atmosphere.

In addition to environmental sources, occupational sources can also produce biologically relevant concentrations of ozone. Exposure to ozone can be an occupational hazard in workplaces due to welding and other electrical processes (Challen 1974; Sandstrom 1995). During normal operation, ozone concentrations in airplane cabins may reach 0.20 ppm (Waters 2002). Ozone exposure is also a potential hazard onboard submarines (Crawl 2003).

While some environmental pollutants are directly toxic to the epithelium of the respiratory system, most biologically relevant environmental oxidant pollutants exert at least some of their toxic effects through the generation of reactive oxygen species (ROS) within the biological system. ROS are generated in all aerobic biological systems during normal cellular respiration. ROS can be generated by the successive single electron reductions of oxygen to water, which occurs during oxidative phosphorylation in mitochondria. These species, including superoxide anion ($O_2^{-}\cdot$), hydrogen peroxide

(H_2O_2), and hydroxyl radical (HO·), are endogenously produced at low levels, and are typically controlled by endogenous antioxidants (Baskin and Salem 1997). They are also produced in the respiratory airways as a result of exposure to exogenous oxidants. For example, exposure of the respiratory tract to ozone leads to epithelial cell injury and concurrent release of O_2^{-}· (Voter et al. 2001), which likely mediates epithelial membrane injury following ozone exposure, rather than ozone itself.

Nitrogen Oxides (NO_x) and Reactive Nitrogen Species

The oxides of nitrogen (nitrogen dioxide, NO_2; nitric oxide, NO) provide another source of environmental oxidants. In the atmosphere, these compounds are predominantly derived from internal combustion engines in motor vehicles (Sandstrom 1995). However, recent source apportionment studies indicate that combustion from stationary sources (e.g. electric power plants) also provides a significant proportion of nitrogen oxides in the environment, particularly in the midwestern United States (Elliott et al. 2007). These anthropogenic sources far exceed the contributions from natural sources, such as lightning and wildfires.

The oxygen bound to nitrogen atoms in a these compounds can undergo reduction, forming a special form of oxygen radical known as a reactive nitrogen species (Elliott et al.). As is the case with ROS, some reactive nitrogen species (Elliott et al.) are produced under controlled conditions *in vivo* (Moncada and Higgs 1991). Of particular importance is nitric oxide, which serves several important roles in the regulation of blood pressure, leukocyte killing functions, and as a neurotransmitter (Baskin and Salem 1997). In excessive amounts, however, nitric oxide can react with other radicals, including

tyrosine radicals, thus inhibiting their normal biological functions. For example, NO· can react with the tyrosyl radical at the active site of ribonucleotide reductase, an enzyme required for the initiation of DNA synthesis, and thereby inhibit cell proliferation (Lepoivre et al. 1994). RNS are also capable of reacting with ROS, yielding more potent oxidizing agents. Reaction of NO· with O_2^{-}· results in the formation of the highly reactive peroxynitrite anion , (ONO_2-), a potent oxidant which can initiate electrophilic attack on both membrane components (lipids, proteins) and low molecular weight ELF molecules, including antioxidants (e.g. ascorbate), yielding reactive cellular components and initiating peroxidation chain reactions (Radi et al. 1991).

In addition to ROS and RNS, many other molecules can contribute to oxidative stress in biological systems. These include organic radicals of amino acid, protein, and lipid oxidation, metal ions (e.g. iron), and reactive carbon species (e.g. CCl_3·) (Bowler and Crapo 2002). Complex gaseous mixtures, such as the components of the gas phase of passive cigarette smoke, provide simultaneous exposure to combinations of potent ROS, RNS, and organic radicals (Jaimes et al. 2004).

ANTIOXIDANT ENZYME SYSTEMS OF THE RAT NASAL EPITHELIUM

Superoxide dismutase

Superoxide dismutases are a family of metal ion-containing enzymes that are present in most aerobic organisms (Stenfors et al. 2004). The major function of these enzymes is to catalyze the dismutation of the superoxide anion radical, O_2^{-}, resulting in the generation of the less reactive oxidants hydrogen peroxide and oxygen gas. Since O_2^{-} does not readily cross cell membranes, it must be detoxified in the cellular compartment

in which it was generated. For this reason, SODs evolved into three distinct forms, which differ in their metal ion content at the active site of the enzyme, and their subcellular locations. In mammals, manganese-SOD (Mn-SOD) is localized to the mitrochondria, and the cytosol contains dimeric copper/zinc-SOD (Cu,Zn-SOD). Mammalian tissues also contain an tetrameric, extracellular form of Cu,Zn-SOD (EC-SOD), that is expressed primarily in the epithelial lining fluid of the lung (Fridovich 1995).

In the Sprague-Dawley rat, immunohistochemical studies have demonstrated that expression of Mn-SOD and Cu,Zn-SOD in olfactory receptor neurons of olfactory epithelium occurs as early as embryonic day 14. While immunoreactivity for Mn-SOD increases throughout the perinatal period to a maximum at postnatal day 11, immunoreactivity for dimeric (cytosolic) Cu,Zn-SOD increases primarily after birth, peaking between postnatal days 11 and 24 (Kulkarni Narla et al. 1997). Similarly, in adult F/344 rats, total SOD activity increases, relative to control, in response to prolonged hyperoxia (Nikula et al. 1991). These findings are supportive of the concept that SOD levels are responsive to increases in oxygen tension during the postnatal period, and that this responsiveness persists into adulthood.

In adult rats, one study using enzyme activity assays demonstrated that total SOD activity is higher in olfactory epithelium than in nasal respiratory epithelium, and that activity in both types of nasal epithelium exceeded that in lung tissue. This study, using Wistar-derived albino rats, also demonstrated, via immunohistochemical localization, that both Mn-SOD and dimeric Cu,Zn-SOD are found primarily within the olfactory epithelium of the dorsal, medial nasal cavity (Reed et al. 2003). Interestingly, a similar distribution of activity was also found with the other enzymatic antioxidants evaluated

(see below). The same distribution of SOD activity was described in a separate study in adult male Wistar rats. This latter study also found that despite the higher total activity of both SOD forms in olfactory epithelium, the ratio of mitochondrial to cytosolic activity was similar in both regions (Lai et al. 1997). This report also found no SOD immunoreactivity in goblet cells or the interstitium of the respiratory epithelium, suggesting that these regions of the nasal mucosa may remain vulnerable to O_2-mediated membrane damage. It is also possible that these areas obtain protection from O_2^- from other sources, including intraepithelial and submucosal mucus. In response to hyperoxia, however, the respiratory epithelium demonstrated greater increases in SOD enzymatic activity relative to control levels (Nikula et al. 1991). This discrepancy may be due to regional differences in the capacity for enzyme upregulation, local differences in the degree or duration of exposure to inhaled oxidants (respiratory epithelium lies primarily in the ventral nasal cavity, while olfactory epithelium lies dorsally), or may represent a point of imbalance in the consumption/repletion kinetics of SOD in these two tissues.

Catalase

Catalase serves a major role in the intrinsic antioxidant cascade in mammalian systems. Its main function is to catalyze the decomposition of hydrogen peroxide to water, thus continuing the cascade of superoxide radical decomposition. Catalase is localized predominantly to peroxisomes, and can be found in this location within epithelial cells and some inflammatory cells, primarily macrophages, (Baskin and Salem 1997).

Within the nasal cavity, catalase activity has been demonstrated in transitional, respiratory, and olfactory epithelium (Nikula et al. 1991; Peshenko et al. 1998), with highest activity found in respiratory epithelium. Catalase activity in lung tissue exceeded both nasal epithelial types (Reed et al. 2003). Catalase activity did not increase in response to hyperoxic (85%) conditions in any of the nasal epithelial types in adult F/344 rats (Nikula et al. 1991). In contrast to the nasal cavity, lung catalase activity showed a 21% increase in response to hyperoxia (95%) in both adult and neonatal Sprague-Dawley albino rats (Frank et al. 1978). This higher activity and upregulation may be necessary in the lung to neutralize the respiratory burst activity from the resident macrophage population in the alveoli.

NAD(P)H:Quinone oxidoreductase (NQO1)

NQO1, also known as DT-diaphorase is an important cytosolic chemoprotective oxido-reductase, involved largely in the metabolism of oxidizing xenobiotic quinones. It is a two-electron quinone reductase, which prevents oxidative damage in cells by preventing the one-electron reduction of quinones, which results in the formation of semiquinones, which can spontaneously dismutate and yield damaging superoxide radicals (Lind et al. 1982). The majority of NQO1 resides in the cytosolic compartment of most cells, with some activity also found in mitochondria (Ernster 1958). In addition to its intracellular activity against xenobiotic quinone oxidants, NQO1 participates in the reduction of endogenous and exogenous quinines in membranes, including cell membrane-bound vitamin E quinones, thereby regenerating antioxidant forms of these

molecules. NQO1 also possesses scavenging activity against exogenously generated superoxide radical anion.

NQO1 activity has been reported in the respiratory and olfactory epithelium of the nasal cavity of Wistar rats. The levels detected were highest in respiratory epithelium, and levels in both respiratory and olfactory were higher than those in lung tissue (Reed et al. 2003). Immunohistochemically, NQO1 has been detected in respiratory, olfactory, and transitional epithelium of the nasal cavity. Unlike the nasal distribution of catalase and SOD, which was primarily dorsal and rostral, NQO1 showed regions of intense detection throughout the nasal cavity of the rat, with the most intense detection in the caudal and ventral regions of the nasal airways (Reed et al. 2003).

Glutathione peroxidase and glutathione reductase

Glutathione peroxidases are a family of enzymes that can be divided into selenium-dependent and selenium-independent systems. Both types can catalyze the reduction of hydrogen peroxide and organic peroxides to water and/or alcohol, but the former group possesses wider substrate specificity. These enzymes exist in cytosolic (monomeric) and cell membrane-bound (tetrameric) forms.

Glutathione peroxidases utilize reduced glutathione (GSH) as an electron donor in the reduction of peroxides, in a mechanism involving glutathione redox cycling. This function of glutathione is independent of its function as a low molecular weight antioxidant in epithelial lining fluids (see below). The glutathione peroxidase reaction results in the formation of the glutathionyl radical (GS·). At high GSH concentrations or

high rates of GSH consumption, GS· quickly dimerizes to form the oxidized form glutathione disulfide (GSSG). Reduced glutathione is regenerated from GSSG by the activity of glutathione reductase, in a reaction requiring reducing potential (NADPH) provided by glucose-6-phosphate dehydrogenase (G6PDH). In this manner, the activities of glutathione peroxidase, glutathione reductase, and G6PDH are interrelated.

Glutathione peroxidase antioxidant activity has been documented in transitional, respiratory (Cassee and Feron 1994), and olfactory epithelium of the rat (Nikula et al. 1991; Reed et al. 2003). Glutathione peroxidase activity in respiratory epithelium is higher in the resting state than olfactory epithelial activity, with glutathione peroxidase activity in the lung intermediate to the two. Glutathione reductase activities are comparable to glutathione peroxidase levels in the nasal transitional and respiratory epithelium, illustrating the close relationship between the two.

Results of glutathione peroxidase activity were widely divergent in the two studies that evaluated this activity in respiratory epithelium (~130nmol/min/mg protein, versus 48.6 μmol/min/mg protein) (Cassee and Feron 1994; Reed et al. 2003). There are several methodological differences between the two studies, however, that may explain these differences. The discrepancy may be due to differences in the ages of the rats (8 weeks versus adult), peroxide substrate differences between the two assays (*tert*-butyl hydroperoxide and cumene hydroperoxide), and differences in standardization methods (cytosolic versus total protein). A similar discrepancy in the measured levels of glutathione reductase activity (~130nmol/min/mg protein versus 275μmol/min/mg protein), between these studies could also be explained by age and standardization

differences; however, the same enzyme substrate (oxidized glutathione) was used in both of these studies (Cassee and Feron 1994; Reed et al. 2003).

Nasal transitional and olfactory epithelium both demonstrate increased levels of glutathione peroxidase activity in response to hyperoxia (85%), while nasal respiratory epithelium showed no significant increase following hyperoxia in adult F/344 rats (Nikula et al. 1991). A separate study found no significant increase in lung glutathione peroxidase activity in response to 95% hyperoxia in adult Sprague-Dawley rats (Frank et al. 1978).

Peroxiredoxin (thioredoxin)

Peroxiredoxins are a broad family of antioxidant proteins that are ubiquitously present in all cells across species. A novel, 28-kDa secretory protein isolated from rat olfactory epithelium was identified as a thiol-specific antioxidant member of the peroxiredoxin family (Peshenko et al. 1998). Peroxiredoxins exhibit substrate specificity similar to that of catalase and glutathione peroxidase, possessing activity against endogenously generated peroxides including hydrogen peroxide.

The 28-kDa peroxiredoxin initially isolated from Wistar rat olfactory epithelium has since been documented in trachea and lung, as well as several other non-respiratory tissues in the rat. Within olfactory epithelium of the Wistar rat, the peroxiredoxin immunoreactivity specifically localizes to the apical portions of the sustentacular cell cytosol and within mucus, both intracellularly and within the airway lumen (Novoselov et al. 1999).

LOW MOLECULAR WEIGHT ANTIOXIDANTS

Glutathione (GSH)

Glutathione is a non-protein tripeptide of γ-glutamate, cysteine, and glycine. Reduced glutathione is the most abundant thiol present in mammalian tissues (Baskin and Salem 1997). GSH serves many roles in living systems. Many of these involve redox functions in biological systems, including serving as an electron donor for reduction of peroxidases via glutathione peroxidase, non-enzymatic reduction of free radicals, structural maintenance of sulfhydryl residues of protein and enzymes, and fulfilling a vital role in the reduction of the α-tocopherol radical and semidehydroascorbate radical, thereby returning them to their functional states as antioxidants (α-tocopherol and ascorbate, respectively) (Buettner 1993). In addition to its many known redox functions, GSH also serves as an important signaling molecule for many cellular processes, including cell proliferation (Shaw and Chou 1986; Luppi et al. 2005; Markovic et al. 2007), and as a sulfhydryl buffer that maintains cysteinyl residues in their reduced states (Halliwell and Gutterudge 2007)

Three different studies have reported GSH values for rat nasal epithelium. Reported concentrations of GSH in two regions of olfactory epithelium (2.32μmol/g tissue in dorsal septal olfactory epithelium, 2.16μmol/g tissue in dorsal meatus olfactory epithelium) in adult F/344 rats are comparable to reported values for respiratory epithelium (2.67μmol/g tissue) in the same study (Potter et al. 1995). Two of these studies reported GSH concentrations relative to total cytosolic protein study. Using a HPLC quantitation method, one group reported concentrations for GSH in nasal

respiratory epithelium per unit cytosolic protein (~2.5μmol/mg cytosolic protein) in 8-week-old Wistar rats (Cassee and Feron 1994). A more recent study reported lower GSH concentrations in the olfactory epithelium (27nmol/mg protein) of Long-Evans rats (Burman et al. 2003); however, these values were obtained in younger rats (5-7 weeks), using a different detection and quantitation method (*o*-phthalaldehyde fluorometric probe).

Ascorbic Acid (Vitamin C)

Ascorbic acid, an essential vitamin in primates, is a water-soluble compound with several important metabolic roles. It is a potent and effective scavenger *in vivo*, capable of reacting with radicals of ROS, RNS, and water-soluble organic radicals, and in this capacity is one of the most important chain-breaking redox agents. One of its principle antioxidant roles is the regeneration of α-tocopherol and uric acid from their respective radicals, (Buettner 1993) which are formed during the metabolism of cell membrane lipid peroxides. The resulting ascorbyl radicals can be reduced back to ascorbic acid via enzymatic systems utilizing GSH or NADH as a reducing agent (Kagan et al. 1992).

Two studies have determined values for ascorbic acid concentrations in rat nasal epithelium, and the reported values are highly variable. Ascorbic acid concentrations in olfactory epithelium (~500μg/mg protein) are 4-fold higher than those reported in respiratory epithelium (~125μg/mg protein), and are comparable to concentrations reported in lung tissue (~400μg/mg protein) of adult Wistar rats (Reed et al. 2003). Another study, however, found significantly lower concentrations (~90nmol/mg protein, or ~16μg/mg protein) of ascorbic acid in olfactory epithelium of 5-7 week-old Long-

Evans rats (Burman et al. 2003). The ascorbic acid in each of these studies was harvested via a phosphoric acid extraction technique; however, the final results were obtained via different detection methods (525nm spectrophotometry versus HPLC).

α-Tocopherol (vitamin E)

Vitamin E is a group of eight naturally occurring lipid-soluble molecules known as the tocopherols. The lipid solubility of α-tocopherol facilitates its role as the major radical (lipid peroxyl) chain-breaking agent in plasma membranes. α-tocopherol is also reactive against superoxide anion radical and hydroxyl radical. α-tocopherol is an integtral part of plasma membranes, and is widely distributed in all types of plasma membranes, including the mitochondrial membranes and the endoplasmic reticulum (Baskin and Salem 1997).

Concentrations of α-tocopherol have been reported in rat nasal epithelium of Wistar rats (Reed et al. 2003). Concentrations of α-tocopherol were 1.4-fold higher in olfactory epithelium than in respiratory epithelium. Pulmonary levels of α-tocopherol were higher than concentrations found in the nasal epithelium.

DISCUSSION

The antioxidant profile and the geographical distribution of antioxidants throughout the nasal cavity can have important implications for susceptibility to inhaled oxidant pollutants and xenobiotics. Olfactory epithelium is enriched with a complement of metabolic enzyme capacity, including cytochrome P450s, glutathione s-transferases, and antioxidant enzymes. This metabolic capacity can be protective, or in some cases,

can exacerbate epithelial injury by generating toxic metabolites. While some antioxidants have wide substrate ranges (e.g. glutathione, ascorbic acid), others catalyze or facilitate specific redox reactions (e.g. SOD, catalase). In health, the complete profile of antioxidant compounds in a living system works in concert to protect the epithelium from oxidant insult. This review illustrates that regional differences exist within species. While other factors are also important (e.g. concentrations of oxidants delivered, airflow patterns through the nose, generation of immune responses), regional differences in antioxidant profiles must be considered in susceptibility studies within species.

This review also raises the question of age differences. While no single study evaluated antioxidant profile in multiple ages within a single species, examination of data from different studies and species suggests that antioxidant levels may vary with age. A similar study has been reported in the lung, which found that the ability to upregulate antioxidant enzyme expression in response to hyperoxia attenuates with age in rabbits and mice (Frank et al. 1978). This finding illustrates the importance of model selection in risk assessment studies, and highlights the need for controlled, comparative studies of multiple animal models and ages.

Several antioxidants that are not reported in this review are important agents in humans. Values for uric acid, heme oxygenase isoforms, and vitamin A, for example, have not been reported in the nasal cavity of the rat. Uric acid is a particularly important antioxidant in the human respiratory tract, and is the major chain-breaking antioxidant in the human nasal cavity (Peden et al. 1990; Peden et al. 1993). Also of importance is the fact that many of the chain-breaking antioxidant molecules, as well as some of the enzymatic antioxidants, reside in both the intracellular compartment and in the overlying

epithelial lining fluid *in vivo*. The concentrations of antioxidants in the intracellular and extracellular pools of the respiratory tract can differ significantly, and their levels may fluctuate independently following perturbation (Buhl et al. 1990; Smith et al. 1992; Testa et al. 1995). Many human studies consider the antioxidant profile of the ELF in risk assessment and kinetics studies. Nasal lavage methods have been developed for the rat, so ELF analysis is a feasible option that should be considered for future studies employing this model.

REFERENCES

Barr, B. C., D. M. Hyde, C. G. Plopper and D. L. Dungworth (1990). "A comparison of terminal airway remodeling in chronic daily versus episodic ozone exposure." *Toxicology & Applied Pharmacology* **106**(3): 384-407.

Barrow, C. S., R. J. Kociba, L. W. Rampy, D. G. Keyes and R. R. Albee (1979). "An inhalation toxicity study of chlorine in Fischer 344 rats following 30 days of exposure." *Toxicol Appl Pharmacol* **49**(1): 77-88.

Baskin, S. I. and H. Salem (1997). Oxidants, antioxidants, and free radicals. Washington, DC, Taylor & Francis.

Bowler, R. P. and J. D. Crapo (2002). "Oxidative stress in airways: is there a role for extracellular superoxide dismutase?" *Am J Respir Crit Care Med* **166**(12 Pt 2): S38-43.

Buettner, G. R. (1993). "The pecking order of free radicals and antioxidants: lipid peroxidation, alpha-tocopherol, and ascorbate." *Archives of biochemistry and biophysics.* **300**(2): 535-43.

Buhl, R., C. Vogelmeier, M. Critenden, R. C. Hubbard, R. F. Hoyt, Jr., E. M. Wilson, A. M. Cantin and R. G. Crystal (1990). "Augmentation of glutathione in the fluid lining the epithelium of the lower respiratory tract by directly administering glutathione aerosol." *Proc Natl Acad Sci U S A* **87**(11): 4063-7.

Burman, D. M., H. G. Shertzer, A. P. Senft, T. P. Dalton and M. B. Genter (2003). "Antioxidant perturbations in the olfactory mucosa of alachlor-treated rats." *Biochem Pharmacol* **66**(9): 1707-15.

Calderon-Garciduenas, L., R. B. Devlin and F. J. Miller (2000). "Respiratory tract pathology and cytokine imbalance in clinically healthy children chronically and sequentially exposed to air pollutants." *Medical Hypotheses* **55**(5): 373-8.

Calderon-Garciduenas, L., A. Mora-Tiscareno, C. J. Chung, G. Valencia, L. A. Fordham, R. Garcia, N. Osnaya, L. Romero, H. Acuna, A. Villarreal-Calderon, R. B. Devlin and H. S. Koren (2000). "Exposure to air pollution is associated with lung hyperinflation in healthy children and adolescents in Southwest Mexico City: a pilot study." *Inhalation Toxicology* **12**(6): 537-61.

Calderon Garciduenas, L., N. Osnaya Brizuela, L. Ramirez Martinez and A. Villarreal Calderon (1996). "DNA strand breaks in human nasal respiratory epithelium are induced upon exposure to urban pollution." *Environ Health Perspect* **104**(2): 160-8.

Calderon Garciduenas, L., N. Osnaya, A. Rodriguez Alcaraz and A. Villarreal Calderon (1997). "DNA damage in nasal respiratory epithelium from children exposed to urban pollution." *Environ Mol Mutagen* **30**(1): 11-20.

Cassee, F. R. and V. J. Feron (1994). "Biochemical and histopathological changes in nasal epithelium of rats after 3-day intermittent exposure to formaldehyde and ozone alone or in combination." *Toxicol Lett* **72**(1-3): 257-68.

Castleman, W. L., D. L. Dungworth, L. W. Schwartz and W. S. Tyler (1980). "Acute respiratory bronchiolitis: an ultrastructural and autoradiographic study of epithelial cell injury and renewal in rhesus monkeys exposed to ozone." *Am J Pathol* **98**(3): 811-40.

Castleman, W. L., D. L. Dungworth and W. S. Tyler (1973). "Histochemically detected enzymatic alterations in rat lung exposed to ozone." *Exp Mol Pathol* **19**(3): 402-21.

Challen, P. J. R. (1974). "Some News on Welding and Welders." *Occup Med (Lond)* **24**(2): 38-47.

Cho, H. Y., J. A. Hotchkiss and J. R. Harkema (1999). "Inflammatory and epithelial responses during the development of ozone-induced mucous cell metaplasia in the nasal epithelium of rats." *Toxicol Sci* **51**(1): 135-45.

Crawl, J. R. (2003). Review/Updating of Limits for Submarine Air Contaminants. First Meeting on Emergency and Continuous Exposure Guidance Levels for Selected Submarine Contaminants, Washington, DC.

Cross, C. E., A. van der Vliet, S. Louie, J. J. Thiele and B. Halliwell (1998). "Oxidative stress and antioxidants at biosurfaces: plants, skin, and respiratory tract surfaces." *Environ Health Perspect* **106 Suppl 5**: 1241-51.

Cross, C. E., A. van der Vliet, C. A. O'Neill, S. Louie and B. Halliwell (1994). "Oxidants, antioxidants, and respiratory tract lining fluids." *Environ Health Perspect* **102 Suppl 10**: 185-91.

Devlin, R. B. (1993). "Identification of subpopulations that are sensitive to ozone exposure: use of end points currently available and potential use of laboratory-based end points under development." *Environmental Health Perspectives* **101 Suppl 4**: 225-30.

Devlin, R. B., W. F. McDonnell, R. Mann, S. Becker, D. E. House, D. Schreinemachers and H. S. Koren (1991). "Exposure of humans to ambient levels of ozone for 6.6 hours causes cellular and biochemical changes in the lung." *Am J Respir Cell Mol Biol* **4**(1): 72-81.

Dungworth, D. L., W. L. Castleman, C. K. Chow, P. W. Mellick, M. G. Mustafa, B. Tarkington and W. S. Tyler (1975). "Effect of ambient levels of ozone on monkeys." *Fed Proc* **34**(8): 1670-4.

Elliott, E. M., C. Kendall, S. D. Wankel, D. A. Burns, E. W. Boyer, K. Harlin, D. J. Bain and T. J. Butler (2007). "Nitrogen isotopes as indicators of NO(x) source contributions to atmospheric nitrate deposition across the midwestern and northeastern United States." *Environ Sci Technol* **41**(22): 7661-7.

Ernster, L. (1958). "Diaphorase Activities in Liver Cytoplasmic Fractions." *Federation Proceedings* **17**(1): 216-216.

Frank, L., J. R. Bucher and R. J. Roberts (1978). "Oxygen toxicity in neonatal and adult animals of various species." *J Appl Physiol* **45**(5): 699-704.

Fridovich, I. (1995). "Superoxide Radical and Superoxide Dismutases." *Annual Review of Biochemistry* **64**(1): 97-112.

Frischer, T. M., J. Kuehr, A. Pullwitt, R. Meinert, J. Forster, M. Studnicka and H. Koren (1993). "Ambient ozone causes upper airways inflammation in children." *Am Rev Respir Dis* **148**(4 Pt 1): 961-4.

Halliwell, B. and J. Gutterudge (2007). Free radicals, other reactive species, and disease. Free Radicals in Biology and Medicine. B. Halliwell. New York, NY, Oxford University Press: 625-638.

Harkema, J. R., P. J. Catalano and J. A. Hotchkiss (1997). "Consequences of prolonged inhalation of ozone on F344/N rats: collaborative studies. Part XII: Atrophy of bone in nasal turbinates." *Res Rep Health Eff Inst*(65 (Pt 12)): 1-19; discussion 21-6.

Harkema, J. R., J. A. Hotchkiss, E. B. Barr, C. B. Bennett, M. Gallup, J. K. Lee and C. Basbaum (1999). "Long-lasting effects of chronic ozone exposure on rat nasal epithelium." *Am J Respir Cell Mol Biol* **20**(3): 517-29.

Harkema, J. R., C. G. Plopper, D. M. Hyde, J. A. St George, D. W. Wilson and D. L. Dungworth (1993). "Response of macaque bronchiolar epithelium to ambient concentrations of ozone." *Am J Pathol* **143**(3): 857-66.

Harkema, J. R., C. G. Plopper, D. M. Hyde, D. W. Wilson, J. A. St George and V. J. Wong (1987). "Nonolfactory surface epithelium of the nasal cavity of the bonnet monkey: a morphologic and morphometric study of the transitional and respiratory epithelium." *Am J Anat* **180**(3): 266-79.

Hatch, G. E., R. Slade, L. P. Harris, W. F. McDonnell, R. B. Devlin, H. S. Koren, D. L. Costa and J. McKee (1994). "Ozone dose and effect in humans and rats. A comparison using oxygen-18 labeling and bronchoalveolar lavage." *Am. J. Respir. Crit. Care Med.* **150**(3): 676-683.

Hester, S. D., G. B. Benavides, M. Sartor, L. Yoon, D. C. Wolf and K. T. Morgan (2002). "Normal gene expression in male F344 rat nasal transitional and respiratory epithelium." *Gene* **285**(1-2): 301-10.

Hotchkiss, J. A., J. R. Harkema, J. D. Sun and R. F. Henderson (1989). "Comparison of acute ozone-induced nasal and pulmonary inflammatory responses in rats." *Toxicol Appl Pharmacol* **98**(2): 289-302.

Ichinose, T., K. Fujii and M. Sagai (1991). "Experimental studies on tumor promotion by nitrogen dioxide." *Toxicology* **67**(2): 211-25.

Jaimes, E. A., E. G. DeMaster, R. X. Tian and L. Raij (2004). "Stable compounds of cigarette smoke induce endothelial superoxide anion production via NADPH oxidase activation." *Arterioscler Thromb Vasc Biol* **24**(6): 1031-6.

Kagan, V. E., A. Shvedova, E. Serbinova, S. Khan, C. Swanson, R. Powell and L. Packer (1992). "Dihydrolipoic acid--a universal antioxidant both in the membrane and in the aqueous phase : Reduction of peroxyl, ascorbyl and chromanoxyl radicals." *Biochemical Pharmacology* **44**(8): 1637-1649.

Koltai, P. J. (1994). "Effects of air pollution on the upper respiratory tract of children." *Otolaryngology - Head & Neck Surgery* **111**(1): 9-11.

Kopp, M. V., C. Ulmer, G. Ihorst, H. H. Seydewitz, T. Frischer, J. Forster and J. Kuehr (1999). "Upper airway inflammation in children exposed to ambient ozone and potential signs of adaptation." *European Respiratory Journal* **14**(4): 854-61.

Kulkarni Narla, A., T. V. Getchell and M. L. Getchell (1997). "Differential expression of manganese and copper-zinc superoxide dismutases in the olfactory and vomeronasal receptor neurons of rats during ontogeny." *J Comp Neurol* **381**(1): 31-40.

Lai, M. T., T. Ohmichi, T. Ogawa, K. Nishizaki and Y. Masuda (1997). "Electron spin resonance spin trapping assay and immunohistochemical localization of superoxide dismutases in the rat nasal mucosa." *Acta Otolaryngol* **117**(3): 437-46.

Lepoivre, M., J. M. Flaman, P. Bobe, G. Lemaire and Y. Henry (1994). "Quenching of the tyrosyl free radical of ribonucleotide reductase by nitric oxide. Relationship to cytostasis induced in tumor cells by cytotoxic macrophages." *J. Biol. Chem.* **269**(34): 21891-21897.

Lind, C., P. Hochstein and L. Ernster (1982). "DT-diaphorase as a quinone reductase: A cellular control device against semiquinone and superoxide radical formation." *Archives of Biochemistry and Biophysics* **216**(1): 178-185.

Luppi, F., J. Aarbiou, S. van Wetering, I. Rahman, W. I. de Boer, K. F. Rabe and P. S. Hiemstra (2005). "Effects of cigarette smoke condensate on proliferation and wound closure of bronchial epithelial cells in vitro: role of glutathione." *Respiratory Research* **6**: 140.

Maples, K. R., K. J. Nikula, B. T. Chen, G. L. Finch, W. C. Griffith and J. R. Harkema (1993). "Effects of Cigarette Smoke on the Glutathione Status of the Upper and Lower Respiratory Tract of Rats." *Inhal Toxicol* **5**: 389-401.

Markovic, J., C. Borras, A. Ortega, J. Sastre, J. Vina and F. V. Pallardo (2007). "Glutathione is recruited into the nucleus in early phases of cell proliferation." *J Biol Chem* **282**(28): 20416-24.

Mautz, W. J., M. T. Kleinman, D. K. Bhalla and R. F. Phalen (2001). "Respiratory tract responses to repeated inhalation of an oxidant and acid gas-particle air pollutant mixture." *Toxicol Sci* **61**(2): 331-41.

Moncada, S. and E. A. Higgs (1991). "Endogenous nitric oxide: physiology, pathology and clinical relevance." *European Journal of Clinical Investigation* **21**(4): 361-374.

Mudway, I. S., A. Blomberg, A. J. Frew, S. T. Holgate, T. Sandstrom and F. J. Kelly (1999). "Antioxidant consumption and repletion kinetics in nasal lavage fluid following exposure of healthy human volunteers to ozone." *Eur Respir J* **13**(6): 1429-38.

Mudway, I. S., N. Stenfors, S. T. Duggan, H. Roxborough, H. Zielinski, S. L. Marklund, A. Blomberg, A. J. Frew, T. Sandstrom and F. J. Kelly (2004). "An in vitro and in vivo investigation of the effects of diesel exhaust on human airway lining fluid antioxidants." *Arch Biochem Biophys* **423**(1): 200-12.

Nikasinovic, L., I. Momas and N. Seta (2003). "Nasal Epithelial and Inflammatory Response to Ozone Exposure: A Review of Laboratory-Based Studies Published Since 1985." *Journal of Toxicology and Environmental Health, Part B* **6**(5): 521 - 568.

Nikula, K. J., P. J. Sabourin, B. C. Frietag, A. J. Birdwhistell, J. A. Hotchkiss and J. R. Harkema (1991). "Biochemical and morphologic responses of rat nasal epithelia to hyperoxia." *Fundam Appl Toxicol* **17**(4): 675-83.

Novoselov, S. V., I. V. Peshenko, V. I. Popov, V. I. Novoselov, M. F. Bystrova, V. J. Evdokimov, S. S. Kamzalov, M. I. Merkulova, T. M. Shuvaeva, V. M. Lipkin and E. E. Fesenko (1999). "Localization of 28-kDa peroxiredoxin in rat epithelial tissues and its antioxidant properties." *Cell Tissue Res* **298**(3): 471-80.

Peden, D. B., R. Hohman, M. E. Brown, R. T. Mason, C. Berkebile, H. M. Fales and M. A. Kaliner (1990). "Uric acid is a major antioxidant in human nasal airway secretions." *Proc Natl Acad Sci U S A* **87**(19): 7638-42.

Peden, D. B., R. W. Setzer, Jr. and R. B. Devlin (1995). "Ozone exposure has both a priming effect on allergen-induced responses and an intrinsic inflammatory action in the nasal airways of perennially allergic asthmatics." *Am. J. Respir. Crit. Care Med.* **151**(5): 1336-1345.

Peden, D. B., M. Swiersz, K. Ohkubo, B. Hahn, B. Emery and M. A. Kaliner (1993). "Nasal secretion of the ozone scavenger uric acid." *Am Rev Respir Dis* **148**(2): 455-61.

Peshenko, I. V., V. I. Novoselov, V. A. Evdokimov, Y. V. Nikolaev, S. S. Kamzalov, T. M. Shuvaeva, V. M. Lipkin and E. E. Fesenko (1998). "Identification of a 28 kDa secretory protein from rat olfactory epithelium as a thiol-specific antioxidant." *Free Radic Biol Med* **25**(6): 654-9.

Plopper, C. G., G. E. Hatch, V. Wong, X. Duan, A. J. Weir, B. K. Tarkington, R. B. Devlin, S. Becker and A. R. Buckpitt (1998). "Relationship of inhaled ozone concentration to acute tracheobronchial epithelial injury, site-specific ozone dose, and glutathione depletion in rhesus monkeys." *Am J Respir Cell Mol Biol* **19**(3): 387-99.

Potter, D. W., L. Finch and J. R. Udinsky (1995). "Glutathione content and turnover in rat nasal epithelia." *Toxicol Appl Pharmacol* **135**(2): 185-91.

Radi, R., J. S. Beckman, K. M. Bush and B. A. Freeman (1991). "Peroxynitrite oxidation of sulfhydryls. The cytotoxic potential of superoxide and nitric oxide." *J. Biol. Chem.* **266**(7): 4244-4250.

Reed, C. J., D. A. Robinson and E. A. Lock (2003). "Antioxidant status of the rat nasal cavity." *Free Radic Biol Med* **34**(5): 607-15.

Sandstrom, T. (1995). "Respiratory effects of air pollutants: experimental studies in humans." *Eur Respir J* **8**(6): 976-95.

Shaw, J. P. and I. N. Chou (1986). "Elevation of intracellular glutathione content associated with mitogenic stimulation of quiescent fibroblasts." *J Cell Physiol* **129**(2): 193-8.

Sienra Monge, J. J., M. Ramirez Aguilar, H. Moreno Macias, N. I. Reyes Ruiz, B. E. Del Rio Navarro, M. X. Ruiz Navarro, G. Hatch, K. Crissman, R. Slade, R. B. Devlin and I. Romieu (2004). "Antioxidant supplementation and nasal inflammatory responses among young asthmatics exposed to high levels of ozone." *Clin Exp Immunol* **138**(2): 317-22.

Slade, R., A. G. Stead, J. A. Graham and G. E. Hatch (1985). "Comparison of lung antioxidant levels in humans and laboratory animals." *Am Rev Respir Dis* **131**(5): 742-6.

Smith, L. J., J. Anderson and M. Shamsuddin (1992). "Glutathione localization and distribution after intratracheal instillation. Implications for treatment." *Am Rev Respir Dis* **145**(1): 153-9.

Stenfors, N., C. Nordenhall, S. S. Salvi, I. Mudway, M. Soderberg, A. Blomberg, R. Helleday, J. O. Levin, S. T. Holgate, F. J. Kelly, A. J. Frew and T. Sandstrom (2004). "Different airway inflammatory responses in asthmatic and healthy humans exposed to diesel." *European Respiratory Journal* **23**(1): 82-6.

Testa, B., M. Mesolella, D. Testa, A. Giuliano, G. Costa, F. Maione and F. Iaccarino (1995). "Glutathione in the upper respiratory tract." *Ann Otol Rhinol Laryngol* **104**(2): 117-9.

Thornton Manning, J. R. and A. R. Dahl (1997). "Metabolic capacity of nasal tissue interspecies comparisons of xenobiotic-metabolizing enzymes." *Mutat Res* **380**(1-2): 43-59.

van der Vliet, A., C. A. O'Neill, C. E. Cross, J. M. Koostra, W. G. Volz, B. Halliwell and S. Louie (1999). "Determination of low-molecular-mass antioxidant concentrations in human respiratory tract lining fluids." *Am J Physiol* **276**(2 Pt 1): L289-96.

Voter, K. Z., J. C. Whitin, A. Torres, P. E. Morrow, C. Cox, Y. Tsai, M. J. Utell and M. W. Frampton (2001). "Ozone exposure and the production of reactive oxygen species by bronchoalveolar cells in humans." *Inhal Toxicol* **13**(6): 465-83.

Wagner, J. G., S. J. Van Dyken, J. R. Wierenga, J. A. Hotchkiss and J. R. Harkema (2003). "Ozone exposure enhances endotoxin-induced mucous cell metaplasia in rat pulmonary airways." *Toxicol Sci* **74**(2): 437-46.

Waters, M. (2002). The Airliner Cabin Environment and the Health of Passengers and Crew: Report to the National Research Council. Washington, DC, National Academies Press.

CHAPTER 3

THREE-DIMENSIONAL MAPPING OF OZONE-INDUCED INJURY, ANTIOXIDANT ALTERATIONS, AND PREDICTED OZONE FLUX, IN THE NASAL AIRWAYS OF MONKEYS USING MAGNETIC RESONANCE IMAGING AND MORPHOMETRIC TECHNIQUES

ABSTRACT

My governing hypothesis is that the spatial and temporal distribution of ozone-induced nasal injury is related to the regulation of intracellular glutathione levels. However, many other factors are likely to contribute to the location and severity of ozone lesions in the nasal cavity. Age-related changes in gross, biochemical and microscopic and structure of the nasal cavity may alter local tissue susceptibility as well as the dose of inhaled toxicant delivered to susceptible sites. This chapter describes a novel method for the use of magnetic resonance imaging, 3-dimensional airway modeling, and morphometric techniques to characterize the distribution and magnitude of ozone-induced nasal injury and site-matched ozone-induced nasal antioxidant fluctuations, following acute and episodic exposures in infant monkeys. Using this method, we generated age-specific, 3-dimensional, epithelial maps of the nasal airways of infant rhesus macaques. These 3-dimensional models were also utilized to perform computational fluid dynamics simulations of ozone uptake in the nasal airways. These simulations were used to determine the influence of airway geometry on local ozone dose, and to compare sites of predicted uptake with sites of injury. Here, we describe the histopathologic, imaging, biochemical, and computational biology methods developed to precisely characterize, localize, quantify, and map these nasal lesions. The principal nasal lesions observed in this primate model of ozone-induced nasal toxicology were neutrophilic rhinitis, along with necrosis and exfoliation of the epithelium lining the anterior maxilloturbinate. These lesions, induced by acute or episodic exposures, were examined by light microscopy, quantified by morphometric techniques, and mapped on 3-dimensional models of the nasal airways. Nasal mucosal samples from these same sites

were processed for intracellular nasal antioxidant content. By combining these techniques, the location and severity of the nasal epithelial injury were correlated with epithelial type, nasal airway geometry, and local biochemical changes on an individual animal basis. These correlations are critical for accurate predictive modeling of exposure-dose-response relationships in the nasal airways, for the determination of factors contributing to epithelial susceptibility to exposure-related injury, and for the extrapolation of nasal findings in animal models to humans for determining risk.

INTRODUCTION

Understanding the pathogenesis of ozone-induced airway injury and remodeling in the upper respiratory tract requires knowledge of the dose delivered to the target airway tissues and the airway tissue's response to exposure. Nasal injury caused by ozone exposure has been shown to be site-specific in both laboratory rodents and primates (Harkema et al. 1987a). The intranasal location of these ozone-induced lesions may be attributable to the local dose of ozone reaching the affected area, the site-specific tissue susceptibility, or a combination of these factors (Morgan and Monticello 1990). The local dose of ozone is dependent upon age-dependent airway geometry, ambient ozone concentration, and airflow-driven delivery. Local tissue susceptibility is a complex factor, dependent upon many components, including the distribution of susceptible epithelial populations in the nasal airways, and the capacity of the local tissue to respond to oxidant challenge. To determine the relative importance of each factor, it is essential to first microscopically identify the ozone-associated lesions in the nasal passages and precisely map the distribution of these specific lesions relative to airway geometry and epithelial susceptibility.

In previous reports, this has been accomplished experimentally using a sequential series of cross-sectional airway profiles covering the entire length of the nasal airways of each experimental animal. This systematic approach has been used to identify patterns of nasal toxicity to inhaled chemicals in adult monkeys (Young 1981; Harkema et al. 1987d; Mery et al. 1994; Kepler 1995), and relies on precise characterization and identification of the distribution of surface epithelial populations (Gross et al. 1982; Gross et al. 1987; Harkema et al. 1987a; Harkema 1991). This type of detailed characterization, however,

has not been previously reported the developing nasal airways of infant monkeys. Age-related differences between adult and infant monkeys in nasal airway geometry and epithelial distribution may cause changes in the exposure-dose-response relationship, and supports the use of infant monkeys as predictive models for nasal toxicology in children.

The rhesus macaque serves as an important animal model of upper airway toxicology because their nasal airways resemble, at a gross and microscopic level, the nasal airways of humans (Harkema 1991; Yeh et al. 1997). Knowledge of the patterns of ozone-induced airway lesions in the developing nasal passages of immature monkeys provides insight into the relative roles played by regional dose and local tissue susceptibility in the toxic responses to ozone in the nose, and ultimately, assists in the assessment of the potential risk of ozone exposure to the health of children. Using a combination of magnetic resonance (MR) imaging, 3-dimensional (3D) modeling, and standard histopathologic and morphometric techniques, we developed a detailed and flexible approach of nasal analysis to identify, localize, and precisely map normal nasal airway epithelium and ozone-induced nasal airway lesions. This method also provides a means to correlate morphologic changes to site-specific biochemical changes in the airways (e.g. regional antioxidant regulation) and with estimates of local ozone dose. Identifying these correlations is essential for developing predictive models of dosimetry, and defining exposure-dose-response relationships in nasal airways of immature non-human primates that are crucial for determining the mode of action in the nasal toxicity of ozone and other inhaled toxicants.

Ozone exposure (0.3 ppm, 8h/day, 6 days) causes epithelial necrosis, followed by epithelial hyperplasia, in the nasal airways of adult monkeys (Harkema et al. 1987c).

These epithelial lesions are confined to the anterior part of the nasal cavity. The effects of ozone exposure on the developing nasal airways of infant monkeys have not been previously investigated. The experiments described in this chapter were designed to determine the morphologic and biochemical effects of cyclic (episodic) ozone exposures on the nasal airways of infant monkeys. These studies were conducted to test the hypothesis that cyclic ozone exposure would cause epithelial necrosis and subsequent epithelial hyperplasia in the anterior nasal cavity of infant monkeys, similar to that described in adult monkeys exposed acutely to ozone (Harkema et al. 1987c). The techniques described here also provide a method to investigate the central hypothesis that the spatial and temporal distribution of ozone-induced nasal epithelial injury and subsequent epithelial proliferation in infant monkeys are dependent upon the local regulation of intracellular glutathione (GSH) concentrations. In addition, these techniques also provide a method to investigate other possible factors contributing to the site-specificity of ozone-induced nasal airway injury (e.g., local ozone dose). This chapter will provide a review of the methods that have been employed for ozone exposure, nasal airway imaging, nasal tissue processing, nasal antioxidant analysis, and 3D nasal airway mapping in the infant rhesus monkey. Attention will be focused on the details of these methods that provide an efficient and comprehensive characterization of airway geometry, nasal histopathology, and nasal antioxidant status, in order to maximize site-matched information obtained from each individual animal.

MATERIALS AND METHODS

Animals and Exposure Regimens

The principal laboratory animal used in our ozone inhalation studies was the infant, male Rhesus macaque (*Macaca mulatta*). All monkeys selected for these studies were born and raised at the California National Primate Research Center. Care and housing of animals before, during, and after treatment complied with the provisions of the Institute of Laboratory Animal Resources and conformed to practices established by the American Association for Accreditation of Laboratory Animal Care (AAALAC).

While several rodent models of environmental airway disease have been previously utilized for human risk assessment, some aspects of the airway anatomy and physiology of rodents make them less desirable for direct extrapolations to humans. For example, rodents are obligate nasal breathers, while humans may alternate between nasal and oronasal breathing. Humans also possess simple nasal turbinates, while rodents possess a very complex nasal turbinate structure (Harkema et al. 2006). Furthermore, the relative surface epithelial populations lining the nasal airways of rodents and humans differ considerably. Approximately 50% of the surface area of the nasal cavity in F344 rats is lined by olfactory epithelium (Gross et al. 1982), while only 3% of human nasal airways are dedicated to this sensory neuroepithelium (Sorokin 1988). Each of these factors ultimately changes the dose of inhaled toxicants delivered to susceptible sites between rodents and humans (Kimbell 2006). A non-human primate model species was selected because the structural and cellular aspects of the nasal airways of monkeys most closely represent those in humans (Yeh et al. 1997). Furthermore, infant rhesus monkeys exposed to ozone represent a more relevant model

of oxidant airway disease in children (Evans et al. 2003; Larson et al. 2004; Fanucchi et al. 2006).

Inhalation studies were designed to compare the epithelial responses to acute ozone exposure to the responses induced by episodic ozone exposure in the nasal airways of infant rhesus monkeys. Thirteen infant male rhesus monkeys were used for this study. Acute regimens consisted of 5 consecutive days of exposure (8h/day) to 0.5 ppm ozone (1 cycle, n=5). Episodic regimens consisted of 5 bi-weekly cycles of alternating filtered air (FA) and ozone exposure (9 consecutive days of 0 ppm [FA], followed by 5 consecutive days of 0.5 ppm ozone, 8h/day; 5 cycle; n=5). 5 cycle exposures were designed to mimic intermittent exposure to clean and polluted air, which likely mimics the nature of exposure experienced by people in high pollution regions (Sram et al. 1996). Control animals were exposed to FA (n=3). Exposures were scheduled so that each animal reached its target age (90 days of age) at the end of the exposure regimen. All exposures were performed at the California National Primate Research Center on the campus of the University of California at Davis.

Ozone exposures were conducted in 4.2 cubic meter (m^3) stainless steel and glass, whole-body inhalation chambers, similar to those previously described (Hinners et al. 1968). Ozone was produced from vaporized liquid, medical grade oxygen by electric discharge ozonizers (Model 03V1-0, Ozone Research Equipment Company, Akron, OH). Generated ozone was diluted with filtered air (24°C, 40-60% relative humidity), and injected into the inlet airflow of the exposure chamber. Filtered air was supplied to the chamber at a flow rate of 2.1m^3 per minute, providing 30 air exchanges per hour. Chamber ozone concentration was monitored throughout exposures with an ultraviolet

ozone analyzer (Model 1003-AH Dasibi Corporation, Glendale, CA). During exposures, a PC-based data acquisition and control system was used (Dell Computer Corporation, Round Rock, TX and GE Fanuc Automation North America, Inc., Charlottesville, VA). In addition to monitoring ozone concentration, this computer system also monitored chamber airflow, temperature, pressure, and humidity.

Necropsy and Tissue Preservation

At the end of exposure, monkeys were sedated using ketamine hydrochloride (10mg/kg IM), followed by induction of deep anesthesia using propofol (*Diprivan*, 0.1-0.2mg/kg/min IV). The trachea, sternum, and abdominal cavity were exposed by a midline incision. Animals were euthanized by exsanguination via the abdominal aorta.

Immediately after sacrifice, the head was removed from the carcass, and the lower jaw, skin, musculature, and brain were removed from the head. The nasal cavity was exposed by splitting the skull sagittally, 1-2mm to the right of midline. This sectioning provided a complete left nasal cavity, including an intact nasal septum, and a free right lateral wall, with the ethmoturbinate and maxilloturbinate attached (Figure 1). The left side of the nasal cavity, including the nasal septum, was flushed with a solution of 1% paraformaldehyde and 0.1% glutaraldehyde, and was then immersed in ~100 ml of the same solution for storage at 4°C until preparation for MR imaging.

The right side of the nasal cavity was used to sample nasal mucosal tissues for biochemical antioxidant analyses. These samples were harvested from three specific locations along the lateral wall of the right nasal cavity, corresponding to the sites examined by light microscopy in the left nasal cavity. Mucosal samples were dissected

from the anterior maxilloturbinate (MT), posterior MT, and anterior ethmoturbinate (ET) (Figure 3-1). The other part from each region was immediately placed into 300μl of 10% metaphosphoric acid containing 50μM desferroxamine, and snap-frozen in liquid nitrogen. Acidified, frozen nasal mucosal samples were later thawed, homogenized for 30 seconds using a Polytron homogenizer, re-frozen, and stored at –80°C until further processing for low molecular weight antioxidant analysis via high performance liquid chromatography (HPLC).

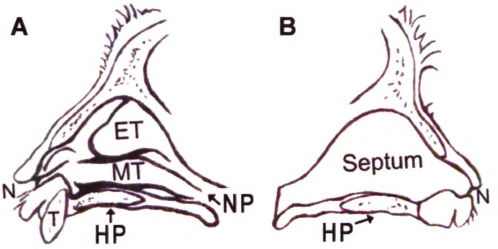

Figure 3-1. Diagram of the right lateral wall **(A)** and the left nasal cavity **(B)** of a 90-day-old Rhesus monkey following sagittal sectioning, showing the intranasal locations of the maxilloturbinate (MT), ethmoturbinate (ET), and the nasopharynx (NP). N = naris; T = 1st incisor tooth; HP = hard palate.

Magnetic Resonance Imaging of Nasal Airways

MR imaging of formalin-fixed nasal cavities has previously been exploited to facilitate geometric measurements of airway geometry in cynomologus monkeys (Harris et al. 2003). In the present study, a similar approach was employed to rapidly compile detailed three-dimensional descriptions of airway architecture post-mortem, but prior to nasal airway sectioning and processing for light microscopic examination.

In preparation for MR imaging, the left nasal cavities were first flushed with a fixative solution of 1% paraformaldehyde/0.1% glutaraldehyde containing the MR contrast agent Magnevist® (gadopentetate dimeglumine, Berlex Laboratories, Wayne, NJ), at a volume concentration of 1 part Magnevist® per 500 parts fixative. Each specimen was then placed in a small container (60ml volume, 42mm I.D., 59mm length), and immersed in the same fixative solution. The use of Magnevist® in the fixative solution ensured that acquired MR images had good signal-to-noise and high contrast between the nasal tissue and the nasal airspaces; thereby, facilitating confident segmentation of airway geometry. In preparation for imaging, each specimen was positioned in the specimen container with the rostral aspect of the nasal cavity facing the bottom of the container, and the plane of the palate parallel to the long axis of the container. The specimen was fixed into this position using soaked 2" x 2" gauze sponges packed around the caudal aspect as needed. Prior to sealing each bottle, the specimen was then degassed to eliminate any small air bubbles that might otherwise adversely affect MR image quality.

All MR imaging was performed at the Environmental Molecular Sciences Laboratory (Richland, WA). High-resolution, 3D MR images of fixed nasal tissue were

acquired at 2.0 Tesla using a Varian UnityPlus spectrometer (Palo Alto, CA) and an in-house fabricated radio frequency (Alderman-Grant) coil with an inner diameter of 5.5 cm. To visualize complex nasal passages raw image data was collected on a $256x128^2$ matrix using a T_2-weighted, 3D spin-echo sequence with a 100 msec echo-time, a 150 msec repetition time, and 4 averages. Each 3D data set therefore required ~2.7 hrs to collect, during which, sample temperature was maintained at ~4° C. After Fourier image reconstruction, all 3D data was stored as a series of 256 2D slices – each showing a squared 4.5 cm field-of-view. Planar resolution within each slice was 350 microns and each slice was 200 microns thick.

Image Analysis and Airway Segmentation

All airway segmentation and mesh generation was performed using methods similar to those already described by Minard *et al* (2006). Briefly, Digital Data Viewer (DDV; Computer Geometry Consulting, http://www.compgeomco.com) was used to identify and digitally segment the airway geometries from the 3D MR image data of each monkey nasal passage. Segmented airways were subsequently used for the development of geometry databases and 3D mesh reconstruction. To facilitate airway segmentation, each set of 256, 2D slices was first read into DDV. The set of images were then viewed in the x, y, and/or z directions, slice by slice. To digitally segment (extract) the nasal passageway, the area on each of the z-slices associated with the airway was highlighted. A separate file ("overlay") was then generated from this extracted data and it was used to create an isosurface rendering of the 3D segmentation (Figure 3-2). During airway segmentation, the x-, y-, and/or z-planes were viewed separately or in any combination

with the isosurface rendering (Figure 3-2) to facilitate comparisons between the segmented airways and the raw MR image data. The isosurface generated from the segmentation files of the MR images, along with the images themselves, could be rotated and viewed from any direction to ensure optimal segmentation. Once completed, this made them ideally suited to serve as guides for subsequent histopathologic and morphometric analyses of nasal passages.

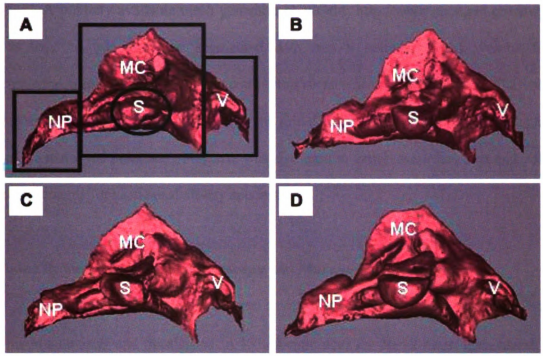

Figure 3-2. Computer assisted 3D isosurface renderings of the nasal passages from two FA-exposed (**A** and **B**) and two 1 cycle ozone-exposed (**C** and **D**) 180-day-old infant monkeys. The black lines in **(A)** delineate the regions of the nasal vestibule (V), the main chamber (MC), the maxillary sinus (S), and the nasopharyngeal meatus (NP).

A publicly available mesh generator (NWGrid; http://www.emsl.pnl.gov/nwgrid) was used to transform the segmented data into a boundary-fitted, volume-filling tetrahedral mesh that was used for computing surface areas and volumes. The volume meshes were designed to be suitable as the initial finite-element mesh for computational fluid dynamics simulations. NWGrid was also used to generate surface area and volume measurements for each nasal airway specimen.

Tissue Processing for Light Microscopy and Morphometric Analysis

After MR imaging, each left nasal cavity specimen was removed from the fixative with Magnevist® and decalcified in 13% formic acid for 10-12 days, then rinsed with distilled water for 2-4 hours. After decalcification, the nasal airways were transversely sectioned at ten or twelve (based on the size of the specimen) specific anatomical locations, using gross dental and palatine landmarks (Figure 3-3). This method produced nasal tissue blocks that had cross sectional profiles similar to those described by Kepler, *et al.* (1995), and has been used in prior studies to obtain accurate geometrical coordinates of nasal airways of non-human primates for computer dosimetry modeling and nasal airway lesion mapping (Kepler et al. 1998). These locations provided transverse sections through the preturbinate region, main nasal airway chamber, and nasopharyngeal region. Each tissue block was embedded in glycol methacrylate (GMA; Immuno-Bed, Polysciences, Inc., Warrington, PA) for airway epithelial mapping and histopathologic analysis.

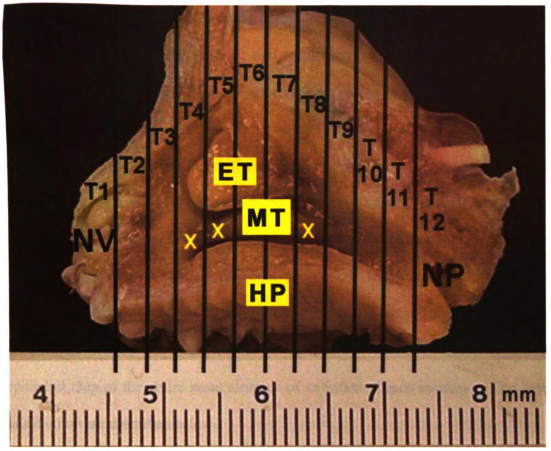

Figure 3-3. Photograph of the lateral wall of the nasal cavity of a 90-day-old Rhesus monkey. The location of the twelve transverse tissue blocks (T1-12) selected for light microscopic examination and morphometric analyses are indicated. NV = nasal vestibule; ET = ethmoturbinate; MT = maxilloturbinate; NP = nasopharynx. The yellow Xs identify the intranasal location of ozone-induced necrotizing rhinitis that is illustrated in Figure 3-8 below.

Three-Dimensional Digital Mapping of Epithelial Distribution

It has been reported that ciliated respiratory epithelium (RE) and non-ciliated transitional epithelium (NTE) in the anterior nasal airways are particularly sensitive to ozone toxicity in adult monkeys (Harkema et al. 1987b; Harkema et al. 1987c), while other epithelial types remain relatively unaffected. In order to accurately assess the morphologic response of the nasal mucosa in infant monkeys, we first had to define the type and extent of epithelial populations in the normal infant monkey. To determine the specific distribution of surface epithelial populations lining the nasal airways, and to provide boundary setting information for computer modeling and site-specific tissue dose predictions, we developed a method to generate a detailed, 3-dimensional digital epithelial map of the entire nasal airspace of an infant, rhesus monkey. The details of this method are described below.

Morphological identification of nasal epithelial types. There are five distinct epithelial populations in the nasal airways of adult macaque monkeys. These include the squamous epithelium (SE), ciliated respiratory epithelium (RE), non-ciliated transitional epithelium (NTE), olfactory epithelium (OE), and lymphoepithelium (LE). The morphological features used to identify each epithelial type for 3D mapping are described here. The reader is referred to a recent review article for a more thorough discussion of the structure and function of these epithelial types and their relevance to nasal toxicologic pathology (Harkema et al. 2006).

Squamous Epithelium

The nasal vestibule is lined with keratinized, stratified squamous epithelium. This nasal epithelial type is composed of basal cells lining the basal lamina, and several layers of squamous epithelial cells, which become progressively flatter toward the luminal surface of the epithelium. The epithelium of the vestibule is contiguous to the epidermis of the skin, and both serve to protect the underlying tissues from exposure to potentially harmful agents in ambient air. In adult monkeys, the squamous epithelium of the nasal vestibule forms an abrupt border with the transitional epithelium that lies immediately distal to it in the main chamber of the nasal airways (Harkema et al. 2006).

Transitional Epithelium

Adjacent to the stratified squamous epithelium of the nasal vestibule, and proximal to the ciliated respiratory epithelium within the main nasal chamber, is a narrow zone of non-ciliated transitional epithelium (NTE). In monkeys, this epithelium is stratified (4-5 cell layers thick), non-keratinized, and consists primarily of cuboidal and columnar epithelial cells with a paucity of mucous goblet cells. In adult monkeys, this epithelium is morphologically distinct from the keratinized squamous epithelium anterior to it, and the RE posterior to it.

Respiratory Epithelium

Most of the main nasal chamber in adult macaque monkeys is lined with ciliated respiratory epithelium. This pseudostratified to columnar epithelium is comprised primarily of ciliated cells, with lesser numbers of narrow non-ciliated (serous) cells, various numbers of mucous (goblet) cells, and basal cells.

Olfactory Epithelium

The olfactory epithelium covers a small region of the dorsal meatus and the dorsal half of the ethmoturbinate in monkeys. The three principal epithelial types that compose the olfactory epithelium are the olfactory sensory neurons, sustentacular cells, and basal cells. The supporting, sustentacular cells form a prominent apical row of nuclei. The olfactory sensory neurons are bipolar neuronal cells interposed between the sustentacular cells. The dendritic portions of these neurons extend above the epithelial surface and terminate into a bulbous olfactory knob, from which extend 10-15 immotile cilia per cell. Basal cells line the basal lamina.

Lymphoepithelium

Lymphoepithelium is a specialized epithelium, found primarily in the walls of the nasopharynx. This epithelium covers discrete, focal aggregates of nasal-associated lymphoid tissue (NALT) in the underlying lamina propria. The lymphoepithelium is composed of cuboidal ciliated cells, few mucous cells, and numerous nonciliated, cuboidal cells with luminal microvilli, called M-cells. These latter cells are similar in structure and function to the analogous immune surveillance cells found in gut- and bronchus-associated lymphoid tissues (GALT and BALT, respectively).

Translation of light microscopic data to 3D epithelial map. One nasal airway specimen from a filtered air-exposed monkey was selected for complete epithelial mapping. Initial slides were taken from the anterior face of each tissue block and stained

with hematoxylin and eosin (H&E) for routine histopathologic examination. Slides were also stained with AB/PAS for detection of acidic and neutral intraepithelial mucosubstances. Additional unstained slides were taken for use in future immunohistochemical analyses (the analyses of intraepithelial mucosubstances and immunohistochemistry are not presented in this report). The remainder of each tissue block was completely sectioned at 50-μm increments, and slides were stained with H&E for routine histopathologic analysis.

Each z-slice of the MR image file was 200μm thick. Sectioning the block at 50μm increments resulted in 4 H&E slides for each image. The H&E slide that best corresponded to the shape of the nasal airspace for each image was selected and examined by light microscopy. Each epithelial type was coded to a color in DDV. The location of nasal epithelial types (squamous epithelium, non-ciliated transitional epithelium, respiratory epithelium, olfactory epithelium, lymphoepithelium) in each section was recorded on the corresponding transverse MR image by drawing a color-coded line along the air-tissue interface at the corresponding site (Figure 3-4). This process was repeated in all transverse images. These data were saved as a DDV overlay file, and were used for generation of a 3-dimensional nasal epithelial map as explained below.

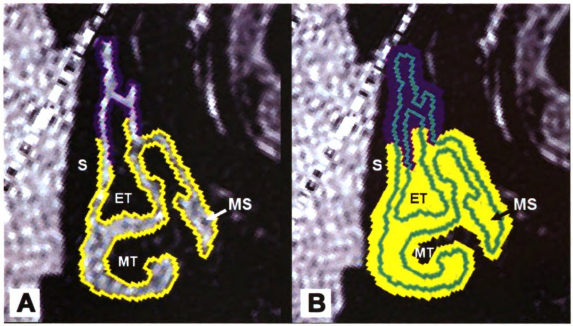

Figure 3-4. Three-dimensional mapping of nasal epithelium. **(A)** Z-plane image of the nasal cavity of a 180-day-old rhesus monkey. Each MR image was visually matched to an H&E slide for epithelial mapping. A color-coded line was drawn for each epithelial type along the air-tissue interface. This process was repeated for each image in the MR file. **(B)** The epithelial tracings were converted to 2D epithelial blobs that extended across the air-tissue interface in each image. The intersection of each epithelial blob with the original nasal airway segmentation (represented by the green line) was used to generate the surface map for each epithelial type. Purple = olfactory epithelium; yellow = respiratory epithelium; MT = maxilloturbinate; ET = ethmoturbinate; MS = maxillary sinus; S = nasal septum.

In computational fluid dynamics (CFD) models, different epithelium-specific gas uptake properties may be accounted for by setting different boundary conditions for gas uptake at epithelium-specific locations on the nasal surface. This requires a seamless, single surface where different epithelial types are defined as regions of the surface. Our approach for producing this surface was to construct separate 3D reconstructions of each epithelial type as well as the entire nasal surface in DDV and import these reconstructions as stereolithography (STL) files into ICEM-CFD (Ansys, Inc., Canonsburg, PA), which is a computer-aided design (CAD) software used for meshing. An STL file defines a surface enclosing a given volume. Therefore, when exporting the epithelial reconstructions created in DDV, we actually exported a volumetric blob that corresponds to the volume defined by the voxels (3D pixels) drawn in DDV while delimiting each epithelial surface (Figure 3-4). The surfaces confining each of these volumetric blobs were intersected with the whole-nose surface in ICEM-CFD to determine the 3-dimensional curves separating the different epithelia. These curves were then used to divide the surface of the model into epithelial regions. The final result was a smooth, seamless, single surface of the nasal airway composed of different parts, each representing a particular epithelial type (e.g. squamous, respiratory) (Figure 3-5). This 3D reconstruction was used to visualize the locations of the major epithelial types, to estimate epithelium-specific surface areas, and as the initial finite element mesh for CFD simulations.

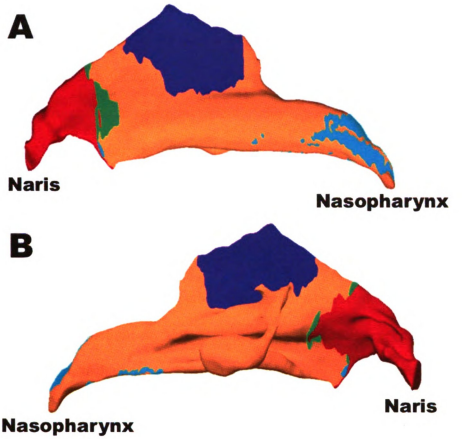

Figure 3-5. Three-dimensional nasal epithelial map. Medial **(A)** and lateral **(B)** views of a three-dimensional reconstruction of the right nasal passage of a 180-day-old rhesus monkey. The locations of the five different epithelial types comprising the nasal airways are indicated by color. Red = squamous epithelium; green = non-ciliated transitional epithelium; orange = respiratory epithelium; purple = olfactory epithelium; light blue = lymphoepithelium.

Morphometric Quantitation of Ozone-Induced Nasal Lesions

Light Microscopic Morphometric Analysis. Nasal airway tissues were processed, decalcified, and embedded as described above. Slides were prepared from the anterior face of each of the 10-12 tissue blocks at a 1-2 μm thickness. Slides were stained with H&E for routine histopathologic examination and morphometric evaluation. Slides from each section were also taken for AB/PAS staining and immunohistochemistry as described above.

The location, nature, and extent of the specific mucosal lesions in each transverse microscopic section were characterized for each animal. The nasal epithelial lesions identified in the current study were confined to the anterior nasal cavity, and were primarily associated with the ciliated respiratory epithelium. To quantitate the loss of respiratory epithelium in this region following ozone exposure, we used standard morphometric techniques to measure the thickness of the respiratory epithelium lining the dorsal surface of the anterior maxilloturbinate (Figure 3-6).

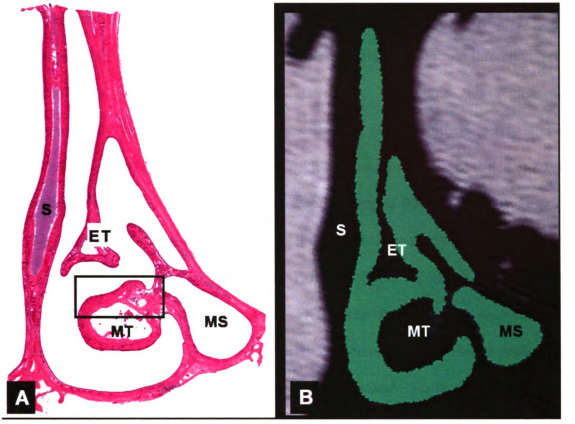

Figure 3-6. **(A)** Photomicrograph of an H&E-stained transverse section (T5) through the left nasal airway of a 90-day-old infant monkey. The region contained within the black box represents the dorsal maxilloturbinate. The epithelium lining this region was selected for morphometric analysis. **(B)** Z-plane MR image of the nasal cavity of the same monkey, obtained at the level corresponding to the transverse section in (A). The overlay of the nasal airspace is highlighted in green. MT = maxilloturbinate; ET = ethmoturbinate; MS = maxillary sinus; S = nasal septum.

Severity of respiratory epithelial cell loss was quantified by measuring the average height of the epithelium overlying the dorsal surface of the first three transverse sections of the maxilloturbinate. Thickness of the RE within this region was morphometrically evaluated as previously described for airway epithelium (Hyde et al. 1990; Hyde et al. 1991; Plopper et al. 1994). All measurements were obtained at a final magnification of 1,710x using a light microscope (Olympus BX40; Olympus America, Inc., Melville, NY) coupled to a 3.3-megapixel digital color camera (Q-Color 3 Camera; Quantitative Imaging Corporation, Burnaby, British Columbia, Canada), and a personal computer (Dimension 8200; Dell, Austin TX). The morphometric analyses were performed using a 135-point cycloid grid overlay with an automated software package for counting points and intercepts within the grid (Stereology Toolbox; Morphometrix, Davis, CA) (Hyde et al. 1990; Hyde et al. 1991). The percent volume density (the proportion of the total epithelial volume), V_v, of cytoplasm, nuclei, and intraepithelial mucosubstances, was determined by point counting and calculated using the following formula:

$$V_v = P_p = P_n/P_t \,, \qquad [1]$$

where P_p is the point fraction of P_n, the number of test points hitting the structure of interest (e.g. cytoplasm), divided by P_t, the total number of points hitting the reference space (i.e. respiratory epithelium). The volume of each epithelial component of interest

per unit of basal lamina length (S_v) was determined by point- (epithelial component) and intercept- (basal lamina) counting and was calculated using the following formula:

$$S_v = 2\, I_O L_\gamma\,, \qquad [2]$$

where I_O is the number of cycloid intercepts with the object (epithelial basal lamina), and L_γ is the length of the test line in the reference volume (epithelium within the test grid). To determine the thickness of the RE, a volume per unit area of basal lamina (cubic micrometers per square micrometer) was calculated using the following formula for arithmetic mean thickness (τ):

$$\tau = V_V / S_v\,. \qquad [3]$$

Statistical Analyses. Statistical analyses for all morphometric parameters were performed using one-way analysis of variance (ANOVA). Pairwise comparisons were selected *a priori,* and were performed using Student-Newman-Keuls multiple comparisons test ($p \leq 0.05$). Statistical outliers were detected using Grubb's test ($p \leq 0.05$).

Three-Dimensional Digital Mapping of Ozone-Induced Nasal Injury

We used a combination of standard histopathologic methods, MR imaging, and computer-assisted, 3D airway modeling to generate subject-specific, 3D maps of ozone-induced nasal lesions. Using DDV, the frontal profile of each transverse section was

visually matched to its corresponding z-plane slice (2D image) in the MRI segmentation (Figure 3-6). The locations of ozone-induced lesions identified on the nasal tissue sections were recorded on the corresponding sites on the z-plane MR images by highlighting the tissue-airspace interface at that site (Figure 3-7). The entire z-plane slice, including the highlighted lesion site, was subsequently superimposed over the isosurface rendering of the entire nasal airspace to provide 3-dimensional lesion localization for that specimen (Figure 3-7). Using the slice plane clip sliders in DDV, the specific Cartesian (x-, y-, and z-plane) coordinates for epithelial lesions can be recorded. These coordinates can be read into NWGrid and translated into the corresponding sites on the surface of the computational volume mesh for that animal. The individual cell faces of the volume mesh corresponding to the site of injury can be digitally highlighted using the General Mesh Viewer (GMV, Los Alamos National Laboratory, http://www-xdiv.lanl.gov/XCM/gmv/GMVHome.html) (Figure 3-7).

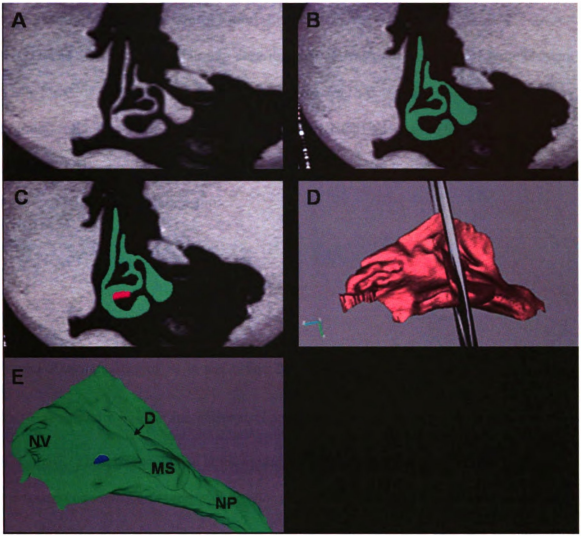

Figure 3-7. Three-dimensional mapping of ozone-induced nasal lesions. **(A)** Z-plane (transverse) MR image of the nasal cavity of a 90-day-old Rhesus monkey. The fixative within the nasal airspace and surrounding the specimen contains Magnevist® MR contrast agent to provide high contrast between nasal tissue and airspaces. **(B)** Using DDV, the geometry of the nasal airspace is selected and highlighted (green) in each z-plane image. **(C)** The locations of specific ozone-induced mucosal lesions are identified on each transverse nasal tissue section, and the region of each lesion is recorded on the tissue-airspace interface of the corresponding z-plane image. In this section, a lesion along the dorsal maxilloturbinate is highlighted. **(D)** The entire z-plane slice can be superimposed over the isosurface rendering for that specimen to provide 3D localization of each lesion. **(E)** The 3D coordinates generated in DDV can be translated into grid coordinates using NWGrid, and mapped on the corresponding site along the surface of the computational volume mesh using GMV, for use in CFD simulations. The area highlighted in blue represents the focal area of injury along the dorsal maxilloturbinate identified in **(C)**. NV = nasal vestibule; MS = maxillary sinus; D = duct to the maxillary sinus; NP = nasopharyngeal meatus.

Computational Fluid Dynamics Simulations

The 3D nasal epithelial map described above was used as an initial finite element mesh for CFD simulations. Airflow simulations were performed for resting breathing (minute volume = 1.0 L/min) using a commercial CFD package (Fidap®, Fluent Inc., Lebanon, NH). For the initial simulation, ozone uptake by the epithelium was assumed to obey the following relationship:

$$Flux_{ozone} = kc_{ozone} \qquad [4],$$

where $\boldsymbol{Flux_{ozone}}$ (kg/m^2·s) is the ozone flux from air into tissue, $\boldsymbol{k}$ is a rate constant (0.023m/s), and $\boldsymbol{c_{ozone}}$ is the ambient concentration of ozone at the air-tissue interface (0.5 ppm). Thus, ozone uptake at the epithelial surface was assumed to be proportional to the ozone concentration at the wall (Taylor et al. 2007), and uniform throughout the nasal airspace. Previous reports suggest that squamous epithelium is resistant to uptake of inhaled reactive gases, including formaldehyde and ozone (Kimbell 1997). To determine the potential influence of the distribution of squamous epithelium on overall ozone uptake in the nasal airways, a second simulation was performed with the same assumptions; however flux over the area of the mesh representing the squamous epithelium was set equal to 0.

Determination of Intracellular Antioxidant Concentrations in Nasal Mucosa

Nasal tissue homogenates were thawed and centrifuged at 12,500 x g for 4 hours. Protein pellets were resuspended in 500µl of PBS, neutralized with 25µl 1N NaOH, and sonicated for 1 hour at 37°C. The protein content of resuspended pellets was measured using the Pierce BCA Protein Assay (Pierce Biotechnology, Rockford, IL). Supernatants were diluted three-fold in 10% meta-phosphoric acid, and filtered through a 0.22µm syringe filter. Triplicate samples of each supernatant were fractioned on a Shimadzu LC-10A*i* HPLC (Shimadzu Scientific Instruments, Columbia, MD), using a Phenomenex Luna C18(2) 250mm x 4.6mm, 5µM reversed phase column, preceded by a Phenomenex ODS 4mm x 3mm guard column (Phenomenex, Torrance, CA). The mobile phase consisted of an isocratic mixture of 50mM phosphate buffer, pH 3.1, containing 50µM octanesulfonic acid and methanol (95:5). Samples were fractioned at a mobile phase flow rate of 1.0ml/min. Reduced glutathione (GSH), oxidized glutathione (disulfide, GSSG), ascorbate (AH_2), and uric acid (UA) were simultaneously detected with an 8-channel ESA CoulArray Model 5600A electrochemical detector (ESA, Chelmsford, MA). GSH, GSSG, AH_2, and UA values were normalized to protein content of centrifuge pellets.

RESULTS

Nasal cavity surface area and volume calculations. Calculations of total surface areas and volumes of the left nasal passages of two FA-exposed and two 1 cycle ozone-exposed 180-day-old rhesus monkeys are presented in Table 3-1. It should be noted here that the calculations of surface area and volume, as well as the data used in epithelial mapping, include the nasal vestibule, starting at the first enclosed nasal transverse

section, and the nasopharyngeal meatus, caudally to the point at which the left and right sides join to form the nasopharynx. The volume and area measurements presented here also include the maxillary sinus. The data presented here show that there was consistency in the nasal surface areas and volume measurements among the age-matched infant monkeys. There was no significant effect of ozone exposure on the nasal surface area and volume measurements obtained in these monkeys. This finding of consistency in nasal size in infant monkeys is in contrast to the significant inter-individual variability in results reported previously for adult monkeys (Schreider 1986; Gross et al. 1987; Kepler 1995).

Monkey (exposure)	Weight (kg)	Volume (cm^3)	Surface Area (cm^2)
A (filtered air)	1.30	0.53	10.3
B (filtered air)	1.50	0.64	13.9
C (1 cycle ozone)	1.55	0.59	13.4
D (1 cycle ozone)	1.32	0.62	13.7

Table 3-1. Calculated total surface areas and volumes of the nasal passages from the four 180-day-old monkeys pictured in Figure 3-2.

Region	Epithelial Surface Area (cm^2)	Percent of Total Surface Area (%)
Squamous	1.81	14.9
Transitional	0.17	1.4
Respiratory	7.92	65.1
Olfactory	1.93	15.9
Lymphoepithelium	0.33	2.7
Total	12.16	100

Table 3-2. Estimated epithelial surface areas for one side of a 180-day-old rhesus monkey.

Digital epithelial mapping and surface area calculations. Complete epithelial mapping of one half of the nasal cavity was performed in one 180-day-old, filtered-air exposed rhesus monkey. Estimated surface areas of the five major epithelial types are presented in Table 3-2. The majority of the nasal airspace in this monkey (65.1%) was lined with ciliated respiratory epithelium, including the ventral half of the main nasal chamber, most of the nasopharyngeal meatus, and the entirety of the maxillary sinus, including the duct. Our results indicated that approximately 16% of the nasal cavity surface area in this infant rhesus monkey was lined by olfactory epithelium. This is consistent with an earlier report estimating that ~14% of the adult rhesus monkey nasal cavity is lined with olfactory epithelium (Gross et al. 1987). We found that the NTE in this infant monkey was confined to a narrow band in the preturbinate region, between the squamous epithelium of the nasal vestibule and the respiratory epithelium of the main nasal chamber. This localization, as well as the finding that NTE comprised approximately 1.4% of the total nasal epithelial surface area in this monkey, is also similar to results obtained from adult rhesus monkeys (Gross et al. 1987). The lymphoepithelium was primarily localized over two discrete aggregations of NALT located in the septal aspect of the nasopharynx. A small island of LE was also found in the ventral aspect of the preturbinate region.

Ozone-induced nasal epithelial injury and morphometry. All monkeys exposed to 1 cycle ozone had a moderate to marked necrotizing rhinitis that was restricted principally to the nasal mucosa lining the middle meatus in the main nasal chamber. There were focal regions of epithelial exfoliation, and these lesions were locally

extensive in the respiratory epithelium lining the dorsal surface of the anterior maxilloturbinate. There was an anterior to posterior decrease in the severity of these intranasal ozone-induced lesions. In 90-day-old monkeys exposed to 1 cycle ozone, the most severely affected areas of the nasal mucosa had near full-thickness necrosis and exfoliation of the surface epithelium with numerous neutrophils, and lesser numbers of eosinophils, infiltrating the subepithelial lamina propria and the remaining surface epithelium (Figure 3-8). Ninety-day-old monkeys that were exposed to 5 cycles of ozone also had ozone-induced rhinitis and epithelial necrosis in relatively the same intranasal locations as the ozone-induced lesions in the 1 cycle ozone-exposed animals.

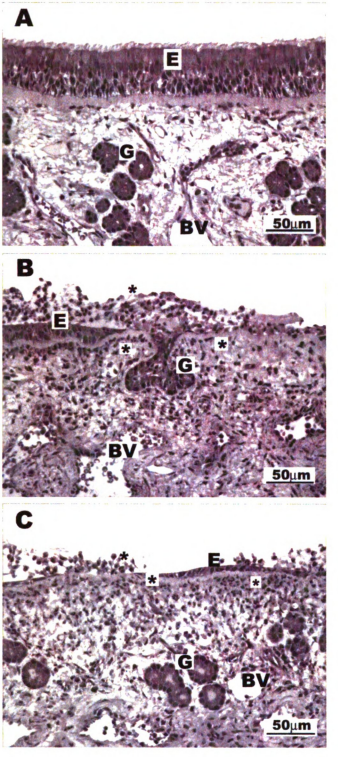

Figure 3-8. Light photomicrographs of the nasal mucosa lining the dorsal surface of the anterior aspect of the maxilloturbinate of 90-day-old monkeys exposed to 0 ppm ozone (filtered air; **A**), 1 cycle ozone (**B**), or 5 cycle ozone (**C**). No microscopic lesions are present in **(A)**. Marked epithelial necrosis and full thickness necrosis of the surface epithelium (E) along with marked neutrophilic inflammation (*) is present throughout the nasal mucosa, including the surface epithelium and underlying lamina propria containing blood vessels (BV) and glands (G).

Morphometric analyses of these ozone-induced nasal lesions indicated that 90-day-old monkeys that were exposed to 1 cycle ozone (0.5 ppm; 8h/day for 5 days) had a 65% reduction (compared to filtered air controls) in the mean thickness of the nasal epithelium lining the dorsal surface of the anterior maxilloturbinate due to toxicant-induced necrosis and exfoliation of this targeted site of nasal airway epithelium. Furthermore, this ozone-induced atrophy of the nasal epithelium resulted in an 88%, 64%, and 59% loss of the volume densities of airway cilia, epithelial cytoplasm, and epithelial nuclei, respectively. Interestingly, the character, severity, and distribution of the ozone-induced nasal epithelial lesions in 5 cycle O_3 exposed monkeys were similar to those in the 1 cycle ozone-exposed infant monkeys of similar age. The loss of mean airway epithelial thickness in monkeys exposed to 5 cycle ozone was only slightly less than in infant monkeys that were exposed to 1 cycle ozone (Figure 3-9).

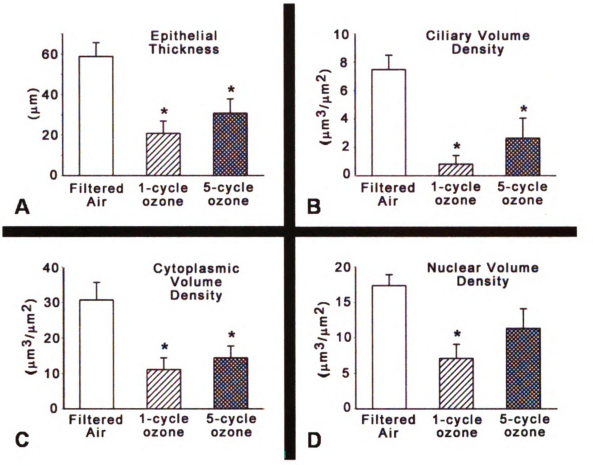

Figure 3-9. Morphometry of ozone-induced nasal epithelial lesions in 90-day-old rhesus monkeys. 1 cycle and 5 cycle ozone-induced epithelial necrosis resulted in attenuation of epithelial thickness **(A)**, and reductions in the volume densities of epithelial cilia **(B)**, epithelial cytoplasm **(C)**, and epithelial nuclei **(D)**.

Computational Fluid Dynamics Simulations. CFD simulations and predictions of ozone uptake in the nasal airspace model are depicted in Figure 10. At an ambient concentration of 0.5 ppm, regions of high ozone uptake are predicted along the ventral aspect of the preturbinate region, and along the septal and lateral walls of the middle and ventral meatus in the region of the anterior maxilloturbinate. A focal region of high ozone uptake (hotspot) is predicted at the dorsal aspect of the anterior maxilloturbinate, at the site of the ozone-induced mucosal injury described earlier. In addition, hotspots are also predicted in regions of the olfactory epithelium, where no ozone-induced injury is observed.

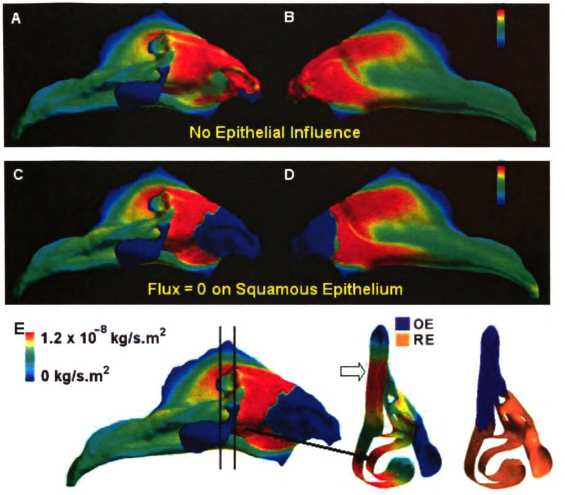

Figure 3-10. Computational fluid dynamics simulations of airflow and ozone uptake in the nasal airways. Lateral **(A)** and septal **(B)** views of CFD predictions of ozone uptake in the model assuming uniform uptake throughout the nasal airways. Lateral **(C)** and septal **(D)** views of CFD predictions of ozone uptake in the model assuming no uptake by the squamous epithelium. **(E)** Transverse section through 3D model at the location of the anterior maxilloturbinate. High uptake (red) is predicted in the respiratory epithelium (RE) at the dorsal aspect of the anterior maxilloturbinate where lesions were observed in inhalation experiments (black arrow). Hotspots are also predicted on the olfactory epithelium (OE), where no lesions were found (white block arrow).

Intracellular concentrations of low molecular weight nasal antioxidants. The intracellular antioxidant measurements in the nasal mucosa are summarized in Figure 3-11. There were no significant differences across the three regions (anterior MT, posterior MT, anterior ET) in the baseline antioxidant concentrations of GSH, GSSG, AH_2, or UA in FA-exposed animals. In animals exposed to 1 cycle or 5 cycle ozone, there was a decrease in GSH, GSSH, AH_2, and UA concentrations in all three nasal regions, compared to FA exposed animals. There was a statistically significant decrease in AH_2 concentrations in the posterior MT following both 1 cycle (63% decrease) and 5 cycle (55% decrease) exposure. There was also a statistically significant decrease in GSSG concentrations in the posterior MT (65% decrease and 82% decrease) and in the anterior ET (85% decrease with both treatments) following 1 cycle and 5 cycle ozone exposure, respectively.

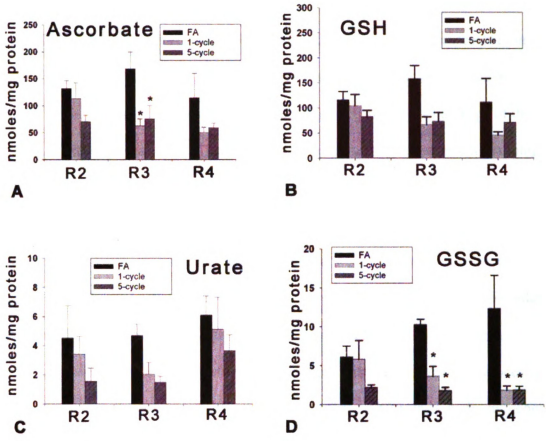

Figure 3-11. Antioxidant concentrations in the nasal mucosa of infant monkeys exposed to 1 cycle ozone and 5 cycle ozone. 1 cycle and 5 cycle ozone exposure resulted in depletion of AH_2 **(A)**, GSH **(B)**, UA **(C)**, and GSSG **(D)**, in mucosal sections from the anterior MT (**R2**), the posterior MT (**R3**), and the anterior ET (**R4**).

DISCUSSION

This is the first report to describe in detail the 3-dimensional representation of the normal epithelial distribution in the nasal airways of an infant, non-human primate model. This technique was designed to develop age-specific epithelial maps of the nasal airways in experimental animal models for use in toxicant-induced lesion mapping and CFD simulations of site-specific tissue dosimetry. Our results in this infant monkey, when compared to a previous report in adults, suggest that the relative amounts of the five epithelial types in the nasal airways of monkeys remained consistent between infancy and adulthood (Gross et al. 1987). However, because there is considerable change in the size and shape of the head of the rhesus monkey from the neonatal to the adult stage, we estimated that there would be significant age-related differences in the location of susceptible epithelial cell populations. These differences in airway geometry and epithelial lining may both contribute to differences in the responses to oxidant pollutant exposure by altering the dose delivered to susceptible epithelial types. This technique allowed for the determination of the specific distribution of susceptible epithelial populations (i.e. RE, NTE), and ultimately, will serve to reduce uncertainty in CFD dosimetry modeling and extrapolation of data from experimental animal models to humans (Kimbell 2006).

It is also crucial to understand the distribution of the normal epithelial populations in infant monkeys in order to be able to adequately distinguish age-related epithelial differences from epithelial alterations induced by toxicant exposure. For example, both squamous metaplasia and respiratory metaplasia of the olfactory epithelium have been reported as adaptive sequelae to toxicant exposure (Harkema et al. 2006). Prior

knowledge of the normal distribution of these epithelial types in the infant nasal airways is needed to make this distinction. A clear limitation to the data reported here is that this map represents the nasal airway from a single, FA-exposed, infant rhesus monkey. In future studies, we plan to complete additional epithelial maps for 90- and 180-day-old FA-exposed animals.

The utility of three-dimensional imaging techniques in laboratory animals for toxicant-induced lesion screening and dosimetry modeling has been previously reviewed (Menache et al. 1997; Wiethoff et al. 2001; Reed et al. 2003). These approaches used semi-quantitative or subjective assessments of airway lesions applied to models of the nasal airspaces of rodents. The use of morphometric techniques for the quantification of respiratory structures has also been the subject of a recent review (Fanucchi et al. 2006). We report the first use of MR imaging, computational biological methods, and standard morphometric techniques to provide a quantitative and site-specific assessment of the nasal responses to inhaled respiratory toxicants in a non-human primate model. The methods described in the current report demonstrate the use of stereologic methods to estimate volume density (*Vs*) of the airway epithelium as a quantitative assessment of the epithelial response to ozone exposure in the nasal airways of infant monkeys. In addition to the *Vs* methods described here for measurement of airway epithelium, other morphometric assessments of the epithelium could be combined with 3D mapping to provide additional information about the response to toxicant challenge. Morphometric techniques may be used to measure the numeric cell density of specific epithelial cells per length of basal lamina (i.e. volume of cells per unit area of basal lamina, $\mu m^3/\mu m^2$) as an assessment of hyperplastic or metaplastic responses. These methods may also be

combined with immunohistochemistry to quantitate other responses, including inflammation (e.g. # of neutrophils per mm basal lamina) and cell proliferation data (e.g. proliferating cell nuclear antigen, PCNA). By providing additional depth to the characterization of the tissue response to toxicant exposure, the measurement of these types of responses is crucial to the establishment of exposure-dose-response relationships in the nasal airways of infant monkeys. Morphometric *quantitation* of these epithelial responses, combined with site-specific 3D mapping, provides objective comparisons of the responses of monkeys to other species, facilitates comparisons to other toxicants, and provides an important basis for extrapolation of experimental data to human risk assessment.

3D mapping of toxicant-induced nasal airway lesions is unique in that the pathology from each individual animal can be applied directly to a three-dimensional model of its own nasal airways for use in CFD simulations. The nasal airway surface area and volume measurements presented in this study, when compared to a previous characterization in adult monkeys (Gross et al. 1987) demonstrated that significant post-natal growth occurs in the nasal airways of monkeys from infancy to adulthood (Table 3-1). This suggests that the nasal deposition patterns of inhaled toxicants would exhibit age-dependent variation, potentially resulting in exposure of different epithelial types to peak doses of toxicant. By providing estimates of toxicant dose relative to airway geometry, CFD simulations provide an effective way to explain the contribution of airway geometry to site-specificity. However, the effectiveness of CFD simulations is limited by the accuracy of the initial model geometry. The three-dimensional models

generated from the MR image segmentations provide a logical framework not only for localizing the airway injury and for correlating injury to susceptible epithelial types, but also to serve as the basis for the initial finite-element meshes to be used for CFD simulations. The Cartesian coordinate system relationships used to record the specific locations of the epithelial lesions in DDV are maintained in the finite element meshes used for predictive dosimetry modeling. This allows for greater accuracy in the correlations between experimentally induced and predicted airway injury, and also allows for more specific testing of hypotheses about transport mechanisms and subsequent extrapolation of animal data to humans. CFD airflow and site-specific tissue dosimetry simulations using tissue dosimetry simulations using this model are in progress.

The nasal injury in the 90-day-old infant monkeys was particularly severe in the ciliated respiratory epithelium along the dorsal surface of the maxilloturbinate. This is consistent with the report that adult monkeys acutely exposed to ozone (0.3 ppm, 8h/day for 6 days) also experienced necrosis and exfoliation of ciliated cells in the anterior nasal cavity (Harkema et al. 1987c). Despite differences in the ozone concentration and duration of exposure, our results indicate that the character and location of the ozone-induced nasal lesions in the 1 cycle ozone-exposed 90-day-old monkeys reported here are similar to those previously reported for adult monkeys acutely exposed to ozone. However, while the character and location of toxicant-induced injury can be compared with previously described methods, the imaging and 3D modeling techniques described in the current study also allow for the assessment of the extent of airway lesions. In future studies, we will section the complete nasal airways of ozone-exposed monkeys, in

a manner similar to the sectioning described above for epithelial mapping. This will allow for the calculation of surface areas for ozone-induced lesions, and facilitate direct comparisons across age groups and ozone doses.

It is possible that the age-related changes in the surface epithelial cell populations alter the susceptibility of the nasal epithelium to ozone toxicity. Another possibility is that age-related differences in airway geometry alter the local delivery of ozone to susceptible epithelial populations within the nasal cavity. Results from our initial simulations in infant monkey models predict that the highest ozone flux occurs in the anterior nasal cavity, in the regions lined by NTE and ciliated RE, and that the presence of squamous epithelium at the naris and nasal vestibule may increase the overall dose of ozone reaching the susceptible epithelial populations (NTE and ciliated RE). These initial simulations are limited, however, for several reasons. First, these simulations assume that the ozone flux is uniform throughout the regions of the nasal cavity lined with mucus. The mucus layer is a dynamic part of the nasal airways, and is locally regulated by many factors. These include the presence or absence of motile cilia, local density of the intraepithelial mucosubstances, and the presence and type of submucosal mucus glands (e.g. Bowman's glands underlying olfactory epithelium versus submucosal mucus glands in respiratory epithelial mucosa). Second, these simulations were performed with an estimate of resting breathing at a constant flow rate. In the living system, airway flow is initiated by the generation of a pressure difference between the intrapulmonary airways and ambient air. This results in a variable flow rate throughout the respiratory cycle. These are both factors that will require consideration for future

CFD simulations in order to increase the accuracy of the predictions. Providing more detailed information to this process will provide valuable information on the relative importance of airway geometry and tissue morphology, as they relate to the location and extent of ozone-induced nasal airway injury in infant monkeys, and ultimately, in children.

We report here that the loss of mean airway epithelial thickness and the volume densities of airway cilia, epithelial cytoplasm, and epithelial nuclei, were not significantly different between infant monkeys receiving 1 cycle or 5 cycle ozone exposures (Figure 9). Neither group of ozone-exposed infant monkeys exhibited mucous cell metaplasia or epithelial hyperplasia in the region of airway injury. We have previously reported that adult monkeys exposed daily (6 or 90 days) to high ambient concentrations (0.3 ppm) of ozone undergo epithelial hyperplasia and mucous cell metaplasia (MCM) in the nasal epithelium. Furthermore, this epithelial remodeling was associated with attenuation of the epithelial necrosis and inflammation in response to subsequent acute ozone exposure. These ozone-induced epithelial adaptations in adult monkeys may render the epithelium less susceptible to tissue injury in response to subsequent ozone challenge (Harkema et al. 1987b; Harkema et al. 1987c). It is important to note, however, that the long-term exposure regimens used in adult monkey studies involved chronic (90 days), daily exposures, while the infant monkeys presented in this report were exposed subchronically (70 days) and episodically. Nevertheless, these findings suggest that infant monkeys acutely or episodically exposed to ozone do not undergo nasal airway epithelial remodeling or adaptation. This also suggests the disturbing possibility that infants may

develop a persistent necrotizing rhinitis following episodic exposures without any protective molecular adaptation or morphologic remodeling of the surface epithelium that would make the nasal airways less susceptible to ozone toxicity. Further studies are needed to determine the responses to longer courses of episodic exposure (Chapter 4), and to investigate the potential long-term consequences of ozone-induced nasal airway injury in childhood.

In addition to anatomic and histologic factors, age-related biochemical changes may also contribute to differential susceptibility to ozone toxicity. Antioxidants in the surface lining fluid and epithelium are considered to provide the first line of defense against inhaled oxidant challenge (Housley et al. 1995; Mudway and Kelly 1998). Nasal antioxidants may play a role in the morphologic responses to ozone exposure. Antioxidant upregulation may contribute to the development of tolerance to oxidant pollutant challenge (Frank et al. 1978; West et al. 2000; Kirschvink et al. 2002). Antioxidant upregulation may play a role in the regulation of oxidant-mediant cell proliferation (Shaw and Chou 1986; Luppi et al. 2005). Ozone exposure also causes site-specific injury in the pulmonary airways of monkeys, which correlates with sites of ozone-induced GSH depletion (Plopper et al. 1998). In several *in vitro* models, the presence of antioxidants in the surface lining fluid serves to augment oxidant pollutant-induced cell membrane damage (Velsor and Postlethwait 1997; Ballinger et al. 2005). We found that all antioxidants measured in the nasal mucosa were depleted at the site of injury (anterior MT) following 1 cycle and 5 cycle ozone exposure. This exposure-related antioxidant depletion may, in part, explain the lack of epithelial remodeling

following 1 cycle and 5 cycle exposure, and may also be related to the persistent susceptibility to ozone-induced injury following cyclic ozone exposure. However, it is important to note that a similar pattern of antioxidant depletion was also observed in the two nasal regions in which no exposure-related injury was observed. This suggests that while age-related differences in the regulation of airway antioxidants may contribute to heterogeneity in the responses of immature models to ozone exposure, other factors are also likely involved. These may include age-related differences in the regulation of inflammation, mucus synthesis and secretion, and mechanisms of epithelial repair.

By splitting the nasal cavity and preserving the right side of the airway for biochemical and molecular analyses, we attained the ability to directly correlate site-specific airway injury and repair with site-specific indicators of tissue susceptibility to ozone toxicity on an individual animal basis. Furthermore, this dissection technique allows for the direct comparison of susceptible and resistant epithelial cell populations within the same animal (e.g. RE vs. OE). The use of morphometry permits correlation of quantified structural features with physiological and biochemical data (Tyler et al. 1985). Using the 3-dimensional mapping technique, this information can be applied to predictive dosimetry models, increasing the specificity of the results obtained from CFD simulations. Employing this technique, however, assumes that the toxicant-induced nasal injury is bilateral and symmetrical, and that it is not significantly influenced by the nasal cycle, the physiologic alternating of airflow from one nasal passage to the other due to periodic cycling of mucosal congestion and decongestion (Flanagan and Eccles 1997).

SUMMARY

Acute and chronic ozone exposures have been shown to cause epithelial hyperplasia in the anterior nasal airways of adult monkeys. In the present study, we have shown that acute and episodic (5 cycle) ozone exposure regimens cause epithelial necrosis, exfoliation, and atrophy in the anterior nasal airways of infant monkeys, with no morphologic evidence of epithelial hyperplasia. The magnitude and spatial distribution of nasal airway injury induced by 1 cycle and 5 cycle exposures were similar. These ozone-induced epithelial alterations were associated with site-matched consumption of GSH and AH_2 in the nasal mucosa. Although these results do not establish a causal relationship between nasal antioxidants and epithelial remodeling, they support the possibility that ozone-induced epithelial hyperplasia and adaptation are dependent upon the regulation of intracellular antioxidants and redox balance. Additional mechanistic studies are needed to further investigate the mechanisms underlying ozone-induced cell proliferation, and the possible role of antioxidants in this process.

The site-specificity of ozone-induced nasal injury necessitates that histopathologic assessment be applied with the same site-specificity. By using the stereologic methods described here, we obtain reliable measurements of the airway epithelium, its individual components, and the components of the underlying basal lamina and lamina propria. These measurements provide a quantifiable assessment of the epithelium and its response to inhaled pollutants. The use of an infant rhesus monkey, while providing data from nasal airways that are grossly and microscopically similar to the nasal airways of children, also presents ethical challenges requiring efficient, robust, and pragmatic experimental design and methods. Combining morphometric techniques with 3D

mapping provides the advantage of applying information about the nature, distribution, and magnitude of nasal airway injury into a single model (Figure 12). Quantitation of these epithelial responses facilitates the comparisons of susceptible and resistant epithelial populations within the same animal. More importantly, this also provides an important method of providing comparisons between experimental animals, and facilitates extrapolations between species with different airway geometries.

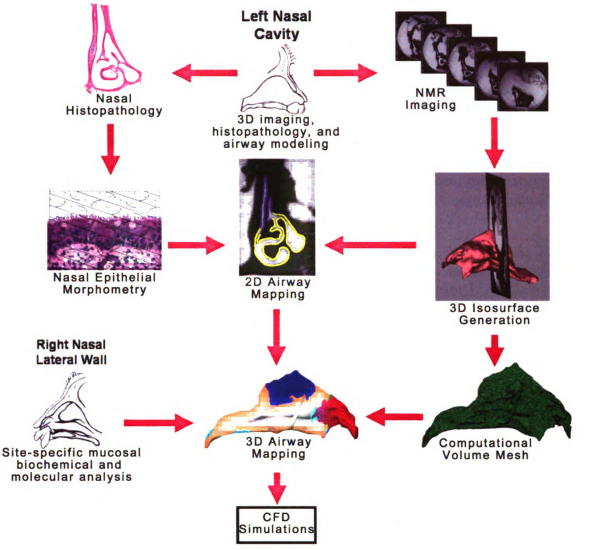

Figure 12. Overview of the imaging, 3D modeling, and histopathologic methods. Sagittal sectioning of the nasal cavity results in a left nasal cavity with nasal septum attached (top), and a right lateral wall (bottom left). The left nasal cavity is fixed and submitted for MR imaging (top right). The resulting stack of 256 MR images is used to digitally segment the nasal airways. This series of 2D segmentations is combined in DDV to generate a 3D isosurface rendering of the nasal airways. Segmentation data generated in DDV are read into NWGrid for translation into a computational volume mesh, which serves as the initial finite element mesh for use in CFD simulations. After MR imaging, the fixed left nasal cavity is decalcified, sectioned, and embedded for histopathologic and morphometric analysis (left). Data obtained from histopathologic analysis are combined with 2D segmentations to generate 2D nasal epithelial and nasal airway injury maps. The 2D data from histopathologic and morphometric analyses, along with site-specific biochemical data from the right nasal specimen (bottom left) can be combined with existing 3D meshes for use in CFD simulations.

REFERENCES

Ballinger, C. A., R. Cueto, G. Squadrito, J. F. Coffin, L. W. Velsor, W. A. Pryor and E. M. Postlethwait (2005). "Antioxidant-mediated augmentation of ozone-induced membrane oxidation." Free radical biology & medicine. **38**(4): 515-26.

Evans, M. J., M. V. Fanucchi, G. L. Baker, L. S. Van Winkle, L. M. Pantle, S. J. Nishio, E. S. Schelegle, L. J. Gershwin, L. A. Miller, D. M. Hyde, P. L. Sannes and C. G. Plopper (2003). "Atypical development of the tracheal basement membrane zone of infant rhesus monkeys exposed to ozone and allergen." American journal of physiology. Lung cellular and molecular physiology. **285**(4): L931-9.

Fanucchi, M. V., C. G. Plopper, M. J. Evans, D. M. Hyde, L. S. Van Winkle, L. J. Gershwin and E. S. Schelegle (2006). "Cyclic exposure to ozone alters distal airway development in infant rhesus monkeys." Am J Physiol Lung Cell Mol Physiol **291**(4): L644-650.

Flanagan, P. and R. Eccles (1997). "Spontaneous changes of unilateral nasal airflow in man. A re-examination of the 'nasal cycle'." Acta Otolaryngol **117**(4): 590-5.

Frank, L., J. R. Bucher and R. J. Roberts (1978). "Oxygen toxicity in neonatal and adult animals of various species." J Appl Physiol **45**(5): 699-704.

Gross, E. A., T. B. Starr, H. W. Randall and M. K.T. (1987). Morphometric analysis fo the primate nasal cavity. Toxicologist.

Gross, E. A., J. A. Swenberg, S. Fields and J. A. Popp (1982). "Comparative morphometry of the nasal cavity in rats and mice." J Anat **135**(Pt 1): 83-8.

Harkema, J. R. (1991). "Comparative aspects of nasal airway anatomy: relevance to inhalation toxicology." Toxicologic Pathology **19**(4 Pt 1): 321-36.

Harkema, J. R., S. A. Carey and J. G. Wagner (2006). "The nose revisited: a brief review of the comparative structure, function, and toxicologic pathology of the nasal epithelium." Toxicologic Pathology **34**(3): 252-69.

Harkema, J. R., C. G. Plopper, D. M. Hyde and J. A. St George (1987a). "Regional differences in quantities of histochemically detectable mucosubstances in nasal, paranasal, and nasopharyngeal epithelium of the bonnet monkey." Journal of Histochemistry & Cytochemistry **35**(3): 279-86.

Harkema, J. R., C. G. Plopper, D. M. Hyde, J. A. St George and D. L. Dungworth (1987b). "Effects of an ambient level of ozone on primate nasal epithelial mucosubstances. Quantitative histochemistry." American Journal of Pathology **127**(1): 90-6.

Harkema, J. R., C. G. Plopper, D. M. Hyde, J. A. St George, D. W. Wilson and D. L. Dungworth (1987c). "Response of the macaque nasal epithelium to ambient levels of ozone. A morphologic and morphometric study of the transitional and respiratory epithelium." American Journal of Pathology **128**(1): 29-44.

Harkema, J. R., C. G. Plopper, D. M. Hyde, D. W. Wilson, J. A. St George and V. J. Wong (1987d). "Nonolfactory surface epithelium of the nasal cavity of the bonnet monkey: a morphologic and morphometric study of the transitional and respiratory epithelium." American Journal of Anatomy **180**(3): 266-79.

Harris, A. J., S. M. Squires, P. D. Hockings, S. P. Campbell, R. W. Greenhill, A. Mould and D. G. Reid (2003). "Determination of surface areas, volumes, and lengths of cynomolgus monkey nasal cavities by ex vivo magnetic resonance imaging." Journal of Aerosol Medicine **16**(2): 99-105.

Hinners, R. G., J. K. Burkart and C. L. Punte (1968). "Animal inhalation exposure chambers." Archives of environmental health. **16**(2): 194-206.

Housley, D. G., I. Mudway, F. J. Kelly, R. Eccles and R. J. Richards (1995). "Depletion of urate in human nasal lavage following in vitro ozone exposure." Int J Biochem Cell Biol **27**(11): 1153-9.

Hyde, D. M., D. J. Magliano and C. G. Plopper (1991). "Morphometric assessment of pulmonary toxicity in the rodent lung." Toxicologic pathology. **19**(4): 428-46.

Hyde, D. M., C. Plopper, J. A. St George and J. R. Harkema (1990). Morphometric cell biology of airspace epithelium. Electron Microscopy of the Lung. D. E. Schraufnagel. New York, Marcel Dekker: 1-120.

Kepler, G. M., D.R. Joyner, A. Fleishman, R.B. Richardson, E.A. Gross, K.T. Morgan, M.N. Godo, and J.S. Kimbell (1995). "Method for obtaining accurate geometrical coordinates on nasal airways for computer dosimetry modeling and lesion mapping,." Inhal Toxicol **7**: 1207-1224.

Kepler, G. M., R. B. Richardson, K. T. Morgan and J. S. Kimbell (1998). "Computer simulation of inspiratory nasal airflow and inhaled gas uptake in a rhesus monkey." Toxicology and applied pharmacology. **150**(1): 1-11.

Kimbell, J. S. (2006). "Nasal dosimetry of inhaled gases and particles: where do inhaled agents go in the nose?" Toxicologic pathology. **34**(3): 270-3.

Kirschvink, N., L. Fievez, F. Bureau, G. Degand, G. Maghuin-Rogister, N. Smith, T. Art and P. Lekeux (2002). "Adaptation to multiday ozone exposure is associated with a sustained increase of bronchoalveolar uric acid." Free Radical Research **36**(1): 23-32.

Larson, S. D., C. G. Plopper, G. Baker, B. K. Tarkington, K. C. Decile, K. Pinkerton, J. K. Mansoor, D. M. Hyde and E. S. Schelegle (2004). "Proximal airway mucous

cells of ovalbumin-sensitized and -challenged Brown Norway rats accumulate the neuropeptide calcitonin gene-related peptide." American journal of physiology. Lung cellular and molecular physiology. **287**(2): L286-95.

Luppi, F., J. Aarbiou, S. van Wetering, I. Rahman, W. I. de Boer, K. F. Rabe and P. S. Hiemstra (2005). "Effects of cigarette smoke condensate on proliferation and wound closure of bronchial epithelial cells in vitro: role of glutathione." Respiratory Research **6**: 140.

Menache, M. G., L. M. Hanna, E. A. Gross, S. R. Lou, S. J. Zinreich, D. A. Leopold, A. M. Jarabek and F. J. Miller (1997). "Upper respiratory tract surface areas and volumes of laboratory animals and humans: considerations for dosimetry models." J Toxicol Environ Health **50**(5): 475-506.

Mery, S., E. A. Gross, D. R. Joyner, M. Godo and K. T. Morgan (1994). "Nasal diagrams: a tool for recording the distribution of nasal lesions in rats and mice." Toxicologic pathology. **22**(4): 353-72.

Minard, K. R., D. R. Einstein, R. E. Jacob, S. Kabilan, A. P. Kuprat, C. A. Timchalk, L. L. Trease and R. A. Corley (2006). "Application of magnetic resonance (MR) imaging for the development and validation of computational fluid dynamic (CFD) models of the rat respiratory system." Inhalation toxicology. **18**(10): 787-94.

Morgan, K. T. and T. M. Monticello (1990). "Airflow, gas deposition, and lesion distribution in the nasal passages." Environmental Health Perspectives **85**: 209-18.

Mudway, I. S. and F. J. Kelly (1998). "Modeling the interactions of ozone with pulmonary epithelial lining fluid antioxidants." Toxicology and applied pharmacology. **148**(1): 91-100.

Plopper, C. G., F. P. Chu, C. J. Haselton, J. Peake, J. Wu and K. E. Pinkerton (1994). "Dose-dependent tolerance to ozone. I. Tracheobronchial epithelial reorganization in rats after 20 months' exposure." American Journal of Pathology **144**(2): 404-20.

Plopper, C. G., G. E. Hatch, V. Wong, X. Duan, A. J. Weir, B. K. Tarkington, R. B. Devlin, S. Becker and A. R. Buckpitt (1998). "Relationship of inhaled ozone concentration to acute tracheobronchial epithelial injury, site-specific ozone dose, and glutathione depletion in rhesus monkeys." Am J Respir Cell Mol Biol **19**(3): 387-99.

Reed, C. J., D. A. Robinson and E. A. Lock (2003). "Antioxidant status of the rat nasal cavity." Free Radic Biol Med **34**(5): 607-15.

Schreider, J. P. (1986). Comparative anatomy and function of the nasal passages. Toxicology of the nasal passages. C. S. Barrow. New York, NY, Hemisphere: 1-25.

Shaw, J. P. and I. N. Chou (1986). "Elevation of intracellular glutathione content associated with mitogenic stimulation of quiescent fibroblasts." J Cell Physiol **129**(2): 193-8.

Sorokin, S. P. (1988). The respiratory system. Cell and tissue biology: A textbook of histology. L. Weiss. Baltimore, Urban & Schwarzenberg: 751-814.

Sram, R. J., I. Benes, B. Binkova, J. Dejmek, D. Horstman, F. Kotesovec, D. Otto, S. D. Perreault, J. Rubes, S. G. Selevan, I. Skalik, R. K. Stevens and J. Lewtas (1996). "Teplice program--the impact of air pollution on human health." Environ Health Perspect **104 Suppl 4**: 699-714.

Taylor, A., A. Borhan and J. Ultman (2007). "Three-Dimensional Simulations of Reactive Gas Uptake in Single Airway Bifurcations." Annals of Biomedical Engineering **35**: 235-249.

Tyler, W. S., D. L. Dungworth, C. Plopper, D. M. Hyde and N. K. Tyler (1985). "Structural evaluation of the respiratory system." Fundamental and Applied Toxicology **5**: 405-422.

Velsor, L. W. and E. M. Postlethwait (1997). "NO2-induced generation of extracellular reactive oxygen is mediated by epithelial lining layer antioxidants." The American journal of physiology. **273**(6): L1265-75.

West, J. A., A. R. Buckpitt and C. G. Plopper (2000). "Elevated airway GSH resynthesis confers protection to Clara cells from naphthalene injury in mice made tolerant by repeated exposures." J Pharmacol Exp Ther **294**(2): 516-23.

Wiethoff, A. J., J. R. Harkema, A. P. Koretsky and W. E. Brown (2001). "Identification of mucosal injury in the murine nasal airways by magnetic resonance imaging: site-specific lesions induced by 3-methylindole." Toxicol Appl Pharmacol **175**(1): 68-75.

Yeh, H. C., R. M. Brinker, J. R. Harkema and B. A. Muggenburg (1997). "A comparative analysis of primate nasal airways using magnetic resonance imaging and nasal casts." J Aerosol Med **10**(4): 319-29.

Young, J. T. (1981). "Histopathologic examination of the rat nasal cavity." Fundamental & Applied Toxicology **1**(4): 309-12.

CHAPTER 4

CORRELATION BETWEEN OZONE-INDUCED SQUAMOUS METAPLASIA AND GLUTATHIONE UPREGULATION IN THE NASAL AIRWAYS OF INFANT MONKEYS

ABSTRACT

Children chronically exposed to high ambient levels of ozone (O_3), the principal oxidant pollutant in photochemical smog, develop epithelial hyperplasia (EH) and squamous metaplasia in the epithelium lining the anterior nasal airways. These nasal alterations may impair normal physiologic functions (e.g. mucociliary clearance) that serve to protect the lower airways from inhaled xenobiotics. Reactions between O_3 and endogenous nasal antioxidants may play a role in the induction of exposure-related cellular injury and repair. The purpose of our study was to determine the effect of cyclic ozone exposures on the developing nasal airways of infant monkeys, and the association between O_3-induced remodeling and nasal antioxidant levels. Infant (180-day-old) rhesus macaques were exposed to 5 consecutive days of O_3 (0.5ppm, 8h/day; "1-cycle") or filtered air (FA), or 11 bi-weekly cycles of O_3 (FA days 1-9; 0.5ppm, 8h/day on days 10-14; "11-cycle"). The left nasal passage was processed for light microscopy and morphometric analysis. Mucosal samples from the right passage were processed for glutathione (GSH), glutathione disulfide (GSSG), ascorbate (AH_2), and uric acid (UA) concentrations. 11-cycle O_3 induced squamous metaplasia and EH along the dorsomedial surface of the maxilloturbinate, resulting in a 39% increase in the numeric density of epithelial cells. 11-cycle O_3 also induced a 65% increase in GSH concentrations at this site, but no change in GSSG, AH_2, or UA levels. 1-cycle O_3 did not cause EH, metaplasia, or changes in antioxidant levels. EH was positively correlated with changes in GSH ($r=0.684$; $p=0.00694$). These findings are consistent with O_3-induced remodeling

observed in children, and provide new insights regarding the role of GSH in O_3-induced cell proliferation.

INTRODUCTION

Ozone, the principal oxidant air pollutant in photochemical smog, causes toxic injury to the nasal (Graham, D. et al. 1988; Koren et al. 1990) and pulmonary (Graham, D. E. and Koren 1990; Devlin et al. 1991) airways in people. The U.S. Environmental Protection Agency estimates that the majority (53%) of children in the United States live in areas that exceed the NAAQS level for ozone (Woodruff et al. 2007). This is of particular concern because recent evidence suggests that children may be more vulnerable to the respiratory health effects of ozone than adults (Kim 2004). Exposure to ambient concentrations of ozone causes acute inflammation in the nasal airways of children (Frischer et al. 1993). Children residing in southwestern Mexico City, a region in which ambient ozone concentrations frequently exceed the NAAQS, experience epistaxis, nasal obstruction, and sinusitis (Calderon-Garciduenas et al. 2001). Nasal biopsies from children in this region exhibit ciliated cell necrosis, ciliary dyskinesia, and squamous metaplasia (Calderon-Garciduenas et al. 2001; Calderon-Garciduenas et al. 2001).

Several studies have characterized ozone-induced nasal airway injury using adult laboratory animal models. Adult monkeys exposed short-term (6 days) to ambient concentrations (0.15 ppm) of ozone develop acute rhinitis, epithelial hyperplasia, and mucous cell metaplasia in the non-ciliated transitional epithelium (NTE) and the ciliated respiratory epithelium (RE). Adult monkeys exposed to long-term ozone (0.15 or 0.30

ppm, 90 days) show an increase in intraepithelial mucus compared to short-term exposure, with resolution of the inflammation and epithelial hyperplasia (Harkema et al. 1987; Harkema et al. 1987). Adult rats also develop acute inflammation, epithelial hyperplasia, and mucous cell metaplasia in the nasal airways following short-term ozone exposure (3 or 7 days, 0.5ppm, 8h/day) (Harkema et al. 1989; Cho et al. 1999). These lesions were also present in adult rats following chronic exposure (13 weeks), and persisted for several weeks after the end of exposure (Harkema et al. 1999). We have recently reported that infant monkeys exposed to cyclic episodes of ozone for two months (5 cycles) also develop acute rhinitis and nasal epithelial necrosis, but do not develop epithelial hyperplasia or mucous cell metaplasia (Carey et al. 2007). Additional controlled studies using immature animal models are needed to better understand the differential effects of ozone exposure on the developing nasal airways of children.

The respiratory tract demonstrates marked heterogeneity with respect to the anatomic site of injury following ozone exposure. In rhesus monkeys, the nature and degree of ozone-induced cellular injury vary significantly by location in both the nasal and pulmonary airways. In the lungs, ozone exposure targets the ciliated respiratory epithelium of the trachea and type I pneumocytes lining the terminal bronchioles (Castleman et al. 1980; Wilson et al. 1984; Nikula et al. 1988). In the nasal airways, ozone-induced injury is confined to the anterior nasal cavity, specifically targeting the NTE and ciliated RE (Harkema et al. 1987; Harkema et al. 1987; Carey et al. 2007).

The site-specificity of ozone-induced injury in the respiratory tract is due to a combination of the local tissue susceptibility and the ozone dose delivered to specific sites. The basis for the variations in tissue susceptibility may be related to the capacity of

that tissue to respond to oxidant challenge. Low molecular weight antioxidants in the epithelium and overlying epithelial lining fluid of the respiratory tract are considered to provide the first line of defense against inhaled oxidant challenge (Cross et al. 1994). The major low molecular weight antioxidants lining the respiratory tract include glutathione (GSH), ascorbate (AH_2), and uric acid (UA). Recent studies suggest that reactions between oxidants and low molecular weight antioxidants are critical to the induction of oxidant-mediated epithelial injury (Ballinger et al. 2005) and repair (Luppi et al. 2005). In primates, GSH is unique among the low molecular weight antioxidants in that it can be synthesized *de novo* and locally regulated by respiratory tract epithelial cells in response to oxidative stress (Dickinson and Forman 2002). In young adult monkeys, ozone exposure causes site-specific depletion of intracellular GSH concentrations at sites of exposure-related injury in the pulmonary airways (Plopper, C. G. et al. 1998). There are also variations in the activities of glutathione S-transferase and glutathione peroxidase, enzymes that require GSH as a substrate, across different regions of monkey lung (Duan et al. 1993).

The association between local antioxidant status and susceptibility to ozone-induced injury in the nasal airways has not been investigated. The purposes of the present study were, 1) to determine the effect of cyclic ozone exposures on the developing nasal airways of infant monkeys, 2) to determine the effect of cyclic ozone exposure on the steady-state levels of intracellular low molecular weight antioxidants, and, 3) to determine the association between ozone-induced injury, remodeling, and nasal antioxidant status. We hypothesized that the site-specificity and temporal pattern of ozone-induced injury and repair are dependent on the local regulation of intracellular

nasal antioxidants. We tested this hypothesis in the nasal airways of infant rhesus monkeys, an animal model whose nasal airways closely resemble those of children. By splitting the nasal cavity, we were able to make direct comparisons between morphologic responses and site-matched cellular and molecular responses to ozone exposure. The results of this study provide new insights into the susceptibility of children to ozone-induced nasal injury, and the potential relationships among nasal antioxidants, epithelial injury, and repair.

MATERIALS AND METHODS

Animals and Ozone Exposure

Fourteen male infant rhesus monkeys (*Macaca mulatta*) were raised from birth in a filtered air environment. All monkeys were obtained from the breeding colony at the California National Primate Research Center at the University of California, Davis. Care and housing of the animals before, during, and after treatment complied with the provisions of the Institute of Laboratory Animal Resources, and conformed to practices established by the American Association for Accreditation of Laboratory Animal Care (AAALAC). While undergoing exposures, animals were housed in stainless steel open-mesh cages. Prior to exposure, animals were housed in small social groups within the exposure chambers in order to allow acclimation to the chamber environment. Five monkeys were exposed to 5 consecutive days of 0.5 parts per million (ppm) ozone for 8 h/day, ending at 6 months of age (1 cycle O_3). Five monkeys were exposed to 9 consecutive days of filtered air (FA) followed by 5 consecutive days of 0.5 ppm ozone, 8h/day, for a total of 11 cycles, beginning at 30 days of age and ending at 6 months of

age (11 cycle O_3). Four control monkeys were exposed to filtered air (FA) only. All animals were 180 +/-3 days of age at the end of exposure.

Ozone exposures were conducted in 4.2-cubic meter (m^3) stainless steel and glass, whole-body inhalation chambers. Ozone was produced from vaporized liquid, medical grade oxygen by electronic discharge ozonizers. Generated ozone was diluted with filtered air (24°C, 40-50% relative humidity) to the appropriate concentration, and injected into the inlet airflow of the exposure chamber. Filtered air was supplied to the exposure chambers at a rate of 2.1m^3 per minute, providing 30 air exchanges per hour. Chamber ozone concentration was monitored throughout exposures with an ultraviolet ozone analyzer (Model 1003-AH, Dasibi Corporation, Glendale, CA).

Necropsy and Tissue Preservation

At the end of exposure, monkeys were sedated using ketamine hydrochloride (10mg/kg IM), followed by induction of deep anesthesia using propofol (*Diprivan*, 0.1-0.2mg/kg/min IV), with the dose adjusted as necessary by an attending veterinarian. The trachea, sternum, and abdominal cavity were exposed by a midline incision. Anesthetized animals were euthanized by exsanguination via the abdominal aorta. Immediately after sacrifice, the head was removed from the carcass, and the lower jaw, skin, brain, and musculature were removed from the head. The nasal cavity was exposed by splitting the skull sagittally, 1-2 mm to the right of midline, yielding a complete left nasal cavity and intact nasal septum, and a free right lateral wall, as previously described (Carey et al. 2007). The left nasal cavity was prepared for histopathologic and morphometric analyses. Briefly, the left nasal cavity was lavaged retrograde through the

nasopharyngeal duct with 2 ml cold phosphate buffered saline, flushed in the same manner with a solution of 1% paraformaldehyde and 0.1% glutaraldehyde (0.01M phosphate buffer, pH 7.4), immersed in ~100 ml of 1% paraformaldehyde and 0.1% glutaraldehyde, and fixed at 4°C for at least 24 hours.

The right side of the nasal cavity was used to harvest site-specific mucosal samples for RNA isolation and biochemical antioxidant analyses corresponding to the sites examined by light microscopy in the left nasal cavity. Mucosal samples were dissected from the anterior maxilloturbinate (MT), posterior MT, and anterior ethmoturbinate (ET) (Figure 4-1, A). Each mucosal sample was divided into two equal parts. One part from each region was stored in 0.5 ml RNA*Later* (Ambion, Austin, TX), held at room temperature for 24 hours, and then stored at-20°C. The samples from the anterior MT were further processed for RNA extraction and gene expression analyses (described below). The other part from each region was immediately placed into 300µl of 10% metaphosphoric acid, and snap-frozen in liquid nitrogen. Acidified, frozen nasal mucosal samples were later thawed, homogenized for 30 seconds using a Polytron homogenizer, re-frozen, and stored at –80°C until further processing for low molecular weight antioxidant analysis via high performance liquid chromatography (HPLC).

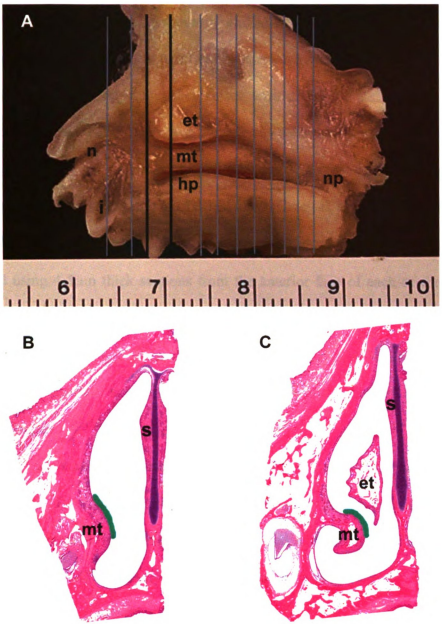

Figure 4-1. Anatomic location of nasal tissues selected for morphometric analysis. (A) Exposed right lateral wall of the nasal cavity of a 180-day-old rhesus monkey. Vertical lines indicate the locations of the twelve transverse sections processed for light microscopy. The two black lines indicate the sections through the anterior maxilloturbinate that were used for morphometric analyses. (B,C) Low magnification photomicrographs of H&E-stained transverse sections through the anterior maxilloturbinate of a FA-exposed monkey. The area highlighted in green represents the dorsomedial surface of the maxilloturbinate. The mucosa underlying this region was selected for morphometric analysis. . n = naris; i = incisor tooth; mt = maxilloturbinate; et = ethmoturbinate; hp = hard palate; np = nasopharyngeal meatus; s = nasal septum.

Tissue Processing for Light Microscopy and Morphometric Analysis

After fixation, each left nasal cavity specimen was decalcified in 200ml of 13% formic acid for 14-16 days, and then rinsed with distilled water for 2-4 hours. After decalcification, each nasal cavity was transversely sectioned at 10-12 specific anatomical locations in a plane perpendicular to the hard palate and nasal septum, using gross dental and palatine landmarks, as previously described (Carey et al. 2007). Each tissue block was embedded in paraffin for light microscopic and morphometric analyses. Slides were prepared using 4-5μm thick sections from the anterior face of each of the 10-12 tissue blocks. A tissue section from each block was stained with hematoxylin and eosin (H&E) for routine histopathologic examination. Another tissue section was stained with Alcian blue (pH 2.5)/periodic acid-Schiff (AB/PAS) for identification of acidic and neutral mucosubstances.

For each animal, the first two transverse tissue sections that included a complete profile of the MT (i.e., the anterior MT) were selected for morphometric analyses (Figure 4-1). A tissue section from these blocks was stained with rabbit-anti-human granulocytic myeloperoxidase (MPO) polyclonal antibody (Lab Vision Corporation, Fremont, CA) for immunohistochemical identification of neutrophils.

Morphometry of Neutrophilic Inflammation and Epithelial Numeric Cell Density

The epithelium lining the dorsomedial surface of the anterior MT of each animal was analyzed through standard morphometric techniques and computerized image analysis (Harkema et al. 1989). Neutrophilic inflammation was assessed on tissue sections immunohistochemically stained for myeloperoxidase. Neutrophil numeric

densities were determined by quantitating the number of nuclear profiles of neutrophils within the surface epithelium, in the lamina propria, and within the subepithelial vasculature of the mucosa lining the dorsomedial MT, and dividing this number by the total length of the basal lamina underlying the epithelium in this region. Neutrophils were identified on the basis of characteristic, multilobed nuclear morphology and cytoplasmic myeloperoxidase immunoreactivity. The basal lamina length was calculated from the contour length of the basal lamina on a digitized image, using image analysis software (Scion Image, Scion Corporation, Frederick, MD). The epithelial cell numeric density was determined by counting the total number of epithelial cell nuclear profiles in the epithelium lining the dorsomedial MT, and dividing this number by the length of the basal lamina. The mucous cell numeric density was determined by counting the total number of AB/PAS positive epithelial cells with nuclear profiles, and dividing this number by the basal lamina length.

Morphometry of Epithelial Metaplasia

Metaplastic changes in the epithelium lining the dorsomedial, anterior MT were quantified using stereologic methods. The volume density of nuclei, cilia, and intraepithelial mucus within this region was morphometrically evaluated as previously described for airway epithelium (Hyde et al. 1990; Hyde et al. 1991; Plopper, C. G. et al. 1994; Carey et al. 2007). All measurements were obtained at a final magnification of 1,710x using a light microscope (Olympus BX40; Olympus America, Inc., Melville, NY) coupled to a 3.3-megapixel digital color camera (Q-Color 3 Camera; Quantitative Imaging Corporation, Brunaby, British Columbia, Canada), and a personal computer

(Dimension 8200, Dell Corporation, Austin, TX). The morphometric analyses were performed using a 135-point cycloid grid overlay with an automated software package for counting points and intercepts within the grid (Stereology Toolbox; Morphometrix, Davis, CA) (Hyde et al. 1990; Hyde et al. 1991). The percent volume density (the proportion of the total epithelial volume), V_v, of the epithelial constituents was determined by point counting and calculated using the following formula:

$$V_v = P_p = P_n/P_t \quad (1)$$

where P_p is the point fraction of P_n, the number of test points hitting the structure of interest (e.g., nuclei), divided by P_t, the total number of points hitting the reference space (i.e., epithelium). The volume of each epithelial component of interest per unit basal lamina length (cubic microns per square micron; S_v) was determined by point- (epithelial component) and intercept- (basal lamina) counting and was calculated using the following formula:

$$S_v = 2I_O L_\gamma \quad (2)$$

where I_O is the number of cycloid intercepts with the object (basal lamina), and L_γ is the length of the test line in the reference volume (epithelium within the test grid). To determine the thickness of the total epithelium, a volume per unit area of basal lamina

(cubic microns per square micron) was calculated using the following formula for arithmetic mean thickness (τ):

$$\tau = V_V/S_V \quad (3)$$

Morphometry of Stored Intraepithelial Mucosubstances

The amount of stored mucosubstances in the surface epithelium of the dorsomedial MT was estimated by quantifying the volume of AB/PAS-stained mucosubstances per unit basal lamina (volume density, Vs), using computerized image analysis and standard morphometric techniques. The area of AB/PAS-stained mucosubstances was calculated by circumscribing the perimeter of the stained material using the Scion Image program. The length of the basal lamina underlying the surface epithelium was calculated as described above. The volume density was estimated using a previously described method (Harkema et al. 1987), and was expressed in nl/mm^2 basal lamina.

Determination of Intracellular Low Molecular Weight Antioxidants Concentrations in Nasal Mucosa

Nasal tissue homogenates were thawed and centrifuged at 12,500 x g for 4 hours. Protein pellets were resuspended in 500µl of PBS, neutralized with 25µl 1N NaOH, and sonicated for 1 hour at 37°C. The protein content of resuspended pellets was measured using the Pierce BCA Protein Assay (Pierce Biotechnology, Rockford, IL). Supernatants were filtered through a 0.22µm syringe filter, and samples were fractioned in triplicate on a Shimadzu LC-10A*i* HPLC (Shimadzu Scientific Instruments, Columbia, MD), using a

Phenomenex Luna C18(2) 250mm x 4.6mm, 5μM reversed phase column, preceded by a Phenomenex ODS 4mm x 3mm guard column (Phenomenex, Torrance, CA). The mobile phase consisted of an isocratic mixture of 50mM phosphate buffer, pH 3.1, containing 50μM octanesulfonic acid and methanol (95:5). Samples were fractioned at a mobile phase flow rate of 0.5 ml/min. Glutathione (GSH), glutathione disulfide (GSSG), ascorbate (AH_2), and uric acid (UA) were simultaneously detected with an 8-channel ESA CoulArray Model 5600A electrochemical detector (ESA, Chelmsford, MA). GSH, GSSG, AH_2, and UA values were normalized to protein content of centrifuge pellets.

Analysis for Glutamate-Cysteine Ligase Catalytic Subunit (GCL-C) and Modifying Subunit (GCL-M) mRNA in Nasal Tissues

Tissue samples for RNA isolation were homogenized using a Polytron homogenizer. Total cellular RNA was isolated with Trizol (Invitrogen, Carlsbad, CA) according to the manufacturer's instructions, from samples stored in RNALater (Ambion). To avoid DNA contamination, RNA pellets were resuspended in nuclease-free water, and Dnase treated with DNA-free (Ambion) for 1 h at 37°C. cDNA was prepared using random hexamer primers (Amersham-Pharmacia Biotech, Inc., Piscataway, NJ) and Moloney murine leukemia virus reverse transcriptase (Invitrogen).

Catalytic and modifying subunit mRNA levels were determined for GCL, the rate-limiting enzyme in de novo GSH biosynthesis, by real-time PCR as previously described (Abel et al. 2005; Wang et al. 2005). Briefly, samples were tested in duplicate, and the PCR for the glyceraldehyde-3-phosphate (GAPDH) housekeeping gene and the target gene from each sample were run in parallel on the same plate. The reaction was

carried out in a 96-well optical plate (Applied Biosystems, Foster City, CA) in a 25µl reaction volume containing 5µl cDNA plus 20µl Mastermix (Applied Biosystems). Sequences were amplified using the 7900 default amplification program (2 min at 50°C, 10 min at 95°C, followed by 40 to 45 cycles of 15 s at 95°C and 1 min at 60°C). The results were analyzed with the SDS 7900 system software, version 2.1 (Applied Biosystems). GCL-C and GCL-M mRNA expression levels were calculated from the normalized ΔC_T values. Fold increases were calculated using the $\Delta\Delta C_T$ method.

Statistical Analyses

All data were expressed as mean group value ± SEM. The differences among groups were analyzed by one-way analysis of variance (ANOVA). Pairwise comparisons were performed *a priori* using Student-Newman-Keuls multiple comparisons test. The relationship between epithelial cell numeric density and intracellular antioxidant concentration was analyzed by using *post hoc* correlation analysis (Pearson product moment correlation). The criterion for statistical significance was set to $p \leq 0.05$ for all analyses. All statistical analyses were performed using a commercial statistical software package (SigmaStat, SPSS Science, Chicago, IL).

RESULTS

Nasal Histopathology

Our histologic and morphometric investigation focused on the epithelium lining the anterior nasal cavity. This region of the nasal cavity has been reported to be the primary site for damage induced by inhaled toxicants in monkeys (Harkema et al. 1987;

Harkema et al. 1987; Harkema et al. 2006) and people (Calderon-Garciduenas et al. 1992; Calderon-Garciduenas et al. 1994; Calderon-Garciduenas et al. 1995; Calderon-Garciduenas et al. 1999; Calderon-Garciduenas et al. 2001; Calderon-Garciduenas et al. 2001).

In FA-exposed (0 ppm) infant monkeys, the preturbinate region of the main chamber was lined with a combination of squamous epithelium, non-ciliated transitional epithelium, and respiratory epithelium (Figure 4-2, A). Most of the remainder of the main chamber of the nasal airways, including the entire surface of maxilloturbinate, was lined with respiratory epithelium. A small region along the dorsal meatus and the dorsal 1/2 to 1/3 of the ethmoturbinate was lined with olfactory epithelium. This epithelial distribution is in accordance with previous reports on the nasal airways of monkeys (Harkema et al. 1987; Harkema et al. 1987; Harkema et al. 2006; Carey et al. 2007). Occasional intraepithelial and sub-epithelial neutrophils were present in the mucosa of the NTE and the RE lining the anterior nasal cavity in FA-exposed monkeys. This mild inflammation was primarily localized near the ducts and luminal openings of submucosal glands, and near the junctions of two adjacent epithelial populations (e.g., the junction of respiratory epithelium and olfactory epithelium). No gross or microscopic exposure-related morphologic alterations were observed in the nasal mucosa of monkeys exposed to FA.

The principal nasal injury in monkeys exposed to 1 cycle O_3 was acute, multifocal, necrotizing rhinitis. This response was restricted primarily to the NTE and ciliated RE lining the ventral half of the anterior main chamber. In all animals exposed to 1 cycle O_3, there were focal areas of epithelial necrosis and exfoliation, localized

primarily to sites along the maxilloturbinate and ventral aspect of the nasal septum. Associated with these areas of necrosis was an influx of neutrophils into the affected epithelium and lamina propria, and endothelial margination of neutrophils in the underlying capacitance vessels of the nasal mucosa.

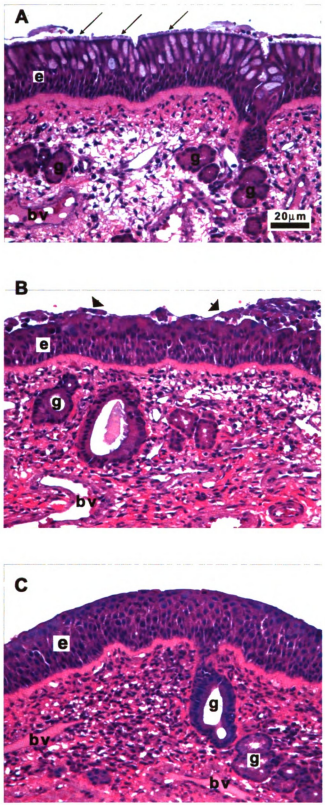

Figure 4-2. Light photomicrographs of the nasal mucosa lining the dorsomedial surface of the maxilloturbinate of 180-day-old monkeys exposed to 0 ppm ozone (filtered air, A), 1 cycle ozone (B), or 11 cycle O_3 (C). The epithelial surface in figure A is lined by an intact layer of cilia (long arrows). Marked epithelial necrosis and exfoliation (arrowheads) of the surface epithelium (e) are present throughout the nasal mucosa following acute ozone exposure (B). Squamous metaplasia and epithelial hyperplasia are present in the surface epithelium following 11 cycle O_3 exposure (C). Note the loss of surface cilia following 1 cycle (B) and 11 cycle (C) ozone exposure. g = glands; bv = blood vessels.

The site of the most severe necrotizing rhinitis in 1 cycle O_3-exposed animals was consistently observed in the respiratory epithelium lining the dorsomedial surface of the anterior MT. This location was further characterized by a conspicuous attenuation or complete loss of cilia, and a reduction in the amount of stored intraepithelial mucosubstances (Figure 4-2, B). No significant histologic abnormalities were noted in the olfactory epithelium, or in the nasal mucosa of the posterior aspect of the nasal cavity in 1 cycle O_3-exposed animals.

The exposure-related injury in 11 cycle O_3 ozone-exposed animals was also restricted to the ventral part of the anterior main chamber, similar to the distribution observed in the 1 cycle O_3-exposed animals. The principal lesions in animals exposed to 11 cycle O_3 were epithelial hyperplasia, squamous metaplasia, and necrotizing rhinitis, located along the dorsomedial surface of the MT (Figure 4-2, C). This location is consistent with the site of maximal injury found in the 1 cycle O_3-exposed animals. However, in contrast to the pseudostratified ciliated respiratory epithelium described in 1 cycle O_3 animals, the surface epithelium at this site in the 11 cycle O_3-exposed animals was 3-4 cells thick, and consisted primarily of layers of small, polygonal epithelial cells devoid of intracellular mucosubstances or surface cilia. There was an overall decrease in the amount of stored intraepithelial mucosubstances in the 11 cycle O_3-exposed animals. However, this overall loss of intraepithelial mucus was accompanied by the appearance of occasional clusters of small, mucus-containing epithelial cells forming intraepithelial mucus glands. Focal areas of acute rhinitis and epithelial necrosis with, and without

exfoliation and loss of cilia, were also present along the ventral septum, ventral meatus, and immediately adjacent to the area of squamous metaplasia along the MT.

Morphometry of Nasal Epithelium

Results of stereologic analysis of the dorsomedial surface of the anterior MT are presented in Figure 4-3. 11 cycle O_3 ozone exposure caused a 30% increase in mean epithelial thickness compared to FA-exposed animals. Furthermore, this ozone-induced epithelial thickening observed in 11 cycle O_3-exposed animals was associated with a significant 2.5-fold-increase in the volume density of epithelial nuclei, compared to FA-exposed animals. There was no significant difference in the mean epithelial height or nuclear volume density between 1 cycle O_3 and FA-exposed animals. Both 1 cycle O_3 and 11 cycle O_3 exposure regimens caused a significant reduction in the volume density of cilia (56% and 91% reductions, respectively) from the surface of the anterior MT, compared to FA exposure.

Quantitation of Intraepithelial Mucosubstances

The epithelial hyperplasia and squamous metaplasia observed in animals exposed to 11 cycle O_3 ozone was also associated with a significant reduction in the amount of stored intraepithelial mucosubstances (88% decrease) and in the numeric density of mucous cells (90% decrease) in the anterior MT, compared to FA exposure (Figure 4-4). 1 cycle O_3 exposure also caused a mild, but not statistically significant, decrease in stored intraepithelial mucosubstances (36% decrease) and mucous cells (7.6% decrease)

compared to FA exposure. There was no significant difference observed in the mucous cell numeric density between FA- and 1 cycle O_3-exposed animals.

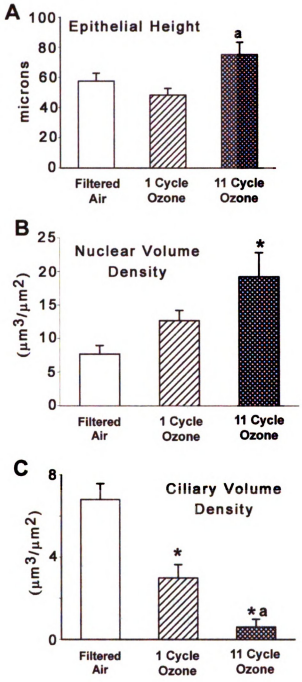

Figure 4-3. Morphometry of ozone-induced nasal epithelial injury in infant rhesus monkeys. 11 cycle O_3 exposure caused epithelial hyperplasia and squamous metaplasia, resulting in an increase in epithelial height (A) and in the volume density of epithelial cell nuclei (B). 1 cycle and 11 cycle ozone exposure each resulted in a reduction in the volume density of cilia (C). Bars represent group mean $\pm$ SEM. * = significantly different from respective FA group ($p \leq 0.05$). a = significantly different from respective acute ozone group ($p \leq 0.05$).

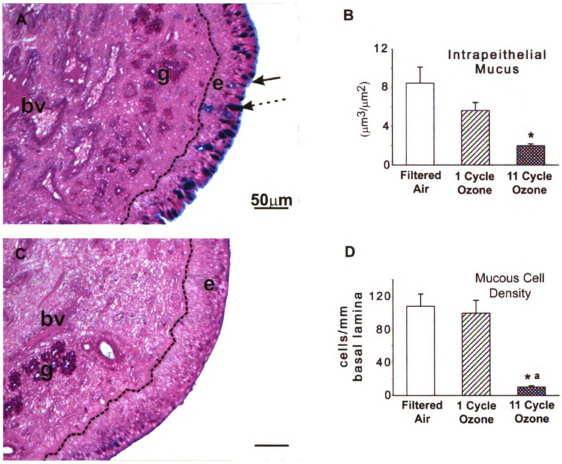

Figure 4-4. (A,C) Light photomicrographs of maxilloturbinates from monkeys exposed to FA (A) or 11 cycle O_3 (C). Tissues were stained with AB/PAS to detect acidic and neutral mucosubstances. Note the presence of cilia (solid arrow) and intraepithelial AB/PAS-stained mucosubstances (dashed arrow) in the epithelium of the FA-exposed monkey, and the loss of these features following 11 cycle O_3 exposure (C). Dotted line – basal lamina between epithelium and lamina propria; e = epithelium; bv = blood vessels; g = glands. (B,D) Morphometry of intraepithelial mucus. Episodic ozone exposure caused a decrease in the volume density of intraepithelial mucosubstances (B) and mucous cell numeric cell density (D). Bars represent group mean $\pm$ SEM. * = significantly different from respective FA group. a = significantly different from respective 1 cycle O_3 group ($p \leq 0.05$).

Morphometry of Neutrophilic Inflammation

The numeric cell densities of neutrophils in the mucosa along the dorsomedial surface of the anterior MT are summarized in Figure 4-5. All ozone-exposed animals (1 cycle or 11 cycle) exhibited neutrophilic rhinitis in the nasal airway mucosa lining the dorsomedial MT. Both of the ozone-exposed groups had ~4-fold more total neutrophils in the nasal mucosa (intraepithelial + interstitial + intravascular) than the FA-exposed group. There was no significant difference in the total or interstitial neutrophil numeric density between 1 cycle O_3 and 11 cycle O_3 animals. However, the 11 cycle O_3 group had significantly more intraepithelial neutrophils (by 2.4-fold), and fewer intravascular neutrophils (75% fewer) along this site than the 1 cycle O_3 group.

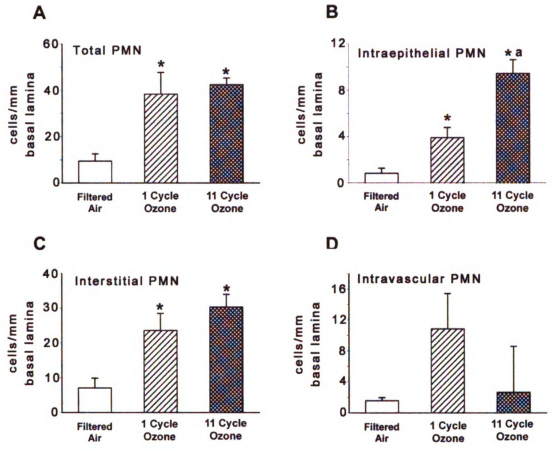

Figure 4-5. Effect of ozone exposure on the numeric cell density of neutrophils (PMNs) in the nasal mucosa along the anterior MT of infant monkeys. (A) Total PMN numeric cell density (intraepithelial PMN + interstitial PMN + intravascular PMN); (B) Intraepithelial PMN; (C) Interstitial PMN; (D) Intravascular PMN. Bars represent group mean $\pm$ SEM. * = significantly different from respective FA group ($p \leq 0.05$). a = significantly different from respective acute ozone group ($p \leq 0.05$).

Intracellular Concentrations of Low Molecular Weight Nasal Antioxidants

The baseline antioxidant concentrations of GSH, GSSG, AH_2, and UA in FA-exposed animals were comparable in the anterior MT, posterior MT, and the anterior ethmoturbinate. The mucosal concentrations of GSH, GSSG, AH_2, and UA did not change significantly in any of the three nasal regions examined following 1 cycle O_3-exposure. However, there were slight decreases observed in the concentrations of GSH, AH_2, and UA in all regions following 1 cycle O_3 exposure compared with FA-exposed animals. In contrast, 11 cycle O_3 exposure caused a significant increase in mucosal GSH concentrations in the anterior MT (65% increase) and in the posterior MT (140% increase) compared to FA exposure (Figure 4-6, A). There was also a moderate increase in GSH concentration in the anterior ethmoturbinate of the 11 cycle O_3 group (75% increase), however this was not statistically significant. There was no change in GSSG concentration in the two MT regions following 11 cycle O_3 exposure, however, the GSSG concentration in the anterior ethmoturbinate increased by ~2.4-fold (Figure 4-6, B). No differences were observed in AH_2 or UA concentrations in any of the three nasal regions examined in 11 cycle O_3 ozone animals (Figure 4-6, C and D).

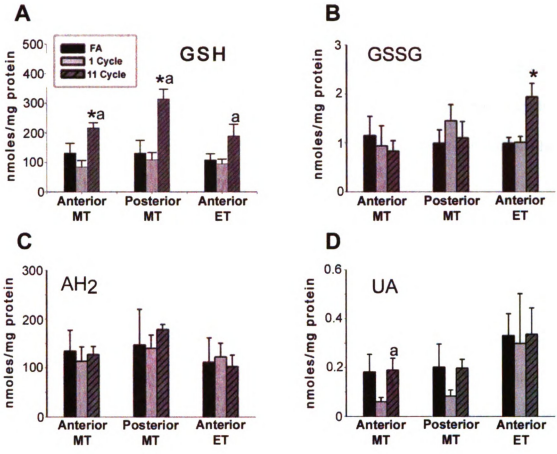

Figure 4-6. Effect of 1 cycle O_3 and 11 cycle O_3 exposure on the intracellular concentrations of GSH (A), GSSG (B), AH_2 (C), and UA (D) in the nasal mucosa from the anterior MT, posterior MT, and anterior ET of infant monkeys. Note the robust increase in intracellular GSH concentrations in all regions of the nasal mucosa following episodic ozone exposure. Bars represent group mean $\pm$ SEM. * = significantly different from respective FA group ($p \leq 0.05$). a = significantly different from respective 1 cycle O_3 group ($p \leq 0.05$).

GCL-C and GCL-M mRNA Expression in the Anterior Maxilloturbinate

11-cycle ozone exposure induced a significant increase (1.4-fold) in the steady-state level of GCL-C mRNA in the anterior MT, compared to FA exposure (Figure 4-7, A). There was no change in GCL-C mRNA expression at this site following 1 cycle O_3 exposure. There were no changes in the expression of GCL-M mRNA following either 1 cycle O_3 or 11 cycle O_3 exposure (Figure 4-7, B).

Correlation Analysis for Epithelial Cell Numeric Density and Antioxidant Concentration Along the Anterior Maxilloturbinate

Correlation analysis was used to determine the association between epithelial cell numeric density and intracellular antioxidant concentration. There was a significant positive correlation between epithelial cell numeric density and intracellular GSH concentration at the anterior MT ($r=0.684$; $p=0.00694$) across all exposure groups (Figure 4-8, A). There were no significant correlations found between epithelial cell numeric density and the intracellular concentrations of AH_2 ($r=0.0215$; $p=0.942$) or UA ($r=0.328$; $p=0.252$) (Figure 4-8, B and C).

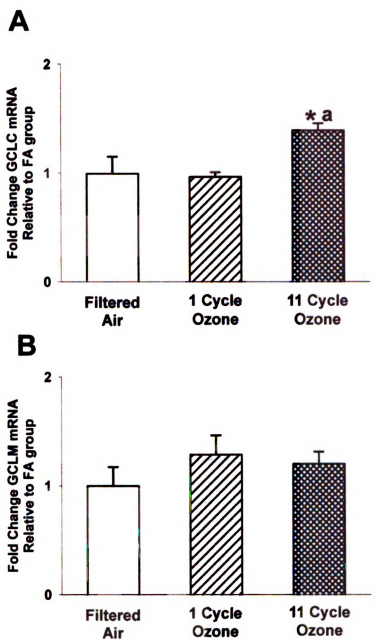

Figure 4-7. Effect of 1 cycle O_3 and 11 cycle O_3 exposure on GCL-C (A) and GCL-M (B) gene expression in the nasal mucosa of the anterior MT. Bars represent group mean $\pm$ SEM. a = significantly different from respective FA group ($p \leq 0.05$). b = significantly different from respective acute ozone group ($p \leq 0.05$).

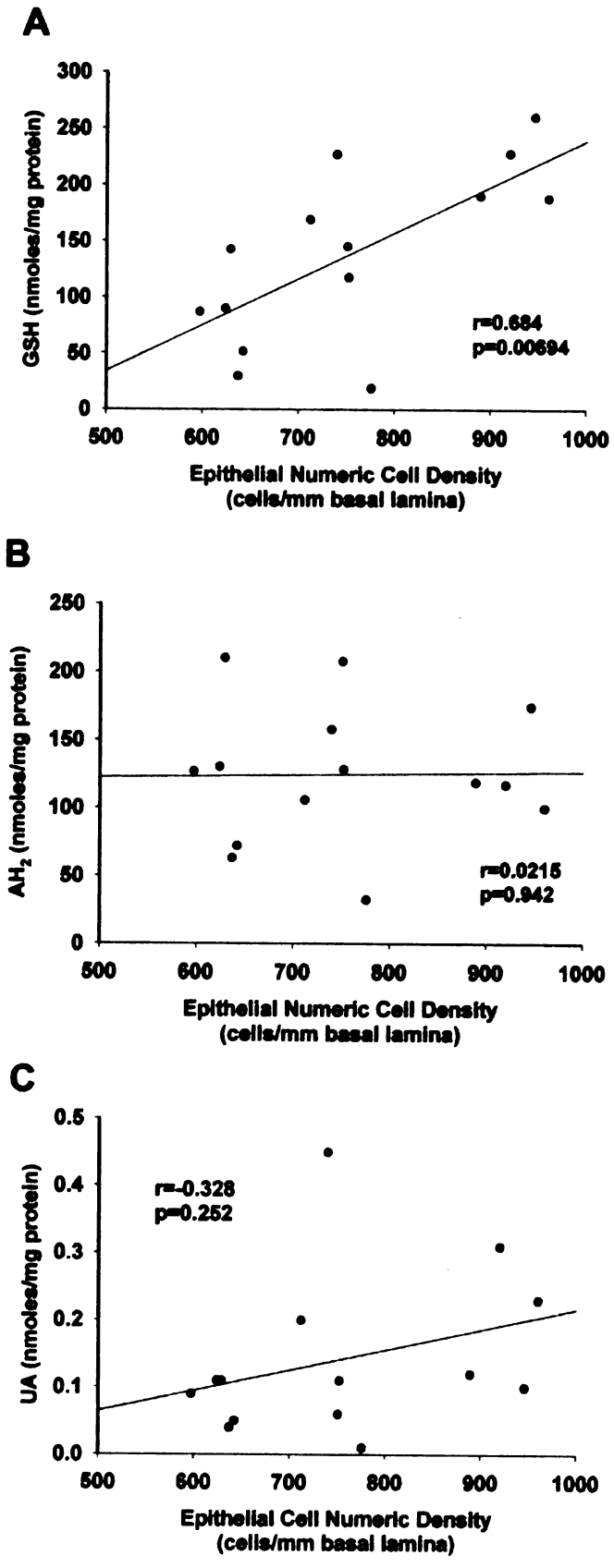

Figure 4-8. Correlations between epithelial hyperplasia (numeric cell density, x-axes) and the intracellular concentrations of GSH (A), AH_2 (B), and UA (C) (y-axes) in the nasal mucosa lining the anterior MT. The associations were described as the Pearson product moment correlation coefficients (r), and were considered significant if $p \leq 0.05$.

DISCUSSION

One purpose of this study was to determine the nature and distribution of mucosal injury and repair in the nasal airway of infant monkeys exposed to ozone. The nasal responses to both acute and chronic, daily ozone exposure in adult monkeys have been extensively characterized. Acute ozone exposure (0.3 ppm, 8h/day, 6 days) causes neutrophilic rhinitis, epithelial necrosis, and ciliated cell loss, confined to the NTE and ciliated RE of the anterior nasal cavity in adult monkeys (Harkema et al. 1987; Harkema et al. 1987). We found that infant (180-day-old) monkeys exposed acutely to ozone (1 cycle O_3) also exhibit epithelial necrosis, ciliated cell loss, and neutrophilic inflammation, which were confined to distinct focal regions in the anterior nasal cavity. The distribution of these lesions was also consistent with those previously described in both younger (90-day-old), infant monkeys (Carey et al. 2007) and in adult monkeys (Harkema et al. 1987a; Harkema et al. 1987b) similarly exposed to ozone. Furthermore, as we have shown here, the sites that exhibited necrosis and ciliated cell injury after 1 cycle O_3 exposure in infant monkeys subsequently developed epithelial hyperplasia and squamous metaplasia following 11 cycle O_3 exposure. The location and nature of this proliferative response to 11 cycle O_3 exposures in these infants was similar to the response previously described in adult macaques (Harkema et al. 1987a) following acute exposure (0.3 ppm, 8h/day for 6 days). These results suggest that the site-specificity of ozone-induced injury is consistent in infants and adults, despite significant post-natal growth of the nasal cavity in non-human primates (Kepler 1995; Carey et al. 2007).

Mucous cell metaplasia is a frequent morphologic feature of airway epithelium following inhaled pollutant challenge (Rogers and Jeffery 1986; Harkema and Hotchkiss 1991; Jany et al. 1991; Hotchkiss et al. 1998; Cho et al. 1999), and is considered a pathologic response following airway epithelial injury (Wagner et al. 2001; Puchelle et al. 2006). Adult monkeys developed mucous cell metaplasia in the anterior nasal airways following both acute (6 days, 8h/day) and chronic (90 days, 8h/day) daily exposure to 0.3ppm ozone (Harkema et al. 1987a). In the present study, neither 1 cycle O_3 nor 11 cycle O_3 ozone exposure caused mucous cell hyperplasia or metaplasia in infant monkeys. In fact, both 1 cycle O_3 and 11 cycle O_3 exposures caused a decrease in the amount of stored intraepithelial mucosubstances in the ciliated RE lining the anterior MT. Our results may be related to age-related differences in the ability of the infant nasal airways to respond to oxidant pollutant exposure. However, since ozone exposure induces mucus hypersecretion in respiratory airways, it is also possible that the higher ozone concentration (0.5 ppm versus 0.3ppm) used for the infant exposures caused a short-term depletion of stored intraepithelial mucosubstances (Nogami et al. 2000).

Squamous metaplasia and hyperplasia of the nasal epithelium have been reported as sequelae of chronic exposure to oxidant pollutants in children (Calderon-Garciduenas et al. 2001; Calderon-Garciduenas et al. 2001). In the present study, monkeys exposed to 11 cycle O_3 exhibited focal areas of epithelial hyperplasia and squamous metaplasia of the ciliated RE lining the anterior MT. This metaplastic change resulted in an increase in epithelial thickness, and was also associated with a loss of surface cilia and a reduction in the amount of stored intraepithelial mucosubstances. These morphologic changes in the nasal airways result in an epithelium that is locally more resistant to uptake of reactive,

pollutant gases (Kimbell et al. 1997), and may serve as protective adaptations. However, these alterations may also serve to disrupt nasal mucociliary clearance and reactive gas absorption in the anterior nasal airways. This loss of normal nasal function could potentially result in delivery of toxic pollutants to more distal sites in the respiratory tract, including the conducting airways and pulmonary parenchyma (Brain 1970; Morgan and Frank 1977). Furthermore, the loss of functional ciliated RE could lead to increased transit times for airborne toxicants trapped in the nasal airways, possibly resulting in prolonged contact with the nasal epithelium and enhanced upper airway toxicity.

We previously reported that infant monkeys exposed episodically to 5 cycles of ozone (0.5 ppm, 8h/day) exhibited persistent neutrophilic rhinitis, similar to that observed following 1 cycle O_3-exposure (Carey et al. 2007). This is in contrast to adult monkeys exposed to 0.3 ppm ozone daily for 6 or 90 days. While adult monkeys exposed for 6 days developed acute neutrophilic rhinitis, this inflammatory response was not observed in animals exposed for 90 days (Harkema et al. 1987a). Another purpose of the present study was to determine the effect of a longer period of episodic ozone exposure on the inflammatory and epithelial responses of the infant monkey nasal cavity. For these experiments, we designed a longer regimen of episodic exposure (11-cycles) to a high ambient concentration of ozone (0.5 ppm, 8h/day). These protocols were designed to mimic intermittent exposures to clean and polluted air, which represents the nature of exposure experienced by people in high pollution regions (Sram et al. 1996). In the present study, we found that infant monkeys exposed to 11 cycle O_3 had a similar distribution and magnitude of neutrophilic rhinitis to that observed in 1 cycle O_3-exposed monkeys. There was no significant difference in neutrophil numeric cell density along

the anterior MT between 1 cycle O_3- and 11 cycle O_3-exposed monkeys (Figure 4-5). The presence of epithelial hyperplasia and squamous metaplasia did not influence ozone-induced inflammation during 11 cycle O_3 exposure. Other reports have also described a decrease in pulmonary inflammation and pro-inflammatory indicators following multi-day ozone exposures (Plopper, Charles G. and Paige 1999; Wesselkamper et al. 2001; Kirschvink et al. 2002). While the mechanisms underlying this acquired tolerance to chronic ozone exposure remain unclear, several reports have hypothesized that epithelial remodeling may serve a protective role against subsequent oxidant pollutant challenge. We did not observe an attenuated inflammatory response in the nasal airways following 11 cycle O_3 exposure, despite the development of significant epithelial remodeling at the site of inflammation. These results indicate that the presence of ozone-induced epithelial hyperplasia alone does not attenuate the inflammatory response to subsequent ozone challenge in infant monkeys, and further suggest that the nasal airways in infant monkeys remain susceptible to oxidant pollutant-induced inflammation following episodic exposures.

Maintenance of neutrophilia at a site of inflammation can be due to persistent chemokine-mediated recruitment of neutrophils from circulation, cytokine-mediated enhancement of neutrophil survival (Dibbert et al. 1999), or a combination of these factors. While altered neutrophil survival has been demonstrated to play a role in the development of pulmonary tolerance to ozone (Fievez et al. 2001), given the duration of the episodic exposure period in our studies, the persistent rhinitis observed following 11 cycle O_3 exposure is most likely the result of continuous or repeated neutrophil recruitment. It is possible that the higher ozone concentration used in our studies

inhibited the development of tolerance. However, these results may also reflect a fundamental difference in the nasal epithelial response to repeated cycles of injury and repair caused by episodic ozone exposure. Future studies are needed to examine the mechanisms behind this differential response to episodic versus daily ozone exposures, and the possible implications toward the nature of ozone exposure experienced by children.

The present study was also designed to test the hypothesis that the site-specificity of ozone-induced epithelial injury, repair, and remodeling in the developing nasal airways of infant monkeys is due, in part, to local differences in the steady-state levels of low molecular weight nasal antioxidants. We compared the baseline and post-exposure tissue concentrations of AH_2, UA, GSH, and GSSG at an intranasal site of ozone-induced injury and repair (anterior MT), and at two sites at which no exposure related morphologic changes were observed (posterior MT, anterior ET). The only exposure-related change in antioxidant levels was an increase in GSH concentration following 11-cycle O_3 exposure. In the lungs, site-specificity of injury and repair induced by inhaled xenobiotics frequently correlates with local changes in the regulation of GSH. Regional changes in GSH status have been correlated with toxicant-induced responses in the lungs of monkeys and rats exposed to ozone (Duan et al. 1996; Plopper, C. G. et al. 1998). Similar GSH responses have been documented in rat lungs following exposure to hyperoxia (Kimball et al. 1976), and in mice exposed to naphthalene (West et al. 2000). A correlation between oxidant pollutant-induced mucosal injury and GSH upregulation has also been demonstrated in the nasal airways of rats exposed to cigarette smoke (Maples et al. 1993). In our study, the ozone-induced upregulation in GSH levels was

not limited to the site of ozone-induced injury, but was found in samples taken throughout the nasal cavity. Furthermore, while no significant differences were discerned among the three regions, the magnitude of this upregulation in GSH concentrations was greatest in the posterior MT, a site with no observed exposure-related morphologic changes. This suggests that the upregulation in mucosal GSH concentration observed in our study was not a site-specific response to ozone-induced injury, but rather a widespread nasal mucosal response to ozone exposure itself.

Acute ozone exposure initially causes site-specific GSH depletion in the respiratory tract (Plopper, C. G. et al. 1998). We hypothesize that the increase in GSH observed following 11 cycle O_3 exposure is an adaptive response to repeated cycles of GSH depletion. Intracellular GSH concentration is maintained by a balance among GSH consumption/degradation, GSH redox cycling (via glutathione reductase), efflux of GSH and GSSG into the ELF, uptake of intact GSH (primarily from the liver), and *de novo* GSH synthesis (van Klaveren et al. 1997). Following acute ozone exposure and GSH consumption, subsequent upregulation of GSH is, at least in part, the result of local *de novo* synthesis. We found only a slight increase in the mRNA levels of the catalytic subunit of GCL, the rate-limiting enzyme in de novo GSH synthesis, in animals exposed to 11 cycle O_3. While the increase in GCL-C expression may explain part of the increase in GSH, other regulators of GSH were also likely involved. Oxidative stress activates signal transduction pathways that lead to activation and nuclear translocation of redox-sensitive transcription factors, including activator protein-1 (AP-1) and nuclear factor-erythroid 2 related factor 2 (Nrf2). In addition to GCL-C and GCL-M, AP-1 and Nrf2 activation controls expression of several other GSH-regulatory genes, including γ-

glutamyl transpeptidase, glutathione reductase, and glutathione synthase (Chan and Kwong 2000; Cho et al. 2006). Increased expression of these genes would promote increases in GSH content via GCL-independent mechanisms (Dickinson and Forman 2002). Changes in cellular redox state can also influence GCL activity in the absence of a transcriptional component. Additional studies are needed to fully elucidate the mechanisms behind ozone-induced GSH upregulation in monkeys.

In the regions lined by respiratory epithelium (anterior and posterior MT), the increase in steady state GSH levels occurred with no significant change in GSSG concentration. In contrast, there was a significant increase in GSSG concentration in the anterior ethmoturbinate, a region lined primarily by olfactory epithelium. This regional difference in glutathione disulfide concentration following 11 cycle O_3 exposure may reflect a local difference in the regulation of GSH and GSSG. Glutathione reductase is an intracellular NADPH-dependent enzyme that catalyzes the reduction of GSSG to GSH. In the rat, glutathione reductase activity is lower in olfactory epithelium than in respiratory epithelium (Reed et al. 2003). Lower glutathione reductase activity could result in higher intracellular concentrations of GSSG, particularly following oxidant challenge. However, it is also possible that reductions in GSH and GSSG efflux rates could contribute to increases in intracellular GSH and GSSG. Future studies that compare intracellular and ELF GSH and GSSG levels would provide valuable information regarding ozone-induced GSH turnover. Regional differences in other GSH regulatory enzymes have not been evaluated for the nasal airways of monkeys.

While the exact role of GSH in cell proliferation remains unclear, a growing body of evidence supports a role for GSH in cell cycle regulation and cell proliferation.

Previous reports indicate that upregulation and subcellular localization of GSH are important in the control of G_1/S transition (Markovic et al. 2007) and DNA synthesis (Thelander and Reichard 1979). The importance of GSH in oxidant-induced cell proliferation has been previously documented in cultured bronchial epithelial cells. Cigarette smoke condensate causes a dose-dependent increase in 5-bromo-2-deoxyuridine (BrdU) incorporation in primary bronchial epithelial cells *in vitro*. This effect is inhibited by glutathione depletion (Luppi et al. 2005). Another recent investigation examined the role of GSH in Nrf2-mediated cell proliferation. Using type II pneomocytes from $Nrf2^{-/-}$ mice, these investigators demonstrate that Nrf2-deficiency leads to impaired cell proliferation *in vitro*, and GSH supplementation restores replicative capacity to $Nrf2^{-/-}$ cells (Reddy et al. 2007). We found a positive correlation between the total numeric density of epithelial cells lining the anterior MT, a measure of epithelial hyperplasia, and the intracellular concentration of GSH at that site. While these experiments were not designed to elucidate the mechanisms behind ozone-induced remodeling, they establish a temporal relationship between increases in the steady state, intracellular levels of GSH and morphologic evidence of cell proliferation. It is important to note, however, that positive correlation analysis does not establish causation, and that GSH upregulation and the onset of epithelial hyperplasia and squamous metaplasia may be coincidental events, both under the influence of additional factors.

We have shown that exposure to repeated episodes of ozone caused acute epithelial injury, epithelial hyperplasia, and squamous metaplasia in the nasal airways of infant monkeys. The nature and distribution of these nasal lesions were consistent with those observed in the nasal airways of children inhabiting chronically polluted

environments. The onset of ozone-induced epithelial remodeling coincides with the ozone-induced upregulation in the steady-state intracellular levels of GSH in the nasal airways. These local biochemical changes in the nasal mucosa correlate with ozone-induced epithelial hyperplasia, and may confer a permissive effect on toxicant-induced cell proliferation. Despite the presence of these ozone-induced morphologic and biochemical alterations, the infant nasal cavity appears to remain susceptible to injury and inflammation induced by repeated ozone exposures. Our results raise concerns about the nature of the mucosal responses to repeated oxidant pollutant exposures in the nasal airways of children.

REFERENCES

Abel, K., D. M. Rocke, B. Chohan, L. Fritts and C. J. Miller (2005). "Temporal and anatomic relationship between virus replication and cytokine gene expression after vaginal simian immunodeficiency virus infection." *J Virol* **79**(19): 12164-72.

Ballinger, C. A., R. Cueto, G. Squadrito, J. F. Coffin, L. W. Velsor, W. A. Pryor and E. M. Postlethwait (2005). "Antioxidant-mediated augmentation of ozone-induced membrane oxidation." *Free radical biology & medicine.* **38**(4): 515-26.

Brain, J. D. (1970). "The uptake of inhaled gases by the nose." *Annals of Otology, Rhinology & Laryngology* **79**(3): 529-39.

Calderon-Garciduenas, L., A. Osorno-Velazquez, H. Bravo-Alvarez, R. Delgado-Chavez and R. Barrios-Marquez (1992). "Histopathologic changes of the nasal mucosa in southwest Metropolitan Mexico City inhabitants." *American Journal of Pathology* **140**(1): 225-32.

Calderon-Garciduenas, L., A. Rodriguez-Alcaraz, R. Garcia, G. Barragan, A. Villarreal-Calderon and M. C. Madden (1999). "Cell proliferation in nasal respiratory epithelium of people exposed to urban pollution." *Carcinogenesis* **20**(3): 383-9.

Calderon-Garciduenas, L., A. Rodriguez-Alcaraz, R. Garcia, L. Ramirez and G. Barragan (1995). "Nasal inflammatory responses in children exposed to a polluted urban atmosphere." *Journal of Toxicology & Environmental Health* **45**(4): 427-37.

Calderon-Garciduenas, L., A. Rodriguez-Alcaraz, R. Garcia, G. Sanchez, G. Barragan, R. Camacho and L. Ramirez (1994). "Human nasal mucosal changes after exposure to urban pollution." *Environmental Health Perspectives* **102**(12): 1074-80.

Calderon-Garciduenas, L., A. Rodriguez-Alcaraz, G. Valencia-Salazar, A. Mora-Tascareno, R. Garcia, N. Osnaya, A. Villarreal-Calderon, R. B. Devlin and T. Van Dyke (2001). "Nasal biopsies of children exposed to air pollutants." *Toxicol Pathol* **29**(5): 558-64.

Calderon-Garciduenas, L., G. Valencia-Salazar, A. Rodriguez-Alcaraz, T. M. Gambling, R. Garcia, N. Osnaya, A. Villarreal-Calderon, R. B. Devlin and J. L. Carson (2001). "Ultrastructural nasal pathology in children chronically and sequentially

exposed to air pollutants." *American Journal of Respiratory Cell & Molecular Biology* **24**(2): 132-8.

Carey, S. A., K. R. Minard, L. L. Trease, J. G. Wagner, G. J. M. Garcia, C. A. Ballinger, J. S. Kimbell, C. Plopper, R. A. Corley, E. M. Postlethwait and J. R. Harkema (2007). "Three-Dimensional Mapping of Ozone-Induced Injury in the Nasal Airways of Monkeys Using Magnetic Resonance Imaging and Morphometric Techniques." *Toxicologic Pathology* **35**(1): 27-40.

Castleman, W. L., D. L. Dungworth, L. W. Schwartz and W. S. Tyler (1980). "Acute respiratory bronchiolitis: an ultrastructural and autoradiographic study of epithelial cell injury and renewal in rhesus monkeys exposed to ozone." *Am J Pathol* **98**(3): 811-40.

Chan, J. Y. and M. Kwong (2000). "Impaired expression of glutathione synthetic enzyme genes in mice with targeted deletion of the Nrf2 basic-leucine zipper protein." *Biochim Biophys Acta* **1517**(1): 19-26.

Cho, H. Y., J. A. Hotchkiss and J. R. Harkema (1999). "Inflammatory and epithelial responses during the development of ozone-induced mucous cell metaplasia in the nasal epithelium of rats." *Toxicological Sciences* **51**(1): 135-45.

Cho, H. Y., S. P. Reddy and S. R. Kleeberger (2006). "Nrf2 defends the lung from oxidative stress." *Antioxid Redox Signal* **8**(1-2): 76-87.

Cross, C. E., A. van der Vliet, C. A. O'Neill, S. Louie and B. Halliwell (1994). "Oxidants, antioxidants, and respiratory tract lining fluids." *Environ Health Perspect* **102 Suppl 10**: 185-91.

Devlin, R. B., W. F. McDonnell, R. Mann, S. Becker, D. E. House, D. Schreinemachers and H. S. Koren (1991). "Exposure of humans to ambient levels of ozone for 6.6 hours causes cellular and biochemical changes in the lung." *Am J Respir Cell Mol Biol* **4**(1): 72-81.

Dibbert, B., M. Weber, W. H. Nikolaizik, P. Vogt, M. H. Schoni, K. Blaser and H. U. Simon (1999). "Cytokine-mediated Bax deficiency and consequent delayed neutrophil apoptosis: a general mechanism to accumulate effector cells in inflammation." *Proc Natl Acad Sci U S A* **96**(23): 13330-5.

Dickinson, D. A. and H. J. Forman (2002). "Glutathione in defense and signaling: lessons from a small thiol." *Ann N Y Acad Sci* **973**: 488-504.

Duan, X., A. R. Buckpitt, K. E. Pinkerton, C. Ji and C. G. Plopper (1996). "Ozone-induced alterations in glutathione in lung subcompartments of rats and monkeys." *American Journal of Respiratory Cell & Molecular Biology* **14**(1): 70-5.

Duan, X., A. R. Buckpitt and C. G. Plopper (1993). "Variation in antioxidant enzyme activities in anatomic subcompartments within rat and rhesus monkey lung." *Toxicol Appl Pharmacol* **123**(1): 73-82.

Fievez, L., N. Kirschvink, S. Dogne, F. Jaspar, M. P. Merville, V. Bours, P. Lekeux and F. Bureau (2001). "Impaired accumulation of granulocytes in the lung during ozone adaptation." *Free Radic Biol Med* **31**(5): 633-41.

Frischer, T. M., J. Kuehr, A. Pullwitt, R. Meinert, J. Forster, M. Studnicka and H. Koren (1993). "Ambient ozone causes upper airways inflammation in children." *Am Rev Respir Dis* **148**(4 Pt 1): 961-4.

Graham, D., F. Henderson and D. House (1988). "Neutrophil influx measured in nasal lavages of humans exposed to ozone." *Arch Environ Health* **43**(3): 228-33.

Graham, D. E. and H. S. Koren (1990). "Biomarkers of inflammation in ozone-exposed humans. Comparison of the nasal and bronchoalveolar lavage." *American Review of Respiratory Disease* **142**(1): 152-6.

Harkema, J. R., S. A. Carey and J. G. Wagner (2006). "The nose revisited: a brief review of the comparative structure, function, and toxicologic pathology of the nasal epithelium." *Toxicol Pathol* **34**(3): 252-269.

Harkema, J. R. and J. A. Hotchkiss (1991). "In vivo effects of endotoxin on nasal epithelial mucosubstances: quantitative histochemistry." *Exp Lung Res* **17**(4): 743-61.

Harkema, J. R., J. A. Hotchkiss, E. B. Barr, C. B. Bennett, M. Gallup, J. K. Lee and C. Basbaum (1999). "Long-lasting effects of chronic ozone exposure on rat nasal epithelium." *Am J Respir Cell Mol Biol* **20**(3): 517-29.

Harkema, J. R., J. A. Hotchkiss and R. F. Henderson (1989). "Effects of 0.12 and 0.80 ppm ozone on rat nasal and nasopharyngeal epithelial mucosubstances: quantitative histochemistry." *Toxicologic Pathology* **17**(3): 525-35.

Harkema, J. R., C. G. Plopper, D. M. Hyde and J. A. St George (1987). "Regional differences in quantities of histochemically detectable mucosubstances in nasal, paranasal, and nasopharyngeal epithelium of the bonnet monkey." *Journal of Histochemistry & Cytochemistry* **35**(3): 279-86.

Harkema, J. R., C. G. Plopper, D. M. Hyde, J. A. St George and D. L. Dungworth (1987). "Effects of an ambient level of ozone on primate nasal epithelial mucosubstances. Quantitative histochemistry." *American Journal of Pathology* **127**(1): 90-6.

Harkema, J. R., C. G. Plopper, D. M. Hyde, J. A. St George, D. W. Wilson and D. L. Dungworth (1987). "Response of the macaque nasal epithelium to ambient levels of ozone. A morphologic and morphometric study of the transitional and respiratory epithelium." *American Journal of Pathology* **128**(1): 29-44.

Hotchkiss, J. A., R. Hilaski, H. Cho, K. Regan, P. Spencer, K. Slack and J. R. Harkema (1998). "Fluticasone propionate attenuates ozone-induced rhinitis and mucous cell metaplasia in rat nasal airway epithelium." *American Journal of Respiratory Cell & Molecular Biology* **18**(1): 91-9.

Hyde, D. M., D. J. Magliano and C. G. Plopper (1991). "Morphometric assessment of pulmonary toxicity in the rodent lung." *Toxicologic pathology.* **19**(4): 428-46.

Hyde, D. M., C. Plopper, J. A. St George and J. R. Harkema (1990). Morphometric cell biology of airspace epithelium. Electron Microscopy of the Lung. D. E. Schraufnagel. New York, Marcel Dekker: 1-120.

Jany, B., M. Gallup, T. Tsuda and C. Basbaum (1991). "Mucin gene expression in rat airways following infection and irritation." *Biochem Biophys Res Commun* **181**(1): 1-8.

Kepler, G. M., D.R. Joyner, A. Fleishman, R.B. Richardson, E.A. Gross, K.T. Morgan, M.N. Godo, and J.S. Kimbell (1995). "Method for obtaining accurate geometrical coordinates on nasal airways for computer dosimetry modeling and lesion mapping,." *Inhal Toxicol* **7**: 1207-1224.

Kim, J. J. (2004). "Ambient air pollution: health hazards to children." *Pediatrics* **114**(6): 1699-707.

Kimball, R. E., K. Reddy, T. H. Peirce, L. W. Schwartz, M. G. Mustafa and C. E. Cross (1976). "Oxygen toxicity: augmentation of antioxidant defense mechanisms in rat lung." *Am J Physiol* **230**(5): 1425-31.

Kimbell, J. S., E. A. Gross, R. B. Richardson, R. B. Conolly and K. T. Morgan (1997). "Correlation of regional formaldehyde flux predictions with the distribution of formaldehyde-induced squamous metaplasia in F344 rat nasal passages." *Mutat Res* **380**(1-2): 143-54.

Kirschvink, N., L. Fievez, F. Bureau, G. Degand, G. Maghuin-Rogister, N. Smith, T. Art and P. Lekeux (2002). "Adaptation to multiday ozone exposure is associated with a sustained increase of bronchoalveolar uric acid." *Free Radical Research* **36**(1): 23-32.

Koren, H. S., G. E. Hatch and D. E. Graham (1990). "Nasal lavage as a tool in assessing acute inflammation in response to inhaled pollutants." *Toxicology* **60**(1-2): 15-25.

Luppi, F., J. Aarbiou, S. van Wetering, I. Rahman, W. I. de Boer, K. F. Rabe and P. S. Hiemstra (2005). "Effects of cigarette smoke condensate on proliferation and wound closure of bronchial epithelial cells in vitro: role of glutathione." *Respiratory Research* **6**: 140.

Maples, K. R., K. J. Nikula, B. T. Chen, G. L. Finch, W. C. Griffith and J. R. Harkema (1993). "Effects of Cigarette Smoke on the Glutathione Status of the Upper and Lower Respiratory Tract of Rats." *Inhal Toxicol* **5**: 389-401.

Markovic, J., C. Borras, A. Ortega, J. Sastre, J. Vina and F. V. Pallardo (2007). "Glutathione is recruited into the nucleus in early phases of cell proliferation." *J Biol Chem* **282**(28): 20416-24.

Morgan, M. and R. Frank (1977). Uptake of pollutant gases by the respiratory system. Respiratory Defense Mechanisms. J. D. Brain, D. F. Proctor and L. M. Reid. New York, NY, Marcell Dekker.

Nikula, K. J., D. W. Wilson, S. N. Giri, C. G. Plopper and D. L. Dungworth (1988). "The response of the rat tracheal epithelium to ozone exposure. Injury, adaptation, and repair." *Am J Pathol* **131**(2): 373-84.

Nogami, H., H. Aizawa, K. Matsumoto, H. Nakano, H. Koto, H. Miyazaki, T. Hirose, S. Nishima and N. Hara (2000). "Neutrophil elastase inhibitor, ONO-5046 suppresses ozone-induced airway mucus hypersecretion in guinea pigs." *Eur J Pharmacol* **390**(1-2): 197-202.

Plopper, C. G., F. P. Chu, C. J. Haselton, J. Peake, J. Wu and K. E. Pinkerton (1994). "Dose-dependent tolerance to ozone. I. Tracheobronchial epithelial reorganization in rats after 20 months' exposure." *American Journal of Pathology* **144**(2): 404-20.

Plopper, C. G., G. E. Hatch, V. Wong, X. Duan, A. J. Weir, B. K. Tarkington, R. B. Devlin, S. Becker and A. R. Buckpitt (1998). "Relationship of inhaled ozone concentration to acute tracheobronchial epithelial injury, site-specific ozone dose, and glutathione depletion in rhesus monkeys." *Am J Respir Cell Mol Biol* **19**(3): 387-99.

Plopper, C. G. and R. C. Paige (1999). Acute and Chronic Effects of Ozone in Animal Models. Air Pollution and Health. S. T. Holgate, J. M. Samet, H. S. Koren and R. L. Maynard. London, Academic Press: 531-557.

Puchelle, E., J. M. Zahm, J. M. Tournier and C. Coraux (2006). "Airway epithelial repair, regeneration, and remodeling after injury in chronic obstructive pulmonary disease." *Proc Am Thorac Soc* **3**(8): 726-33.

Reddy, N. M., S. R. Kleeberger, H. Y. Cho, M. Yamamoto, T. W. Kensler, S. Biswal and S. P. Reddy (2007). "Deficiency in Nrf2-GSH signaling impairs type II cell growth and enhances sensitivity to oxidants." *Am J Respir Cell Mol Biol* **37**(1): 3-8.

Reed, C. J., D. A. Robinson and E. A. Lock (2003). "Antioxidant status of the rat nasal cavity." *Free Radic Biol Med* **34**(5): 607-15.

Rogers, D. F. and P. K. Jeffery (1986). "Inhibition of cigarette smoke-induced airway secretory cell hyperplasia by indomethacin, dexamethasone, prednisolone, or hydrocortisone in the rat." *Exp Lung Res* **10**(3): 285-98.

Sram, R. J., I. Benes, B. Binkova, J. Dejmek, D. Horstman, F. Kotesovec, D. Otto, S. D. Perreault, J. Rubes, S. G. Selevan, I. Skalik, R. K. Stevens and J. Lewtas (1996). "Teplice program--the impact of air pollution on human health." *Environ Health Perspect* **104 Suppl 4**: 699-714.

Thelander, L. and P. Reichard (1979). "Reduction of ribonucleotides." *Annu Rev Biochem* **48**: 133-58.

van Klaveren, R. J., M. Demedts and B. Nemery (1997). "Cellular glutathione turnover in vitro, with emphasis on type II pneumocytes." *Eur Respir J* **10**(6): 1392-1400.

Wagner, J. G., J. A. Hotchkiss and J. R. Harkema (2001). "Effects of ozone and endotoxin coexposure on rat airway epithelium: potentiation of toxicant-induced alterations." *Environ Health Perspect* **109 Suppl 4**: 591-8.

Wang, Y., K. Abel, K. Lantz, A. M. Krieg, M. B. McChesney and C. J. Miller (2005). "The Toll-like receptor 7 (TLR7) agonist, imiquimod, and the TLR9 agonist, CpG ODN, induce antiviral cytokines and chemokines but do not prevent vaginal transmission of simian immunodeficiency virus when applied intravaginally to rhesus macaques." *J Virol* **79**(22): 14355-70.

Wesselkamper, S. C., L. C. Chen, S. R. Kleeberger and T. Gordon (2001). "Genetic variability in the development of pulmonary tolerance to inhaled pollutants in inbred mice." *Am J Physiol Lung Cell Mol Physiol* **281**(5): L1200-9.

West, J. A., A. R. Buckpitt and C. G. Plopper (2000). "Elevated airway GSH resynthesis confers protection to Clara cells from naphthalene injury in mice made tolerant by repeated exposures." *J Pharmacol Exp Ther* **294**(2): 516-23.

Wilson, D. W., C. G. Plopper and D. L. Dungworth (1984). "The response of the macaque tracheobronchial epithelium to acute ozone injury. A quantitative ultrastructural and autoradiographic study." *Am J Pathol* **116**(2): 193-206.

Woodruff, T. J., D. A. Axelrad, A. D. Kyle, O. Nweke and G. G. Miller (2007). America's Children and the Environment. Washington, DC, United States Environmental Protection Agency: 1-176.

CHAPTER 5

ROLE OF GSH IN THE PATHOGENESIS OF OZONE-INDUCED EPITHELIAL HYPERPLASIA IN RAT NASAL AIRWAYS

INTRODUCTION

The governing hypothesis in these studies was that ozone-induced epithelial hyperplasia in the nasal airways of infant monkeys and rats is a glutathione-dependent process. In our previous studies, we demonstrated that chronic, episodic ozone exposure causes epithelial hyperplasia and squamous metaplasia in the anterior nasal airways of infant monkeys, and that this hyperplastic response is correlated with the local upregulation of intracellular glutathione (GSH) concentrations. Although the results from these studies demonstrate a temporal and spatial association between ozone-induced epithelial hyperplasia and local GSH concentrations in the nasal airways, they do not establish a mechanistic relationship among oxidant exposure, cell survival and proliferation, and the regulation of steady-state GSH levels.

Oxidant-induced nasal epithelial hyperplasia is a multifactorial process. Early exposures to ozone cause epithelial necrosis in the nasal airways (Hotchkiss et al. 1997). The resulting epithelial proliferation is a response of the surviving epithelial cell population to regenerate and repair (Henderson et al. 1993). The early responses to ozone exposure must include mechanisms that can enhance cell survival following oxidant challenge. Ozone exposure leads to the rapid induction of oxidant response genes in the respiratory airways. Heme-oxygenase 1 (HO-1) and inducible nitric oxide synthase (iNOS) are both inducible forms of anti-oxidant enzymes that are upregulated early during oxidant exposure (Foucaud et al. 2006), and are considered common indicators of oxidative stress in the respiratory airways (Morse and Choi 2005). Both enzymes confer cytoprotective benefits during early ozone exposures that may provide protection to surviving epithelial cells during repeated oxidant pollutant exposures (Joshi

et al. 1999; Jin and Choi 2005). Furthermore, both enzymes may be directly related to control of cell cycle and cell proliferation following oxidant exposure or oxidant-induced cytokine stimulation (Romanska et al. 2002; Colombrita et al. 2003).

Ozone exposure in humans causes secretion of pro-inflammatory cytokines and chemokines into the respiratory airways. Many of these, including IL-6, TNF-α, and IL-8, have been implicated in cellular processes related to ozone-induced epithelial injury and repair (Koren et al. 1989; Devlin et al. 1991; Devlin 1993). Both TNF-α and IL-6 are important regulators of inflammation following ozone exposure (Pendino et al. 1994; Leikauf et al. 1995). IL-6 also plays an important role in the regulation of epithelial repair and cell proliferation in the pulmonary airways following ozone exposure. Yu, et al., demonstrated that ozone-induced cell proliferation is inhibited in the pulmonary airways of IL-6 knockout mice and in mice treated with anti-IL-6 neutralizing antibodies (Yu et al. 2002). IL-8, a member of the CXC chemokine family, is a potent neutrophil chemoattractant molecule in humans and non-human primates. Studies conducted in monkeys (Hyde et al. 1992) and rats (Salmon et al. 1998) provide support for the contribution of neutrophil chemotaxis in the pathogenesis of lung injury and repair following short-term ozone exposure. The specific functions of these cytokines and chemokines in the pathogenesis of ozone-induced nasal epithelial hyperplasia have not been determined.

The same factors that contribute to activation of cytoprotective and pro-inflammatory cell signaling cascades may also lead to alterations in the intracellular regulation of GSH. One of the effects of oxidative stress is the activation of antioxidant response transcription factors, including nuclear factor E2-related factor-2 (Nrf2). In

humans, activation of Nrf2 leads to nuclear translocation and binding to promoter sequences of several antioxidant response genes. Among these are the genes for several GSH synthetic enzymes, including the catalytic and modulatory subunits of glutamate cysteine ligase (GCL-C and GCL-M), glutathione synthase (GS), and γ-glutamyltranspeptidase (GGT) (Lu 2008). Increased expression of these enzymes is one possible mechanism for local upregulation in GSH levels observed in the nasal airways of infant monkeys following ozone exposure (Chapter 4), as well as similar mucosal responses following oxidant exposure in the nasal airways of rats (Maples et al. 1993) and pulmonary airways of monkeys (Plopper et al. 1998).

Oxidative (or nitrosative) stress can also cause DNA lesions or inhibit DNA repair mechanisms in susceptible cell populations. This genotoxicity can lead to oxidant-induced cell cycle arrest at either of the two major cell cycle checkpoints, G_1/S or G_2/M. Recent studies provide evidence for the role of intracellular GSH in mediating cell cycle progression through G_1/S (Lu et al. 2007) or G_2/M (Reddy et al. 2008) following oxidative stress. Previous studies also provide evidence supporting a role for GSH upregulation in progression through G_1/S transition (Shaw and Chou 1986; Kavanagh et al. 1990). Results from recent *in vitro* studies indicate that GSH depletion inhibits oxidant-induced cell proliferation in cultured human bronchial epithelial cells, and that the cysteine donor N-acetylcysteine, a precursor to GSH synthesis, restores replicative capacity (Luppi et al. 2005).

The two studies described in this chapter were designed to test the hypotheses that (1) early ozone exposures cause oxidative stress, expression of pro-inflammatory cytokines and chemokines, and expression of GSH synthetic enzymes in the nasal

airways of immature rats prior to the development of ozone-induced epithelial hyperplasia, (2) that these early molecular responses would lead to upregulation of intracellular GSH concentrations in rat nasal tissues, and that (3) inhibition of GSH synthesis during ozone exposures would inhibit the development of ozone-induced epithelial hyperplasia in the anterior nasal airways of immature rats. In ***Study 1***, we examined the changes in the expression levels of indicators of oxidative stress (HO-1, iNOS), pro-inflammatory cytokines (TNF-α, IL-6), CXC chemokines (MIP-2, CINC), and GSH synthesis enzymes (GCL-C, GCL-M) in the nasal airways of rats, and compared these with the timing of BrdU incorporation, an indicator of cell proliferation, following 1 day and 2 days of daily ozone exposure. In ***Study 2***, we examined the changes in intracellular concentrations of GSH, glutathione disulfide (GSSG), and ascorbate (AH_2) during the development of ozone-induced nasal epithelial hyperplasia. Finally, we examined the effect of potent GSH synthesis inhibition (buthionine sulfoximine, an inhibitor of GCL) on intracellular GSH concentrations, and on the development of ozone-induced epithelial hyperplasia.

STUDY 1: EARLY CELLULAR AND MOLECULAR EVENTS PRECEEDING OZONE-INDUCED EPITHELIAL HYPERPLASIA IN THE NASAL AIRWAYS OF IMMATURE RATS

MATERIALS AND METHODS

Animals, Ozone Exposure, and BrdU Treatment

Eighteen male Fischer 344/N rats (Harlan Sprague-Dawley, Indianapolis, IN), 28-days-old, were used in ***Study 1***. All animals were free of pathogens, and used in accordance with guidelines set forth by the All-University Committee on Animal Use and Care at Michigan State University. Rats were housed, three animals per cage, in polycarbonate shoebox-type cages with filter tops. Water and food (Tek-Lab 1640, Harlan Sprague-Dawley) were provided *ad libitum*. Rats were maintained on a 12-h light/12-h dark cycle, in a temperature- and humidity-controlled environment (16-25°C; 40-70% relative humidity).

All inhalation exposures were conducted in whole-body exposure chambers (HC-1000; Lab Products, Maywood, NJ). The rats were acclimated to the exposure chambers, supplied with filtered air (FA), for 8 hours on the day prior to the start of inhalation exposures. The rats were individually housed in rack-mounted stainless steel wire cages with free access to water during acclimation. The exposure chamber temperature, relative humidity, and light cycle were maintained as described earlier for animal housing.

To determine the effect of ozone exposure on the molecular responses of the nasal airways prior to the development of ozone-induced epithelial hyperplasia, we randomly assigned 18 rats to three experimental groups (n = 6/group). One group of rats was exposed to 0.8 ppm ozone for 8h/day for one day. A second group of rats was exposed to 0.8 ppm ozone for 8h/day for two consecutive days. A control group of rats was exposed to FA (0 ppm) for 8h/day for one day. In previous chapters, we utilized a concentration of 0.5 ppm ozone for non-human primate studies. We selected a higher ozone concentration (0.8 ppm) for the rodent experiments based on comparative dosimetry

studies which suggest that the respiratory airways of rodents are less susceptible to the health effects of ozone exposure, and require up to five-fold higher ozone concentrations to elicit comparable levels of respiratory injury (Hatch et al. 1994). Three animals from each group were dedicated for nasal histopathology and morphometry. The remaining three animals from each group were dedicated for nasal RNA isolation and mRNA analysis. At the end of the last day of exposure, each rat dedicated for nasal histopathology was injected with 5-bromo, 2-deoxyuridine (50mg/kg, intraperitoneally) to label cells in the S-phase (DNA synthesis) of the cell cycle. All rats in ***Study 1*** were euthanized two hours following the end of exposure.

Ozone exposures were conducted nightly, from 11:00 p.m. to 7:00 a.m., while the animals were most active. All exposures were conducted in the Inhalation Toxicology Exposure Laboratory of the University Research Containment Facility at Michigan State University. Food was removed, but animals had free access to water during ozone exposures. Ozone was generated with an OREC Model O3VI-O ozonizer (Ozone Research and Equipment, Phoenix, AZ), using compressed air (AirGas, Lansing, MI) as an oxygen source. Ozone was diluted with filtered room air and delivered to the ozone chambers through Teflon tubing. The total airflow through the exposure chambers was maintained at approximately 250 L/min, to provide 15 chamber air changes per hour. Chamber temperature and relative humidity were maintained at the same levels as during the chamber acclimation period. The concentration of ozone within the chamber was controlled by adjusting the voltage of the ultraviolet lamp within the ozonizer. Ozone concentration was monitored during exposure with ozone monitors (Model 1003-AH; Dasibi Environmental Corporation, Glendale, CA), and recorded with a strip chart

recorder (Model 707; Chrono-Log Corporation, Havertown, PA). The probes for sampling the exposure atmosphere were positioned in the breathing zone of the rats within the ozone exposure chambers. The chamber ozone concentrations during exposure to 0.8 ppm ozone were 0.786 $\pm$ 0.028 ppm (mean $\pm$ SD). The chamber ozone concentrations during exposure to filtered air were maintained at less than 0.050 ppm.

Necropsy and Tissue Preparation for Morphometric Analyses

Two hours following the end of exposure, rats were anesthetized with pentobarbital (50mg/kg, i.p.), and then killed by exsanguination via the abdominal aorta. After death, the head of each rat was removed from the carcass, and the eyes, lower jaw, skin, and musculature was removed. For animals in ***Study 1***, the entire nasal cavity was processed for histopathology. The nasal cavities were flushed in a retrograde manner through the nasopharyngeal orifice with 2ml of 10% neutral buffered formalin, and then immersed in a large volume of the same fixative for a minimum of 24 hours.

The formalin-fixed nasal cavities were decalcified in 13% formic acid for 5 days, and were then rinsed in reverse osmosis filtered water for 2 hours as previously described (Harkema et al. 1988). A tissue block was removed from the anterior aspect of the left nasal cavity by making two transverse cuts perpendicular to the hard palate. The first cut was made immediately posterior to the upper incisor tooth (Figure 5-1). The second cut was made at the level of the incisive papilla. The tissue blocks were embedded in paraffin, and 5μM-thick sections were cut from the anterior face of the block. Tissue sections from each animal were histochemically stained with hematoxylin and eosin (H&E) for routine histopathologic examination (results presented and discussed in ***Study***

2). Other tissue sections were immunohistochemically stained with anti-BrdU antibody (Becton Dickinson Immunocytometry Systems, San Jose, CA) to detect BrdU-labeled nuclei, and counter stained with hematoxylin (Johnson et al. 1990).

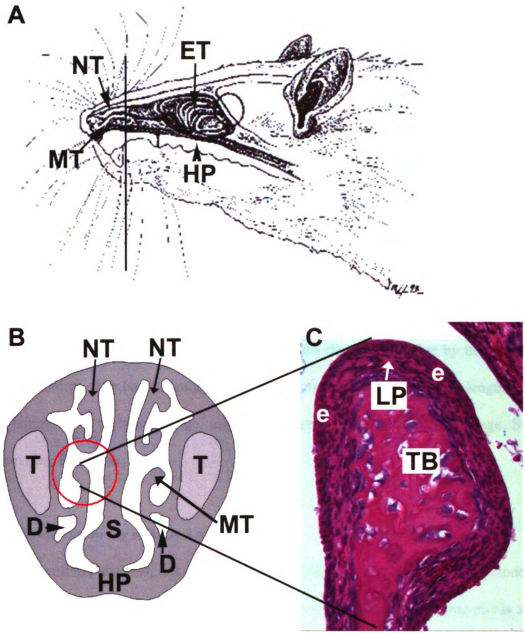

Figure 5-1. Anatomic location of nasal tissues selected for morphometric analyses. (A) Exposed right lateral wall of rat nasal cavity. MT = maxilloturbinate; NT = nasoturbinate; ET = ethmoturbinate; HP = hard palate. Vertical line indicates the anterior surface of the tissue block sectioned for morphometric analyses. (B) Diagram of the anterior face of a tissue block from the anterior nasal cavity. S = nasal septum; T = root of incisor tooth; D = nasolacrimal duct. Red circle illustrates the profile of the anterior maxilloturbinate. (C) Enlarged photomicrograph of the maxilloturbinate from a FA-exposed rat, illustrating the major tissue compartments. e = non-ciliated transitional epithelium (NTE); TB = turbinate bone; LP = lamina propria. The normal NTE is a non-ciliated cuboidal epithelium consisting of 1-2 cell layers.

Morphometry of Cellular Injury and Cell Proliferation

Non-ciliated transitional epithelium (NTE) overlying the dorsal aspect of the anterior maxilloturbinate (Figure 5-1) of each animal was analyzed using computerized image analysis and standard morphometric techniques (Hotchkiss, Harkema, Henderson Exp Lung Res 1991). In ***Study 1***, the BrdU labeling index was calculated as an indicator of reparative DNA synthesis in response to ozone-induced cell injury (Rajini et al. 1993). The number of BrdU-labeled epithelial cell nuclei was counted, divided by the total number of epithelial cell nuclei, and multiplied by 100 to yield the percentage of BrdU-labeled epithelial cell nuclei. The BrdU+ numeric cell density was calculated by counting the number of BrdU-labeled nuclei, and dividing this number by the length of the basal lamina. The basal lamina length was calculated from the contour length of the basal lamina on a digitized image, using image analysis software (Scion Image, Scion Corporation, Frederick, MD).

Tissue Preparation for mRNA Analysis

For mRNA analysis, rats exposed to filtered air for 1 day, or exposed to ozone for 1 or 2 days, were killed 2 hours following the end of exposure. These time points were chosen for pro-inflammatory, GSH synthesis, and oxidative stress gene expression analysis on the basis of previous findings in adult rats that neutrophilic inflammation and cellular injury reach peak levels within the first 2 days of daily ozone exposure (Cho et al. 1999). The head of each rat dedicated for mRNA isolation was removed and sagittally split 1mm to the right of midline. This sectioning process yielded a left nasal cavity, with the septum attached, and a free right nasal lateral wall. The right side of the nasal cavity

was immersed in 10ml RNA*Later* (Ambion; Austin, TX), and stored at room temperature for 24 hours, then stored at –20°C until microdissection.

Total RNA Isolation from Nasal Tissues

Maxilloturbinates were microdissected from RNA*Later*-preserved, frozen nasal cavities of each animal. Total cellular RNA was extracted from the maxilloturbinate according to the manufacturer's protocol (RN*Easy* Mini Kit, Qiagen, Valencia, CA). Briefly, tissues were homogenized in buffer RLT containing β-mercaptoethanol with a 5mm Rotor-sator homogenizer (PRO Scientific, Oxford, CT), and centrifuged at 12,000 x g for 3 minutes. RNA was purified from the supernatant using the RN*Easy* capture column. Samples were treated with Qiagen RNAse-Free DNAse set on the column for 30 minutes. Eluted RNA was diluted 1:5, and was quantified using a Genequant Pro spectrophotometer (BioCrom, Cambridge, England).

Reverse transcription was performed using High Capacity cDNA Reverse Transcription Kit reagents (Applied Biosystems, Foster City, CA). Each RT reaction was run in a 50-µl reaction volume containing 5-µg of total RNA and cDNA Master Mix prepared according to the manufacturer's protocol. Reverse transcription was performed in a GeneAmp PCR System 9700 Thermocycler PE (Applied Biosystems) at 25°C for 10 minutes, 37°C for 2 hours, and held at 4°C.

Real-time Reverse Transcription Polymerase Chain Reaction

cDNA samples were diluted to 5ng/µl and dispensed (in duplicate) into a 384-well reaction plate using the BioMek 2000 Automated Workstation (Beckman Coulter,

Fullerton, CA). Quantitative mRNA expression analyses were performed with the ABI PRISM 7900 HT Sequence Detection System using Taqman Gene Expression Assay reagents for GCL-C, GCL-M, iNos, HO-1, macrophage inflammatory protein 2 (MIP-2, CXCL2), and cytokine-induced neutrophil chemoattractant 1 (CINC, CXCL1) (Applied Biosystems). The cycling parameters were 48°C for 2 minutes, 95°C for 10 minutes, and 40 cycles of 95°C for 15 seconds followed by 60°C for 1 minute. All mRNA expression levels were reported as fold-increase (FI) of mRNA in experimental samples compared to a control sample. Real-time PCR amplifications were relatively quantified using the ΔΔCt method normalized to the geometric mean of 3 endogenous controls (18S, β-actin, and GAPDH). This normalization strategy has been utilized for accurate RT-PCR expression profiling in biological samples with small expression differences (Vandesompele et al. 2002). The delta Ct (ΔCt) value for the experimental sample is subtracted from the ΔCt value of the corresponding control sample (ΔΔCt). The FI in experimental samples relative to control samples is then calculated as: $FI = 2^{-\Delta\Delta Ct}$.

Statistical Analyses

All data were expressed as mean group value ± SEM. The differences among groups in ***Study 1*** were analyzed by one-way analysis of variance (ANOVA). Pairwise comparisons were performed *a priori* using Student-Newman-Keuls multiple comparisons test. The criterion for statistical significance was set to $p \leq 0.05$ for all analyses. All statistical analyses were performed using a commercial statistical software package (SigmaStat, SPSS Science, Chicago, IL).

RESULTS

Ozone-Induced BrdU Incorporation in Immature Rat Nasal Airways

Ozone exposure induced increases in the BrdU numeric cell density along the dorsal maxilloturbinate in rats exposed for 1-day (6.6-fold increase) and for 2-days (21-fold increase), compared to rats exposed to filtered air. Ozone exposure also induced similar increases in the BrdU labeling index following both 1-day and 2-day exposures (7-fold and 22-fold increases, respectively). The increases in both BrdU numeric cell density and BrdU labeling index following 2-day exposure were significantly different from both FA-exposed and 1-day ozone-exposed rats (Figure 5-2).

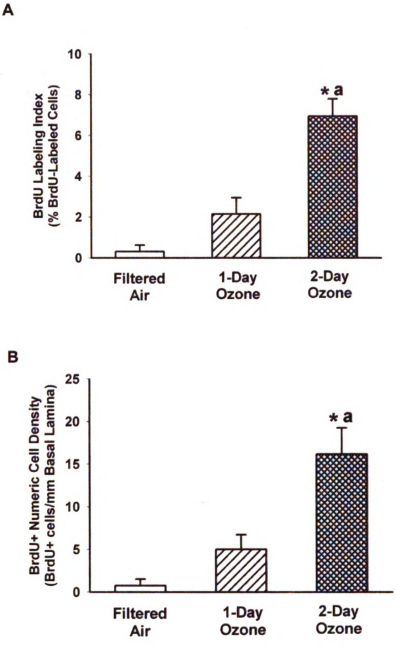

Figure 5-2. Effect of ozone exposure on BrdU labeling index (A) and BrdU numeric cell density in the NTE. Bars represent group mean $\pm$ SEM (n = 3/group). * = significantly different from FA-exposed rats ($p \leq 0.05$). a = Significantly different from rats exposed to 1-day ozone ($p \leq 0.05$).

Ozone-Induced Oxidative Stress Gene Expression

Ozone exposure induced an increase in HO-1 mRNA expression in rat nasal airways following both 1-day and 2-day exposures (2.7-fold and 2.4-fold increases, respectively) (Figure 5-3). Ozone caused an increase in iNOS mRNA expression in rat nasal mucosa following 2-day exposure (3.8-fold increase versus FA). The increase in iNOS expression in 2-day-exposed rats was significantly different from both FA-exposed and 1-day-exposed rats (Figure 5-3). There were no significant effects of ozone exposure on the expression of GCL-C or GCL-M following either 1-day or 2-day exposure (Figure 5-4).

Ozone-Induced Pro-Inflammatory Gene Expression

2-day ozone exposure induced a significant increase in the steady state levels of TNF-α mRNA (3.4-fold increase) and IL-6 mRNA (30-fold increase) versus FA exposure. TNF-α and IL-6 mRNA levels were also increased following 1-day ozone exposure (1.7-fold and 8.2-fold, respectively). These changes were not significantly different from FA-exposed controls, but were significantly different from 2-day ozone exposed rats (Figure 5-5).

Ozone-Induced CXC Chemokine Gene Expression

Two-day ozone exposure caused significant increases in MIP-2 (10-fold) and CINC (13-fold) mRNA expression versus FA. The increases in mRNA expression for each of these genes following 2-day exposure were also significantly different from 1-day

ozone exposure. There were no significant differences versus FA in MIP-2 or CINC mRNA levels following 1-day ozone exposure (Figure 5-6).

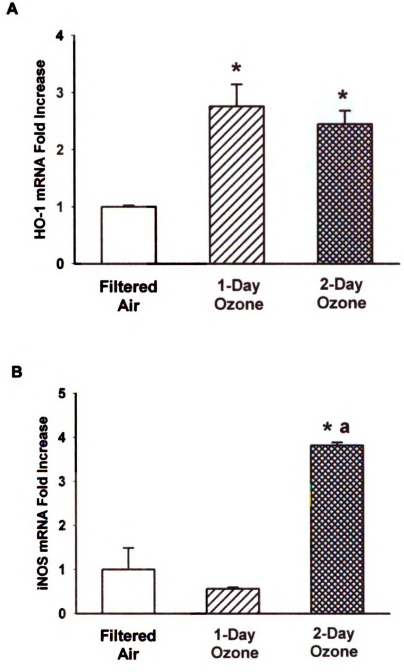

Figure 5-3. Effect of ozone exposure on expression of HO-1 mRNA (A) and iNOS mRNA (B) in rat nasal mucosa. Bars represent group mean $\pm$ SEM (n = 3/group). * = significantly different from FA-exposed rats ($p \leq 0.05$). a = Significantly different from rats exposed to 1-day ozone ($p \leq 0.05$).

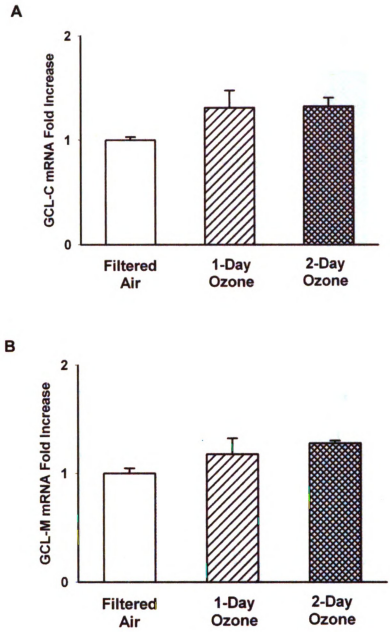

Figure 5-4. Effect of ozone exposure on expression of GCL-C mRNA (A) and GCL-M mRNA (B) in rat nasal mucosa. Bars represent group mean $\pm$ SEM (n = 3/group).

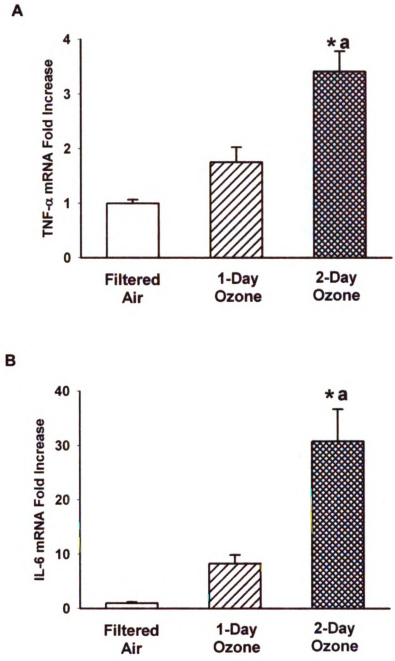

Figure 5-5. Effect of ozone exposure on expression of TNF-α mRNA (A) and IL-6 mRNA (B) in rat nasal mucosa. Bars represent group mean $\pm$ SEM (n = 3/group). * = significantly different from FA-exposed rats ($p \leq 0.05$). a = Significantly different from rats exposed to 1-day ozone ($p \leq 0.05$).

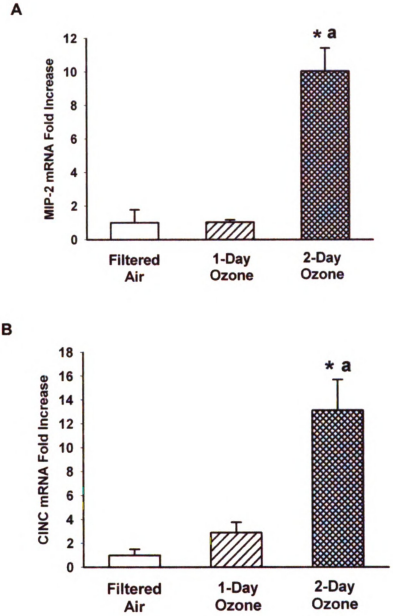

Figure 5-6. Effect of ozone exposure on expression of MIP-2 mRNA (A) and CINC mRNA (B) in rat nasal mucosa. Bars represent group mean $\pm$ SEM (n = 3/group). * = significantly different from FA-exposed rats ($p \leq 0.05$). a = Significantly different from rats exposed to 1-day ozone ($p \leq 0.05$).

DISCUSSION

This study was designed to examine the early molecular events preceding ozone-induced epithelial hyperplasia in the nasal airways of immature rats. Specifically, we hypothesized that early ozone exposure causes oxidative stress, pro-inflammatory gene expression, neutrophil chemotaxis, and upregulation of GSH synthesis genes in the nasal mucosa of immature rats, and that these changes would precede or coincide with the onset of ozone-induced DNA synthesis. In the present study, we found that daily exposure to 0.8 ppm ozone (8h/day) induced epithelial damage and triggered cell proliferation in the nasal airways of immature rats within 2 days of daily exposure. This finding is similar to results observed in adult rats during daily exposures to 0.5 ppm ozone (8h/day for three days), which caused peak increases in BrdU incorporation on day 2 of exposure (Cho et al. 1999).

Ozone exposure caused a rapid increase in nasal HO-1 mRNA expression following 1-day ozone exposure that was maintained following 2-day exposure. Ozone exposure caused a delayed increase in nasal iNOS mRNA expression, with a significant increase only observed following 2-day ozone exposure. Both indices of oxidative stress were elevated by the onset of the ozone-induced increase in S-phase DNA synthesis (BrdU incorporation) on day 2. Our results support the conclusion that early exposure to ozone causes upregulation of cytoprotective antioxidant enzyme systems in the nasal airways. In multi-day ozone exposures, this early upregulation may influence cell survival in the remaining cell populations in the face of subsequent ozone exposures, and allow time for the prerequisite mechanisms for cell proliferation to become established. Interestingly, despite the observed increase in HO-1 and iNOS expression, there was no

significant increase observed in the expression of the GSH synthetic enzyme heterodimers GCL-C and GCL-M. GCL is the rate-limiting enzyme in *de novo* GSH synthesis, and its expression is responsive to local decreases in the redox state of the cell (Iles and Liu 2005). We hypothesized that early ozone exposures would cause oxidative stress in the nasal airways, resulting in GSH consumption and a transient decrease in local redox state, thus increasing gene expression of GCL. In addition to changes in GCL mRNA expression, intracellular GSH concentrations are regulated by several other factors, including changes in GCL mRNA stability, variations in GCL-C activity, and changes in gene expression of other GSH regulatory enzymes, including GGT and GS. It is possible that these other factors could maintain intracellular redox balance without necessitating an increase in GCL expression.

We demonstrated a significant induction of mRNA for the pro-inflammatory cytokines TNF-α and IL-6 in the nasal airways during early exposure to ozone. We also demonstrated coordinated increases in the expression of the CXC chemokines MIP-2 and CINC in the nasal airways. In particular, there was a dramatic increase in IL-6 mRNA induction (30-fold increase versus FA) by day 2 of exposure, which may influence ozone-induced DNA synthesis and cell proliferation. TNF-α and IL-6 are pleiotropic cytokines, which may play different roles at different times during the process of airway injury, inflammation, and epithelial repair. Yu, et al., showed that IL-6 knockout mice exhibit attenuated lung injury, decreased airway inflammation, and decreased DNA synthesis following ozone exposure (Yu et al. 2002). In contrast, McKinney, et al., showed that pre-treatment with IL-6 attenuated ozone-induced lung inflammation, while pre-treatment with an anti-IL-6 neutralizing antibody augmented ozone-induced

inflammation (McKinney et al. 1998). Pre-treatment with TNF-α or IL-1 also attenuated ozone-induced epithelial injury in the nasal airways of rats (Hotchkiss and Harkema 1992). However, another study demonstrated that pre-treatment with anti-TNF-α antibodies ameliorated ozone-induced lung injury. In addition, this study found that early blockade of TNF-α activity inhibited the ozone-induced expression of IL-6 (Bhalla et al. 2002). It is possible that expression of IL-6 and TNF-α prior to ozone exposure serves to limit or inhibit inflammation, while their expression during the first few days of exposure may serve to amplify pro-inflammatory signals. It is also possible that their functions may be dependent upon the concurrent expression levels of other pro-inflammatory cytokines (e.g., IL-1). In our study, the timing of IL-6 and TNF-α upregulation, along with the concurrent increase in the expression of CXC chemokines, support a pro-inflammatory role for these cytokines in the nasal airways during early ozone exposure. However, given the complexity of the inflammatory responses to IL-6 and TNF-α manipulation, further investigation into the early interactions between these two important cytokines is needed.

STUDY 2: EFFECT OF GSH DEPLETION ON OZONE-INDUCED EPITHELIAL HYPERPLASIA.

MATERIALS AND METHODS

Animals, Ozone Exposures, and Glutathione Depletion

To determine the effect of ozone exposure on the steady-state intracellular concentrations of GSH in the nasal airways, and to determine the effect of GSH depletion on the development of ozone-induced epithelial hyperplasia, we randomly assigned 72 rats to twelve experimental groups (n = 6/group). Two groups of animals were exposed to FA for 8 hours. Two groups of animals each were exposed to 0.8 ppm ozone, 8h/day, for 1, 2, or 3 consecutive days, and were euthanized two hours following the end of exposure. Rats in the remaining four groups were exposed to 0.8 ppm ozone, 8h/day, for three consecutive days, and then allowed to recover for 24 or 48 hours post-exposure prior to euthanasia. One hour prior to the start of each daily inhalation exposure, half of the rats were treated with L-buthionine-[S,R]-sulfoximine (1g/kg, intraperitoneally, i.p.; BSO, Sigma Chemical Co., St. Louis, MO), an inhibitor of glutathione synthesis (Haddad 2001). The goal of BSO therapy was to cause a ~50% depletion in nasal mucosal GSH levels. This degree of GSH depletion has been successfully achieved *in vitro* and *in vivo* in previous studies without causing systemic side effects or cellular dysfunction (Canals et al. 2001; Heales et al. 1996). The other half of the animals received saline vehicle intraperitoneally (10ml/kg BWT). Animals that were allowed to recover for 24 or 48 hours post-exposure also received BSO or saline at the same time of day on post-exposure days.

Necropsy and Tissue Preparation for Morphometric Analyses

Two hours, 1 day, or 2 days following the end of exposure, rats were anesthetized with pentobarbital (50mg/kg, i.p.), and then killed by exsanguination via the abdominal aorta. After death, the head of each rat was removed from the carcass, and the eyes,

lower jaw, skin, and musculature was removed. For animals in ***Study 2***, the nasal cavity was sagittally split 1mm to the right of the midline, yielding an intact left nasal cavity with septum attached, and a free right lateral nasal wall. The left nasal cavity was further processed for histopathology as described in ***Study 1***.

One nasal section from each animal was histochemically stained with hematoxylin and eosin (H&E) for morphologic examination and morphometric analyses. For animals in ***Study 2***, a tissue section was immunohistochemically stained with monoclonal mouse anti-proliferating cell nuclear antigen, clone PC10 (PCNA; Dako North America, Carpinteria, CA).

Morphometry of Neutrophilic Inflammation, Epithelial Numeric Cell Density, and Cell Proliferation

The non-ciliated transitional epithelium (NTE) overlying the dorsal aspect of the anterior maxilloturbinate of each animal (Figure 5-1) was analyzed using computerized image analysis and standard morphometric techniques (Hotchkiss et al. 1991). Neutrophilic inflammation was quantified by counting the number of nuclear profiles of neutrophils in the surface epithelium of the dorsal maxilloturbinate, and dividing this number by the total length of the basal lamina underlying this epithelium (i.e., intraepithelial neutrophils per mm basal lamina). Neutrophils were identified on H&E-stained slides by morphologic characteristics, including a multi-lobed nucleus and clear cytoplasm with non-staining granules. The basal lamina length was calculated from the contour length of the basal lamina on a digitized image, using image analysis software (Scion Image, Scion Corporation, Frederick, MD). The epithelial cell numeric density

was determined by counting the total number of epithelial cell nuclear profiles in the epithelium lining the dorsal maxilloturbinate, and dividing this number by the length of the basal lamina.

The expression of PCNA was used as an indicator of cell injury and proliferation (Muskhelishvili et al. 2003). PCNA is an auxiliary protein of the DNA polymerase-δ complex that is expressed in the nuclear compartment of proliferating cells. For ***Study 2***, PCNA was used as a marker of cell proliferation instead of BrdU, in order to avoid possible inconsistencies in BrdU absorption following repeated intraperitoneal BSO injections. The PCNA labeling index was determined by counting the number of PCNA-labeled epithelial cell nuclei, dividing this number by the total number of epithelial cell nuclei, and multiplying by 100 to yield the percentage of PCNA-labeled epithelial cell nuclei in the surface epithelium. The PCNA numeric cell density (unit-length labeling index) was calculated by counting the number of PCNA-labeled nuclei, and dividing this number by the length of the basal lamina.

Tissue Preparation for HPLC Antioxidant Analysis

The right half of the nasal cavity was processed for HPLC antioxidant analysis. The head was dissected and split as previously described. The maxilloturbinate from each animal was microdissected from the right lateral wall, and was immediately placed into 300µl of 10% metaphosphoric acid, and snap-frozen in liquid nitrogen. Acidified, frozen nasal mucosal samples were later thawed, homogenized for 30 seconds using a Polytron homogenizer, re-frozen, and stored at –80°C until further processing for low

molecular weight antioxidant analysis via high performance liquid chromatography (HPLC).

Analysis of Intracellular Concentrations of Low Molecular Weight Nasal Antioxidants

Nasal tissue homogenates were thawed and centrifuged at 12,500 x g for 4 hours. Protein pellets were resuspended in 500µl of PBS, neutralized with 25µl 1N NaOH, and sonicated for 1 hour at 37°C. The protein content of resuspended pellets was measured using the Pierce BCA Protein Assay (Pierce Biotechnology, Rockford, IL). Supernatants were diluted three-fold in 10% meta-phosphoric acid, and filtered through a 0.22µm syringe filter. Triplicate samples of each supernatant were fractioned on a Shimadzu LC-10A*i* HPLC (Shimadzu Scientific Instruments, Columbia, MD), using a Phenomenex Luna C18(2) 250mm x 4.6mm, 5µM reversed phase column, preceded by a Phenomenex ODS 4mm x 3mm guard column (Phenomenex, Torrance, CA). The mobile phase consisted of an isocratic mixture of 50mM phosphate buffer, pH 3.1, containing 50µM octanesulfonic acid and methanol (95:5). Samples were fractioned at a mobile phase flow rate of 1.0ml/min. Reduced glutathione (GSH), oxidized glutathione (GSSG), and ascorbate (AH_2), were simultaneously detected with an 8-channel ESA CoulArray Model 5600A electrochemical detector (ESA, Chelmsford, MA). GSH, GSSG, and AH_2 values were normalized to protein content of centrifuge pellets.

Statistical Analyses

All data were expressed as mean group value ± SEM. The differences among groups in ***Study 2*** were analyzed by two-way ANOVA with interactions. Pairwise comparisons were performed *a priori* using Student-Newman-Keuls multiple comparisons test. The criterion for statistical significance was set to $p \leq 0.05$ for all analyses. All statistical analyses were performed using a commercial statistical software package (SigmaStat, SPSS Science, Chicago, IL).

RESULTS

Determination of Low Molecular Weight Nasal Antioxidant Concentrations

There was no significant effect of ozone exposure observed in the steady-state nasal mucosal concentrations of GSH, GSSH, or AH_2 at any of the exposure or post-exposure time points. There was a tendency toward increased concentrations of GSH and GSSG in all saline-treated, ozone-exposure groups compared to their respective FA exposed controls (all GSH and GSSG values in ozone-exposed groups were higher than their respective control values); however, none of these differences was statistically significant.

BSO treatment caused a 45% decrease in the mucosal GSH concentration in FA-exposed rats. BSO treatment also caused a decrease in nasal mucosal concentrations in all ozone-exposed rats compared to similarly exposed, saline-treated rats. This decrease was statistically significant following 1-day (57% decrease) and 2-day (65% decrease) exposures, and following 3-day exposures + 24 hour (71% decrease) and 48 hour (69% decrease) recovery periods (Figure 5-7).

Following 3-day ozone exposure, BSO treatment caused a significant (69%) decrease in mucosal GSSG concentrations versus saline-treated rats exposed to ozone for 3 days. BSO treatment caused a decrease in the mucosal GSSG concentrations in all ozone-exposed rats compared to similarly exposed, saline-treated rats (Figure 5-8).

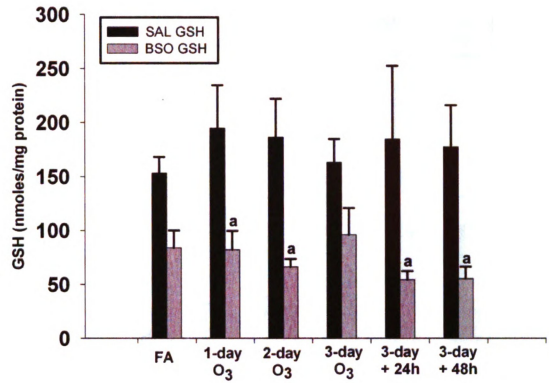

Figure 5-7. Effect of ozone exposure +/- BSO treatment on intracellular GSH concentrations in rat nasal mucosa lining the anterior maxilloturbinate. Bars represent group mean $\pm$ SEM (n = 6/group). a = significantly different from respective saline-treated rats.

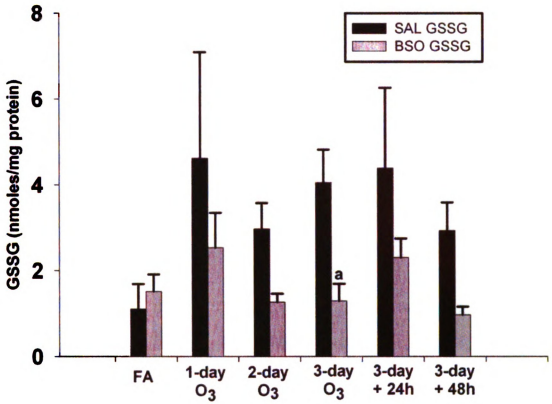

Figure 5-8. Effect of ozone exposure +/- BSO treatment on intracellular GSSG concentrations in rat nasal mucosa lining the anterior maxilloturbinate. Bars represent group mean ± SEM (n = 6/group). a = significantly different from respective saline-treated rats.

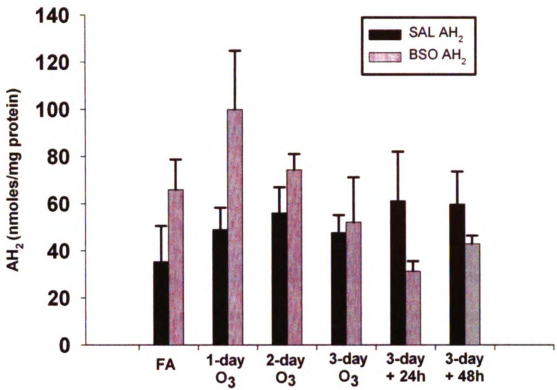

Figure 5-9. Effect of ozone exposure +/- BSO treatment on intracellular AH_2 concentrations in rat nasal mucosa lining the anterior maxilloturbinate. Bars represent group mean $\pm$ SEM (n = 6/group).

There was no statistically significant effect of BSO treatment on the steady state nasal mucosal concentrations of AH_2 in FA- or ozone-exposed rats. There were trends toward increases in nasal mucosal AH_2 concentrations of BSO-treated rats observed following FA-exposure and 1-day ozone exposure; however, these changes were not statistically significant (Figure 5-9).

Nasal Histopathology

Light photomicrographs of representative maxilloturbinates that summarize the time-dependent progression of inflammatory and epithelial responses to ozone exposure +/- BSO treatment are illustrated in Figure 5-10. No exposure related lesions were identified in the nasal airways of rats treated with either saline or BSO and exposed to filtered air (0 ppm). In all ozone-exposed animals, nasal lesions were restricted to the nasal transitional epithelium (NTE) lining the lateral meatus of the anterior nasal cavity. There were no significant microscopic differences observed between saline- and BSO-treated animals in the time-dependent progression of ozone-induced epithelial injury in the anterior nasal cavity.

In rats treated with saline or BSO and exposed to 1 day of 0.8 ppm ozone, the principal morphologic alterations observed were epithelial degeneration and necrosis in the NTE. These lesions were most severe in the NTE lining the dorsal aspect of the maxilloturbinate, the ventral surface of the nasoturbinate, and the lateral wall adjacent to the maxilloturbinate. An influx of neutrophils was observed in the epithelium and lamina propria lining the maxilloturbinate, nasoturbinate, and lateral nasal wall.

Figure 5-10. Light photomicrographs of the dorsal aspect of maxilloturbinates from rats treated with saline (A, B, C) or BSO (D, E, F) and exposed to 0 ppm ozone (A and D), exposed to 0.8 ppm ozone for 2 days (B and D), or exposed to 0.8 ppm ozone for 3 days and killed 48 hours post-exposure (C and F). Tissues were stained with H&E. Note the presence of scattered mitotic figures (*black arrows*) in the NTE, along with the influx of neutrophils (*white arrows*) into the epithelium (e) and underlying lamina propria (lp) in the maxilloturbinates of rats exposed to 0.8 ppm ozone for 2 days (B and D). TB = turbinate bone; bv = blood vessel.

A
SALINE
e
lp
tb
50µm
B
SALINE
lp
tb
e
C
SALINE
lp
tb
e
D
FA
BSO
lp
e
tb
bv
E
0.8 PPM 2 Days
BSO
lp
tb
e
F
0.8 PPM 3 Days +48h
BSO
e
lp
tb

Figure 5-10

After 2 days of ozone exposure, the principal morphologic alterations in the NTE of saline- and BSO-treated rats were basal cell hyperplasia and progressive neutrophilic rhinitis. The NTE lining the dorsal maxilloturbinate exhibited cytoplasmic basophilia, particularly along the basal cell layer, consistent with epithelial regeneration. Occasional mitotic figures were observed within the NTE. The degeneration of surface epithelial cells noted following 1-day exposure was also present on day 2. Neutrophil infiltration into the nasal mucosa was increased from day 1.

At the end of 3 days of ozone exposure, saline- and BSO-treated rats exhibited epithelial hyperplasia of the NTE. In 3-day ozone animals, the epithelium lining the dorsal maxilloturbinate was 3-4 cell layers thick, compared to 1-2 cell layers in the NTE of FA-exposed rats. Concurrent with the increase in epithelial thickness was a decrease in the influx of neutrophils into the nasal mucosa following 3-day ozone exposure.

Epithelial morphology was similar in saline- and BSO-treated rats exposed to ozone for 3 days and allowed to recover for either 24 or 48 hours post-exposure. The principal lesion observed in these animals was marked epithelial hyperplasia in the NTE lining the maxilloturbinate, and moderate hyperplasia of the epithelium lining the lateral wall and ventral surface of the nasoturbinate. A mild neutrophilic rhinitis persisted in the epithelium and lamina propria lining the maxilloturbinates.

Morphometric Quantitation of Epithelial Hyperplasia

PCNA labeling of maxilloturbinates in saline- and BSO-treated, ozone-exposed rats is illustrated in Figure 5-11. Ozone induced a significant increase in the PCNA labeling index in both saline- and BSO-treated rats (96-fold and 86-fold, respectively)

exposed to 0.8 ppm ozone for 2 days, compared to FA-exposed rats (Figure 5-12). There were no significant differences in the PCNA labeling index observed at any other exposure time, compared to FA exposure. Interestingly, the labeling index in saline-treated rats following 1-day of exposure was significantly greater (10-fold higher) than that observed in BSO-treated rats at the same time point. However, neither was significantly different from FA-exposed rats. PCNA labeling was similar between saline- and BSO-treated rats at all other time points.

Accordingly, ozone exposure also induced a significant increase in the PCNA numeric cell density in both saline- and BSO-treated rats following 2-day exposure (200-fold and 75-fold increases, respectively), compared to controls. PCNA numeric cell densities in saline-treated rats were also higher than control levels following 3-day exposure + 24 hour recovery (160-fold higher) and 48 hour recovery (160-fold). The PCNA numeric cell density in saline-treated rats exposed to 1-day of ozone was 12-fold higher than in similarly exposed BSO-treated rats, however, this difference was not statistically significant (Figure 5-13).

Figure 5-11. Light photomicrographs of maxilloturbinates from rats treated with saline and exposed to 0 ppm ozone (filtered air, A), and from rats treated with saline (B) or BSO (C) and exposed to 0.8 ppm ozone for 2 days. Tissues were immunohistochemically stained with anti-PCNA antibody to detect proliferating cells. Note the nuclear uptake of brown chromagen (black arrows) in the epithelium (e) lining the dorsal maxilloturbinate and lateral wall (LW) of the anterior nasal cavity in saline- (B) and BSO-treated (C), ozone exposed rats, indicating PCNA expression. tb = turbinate bone.

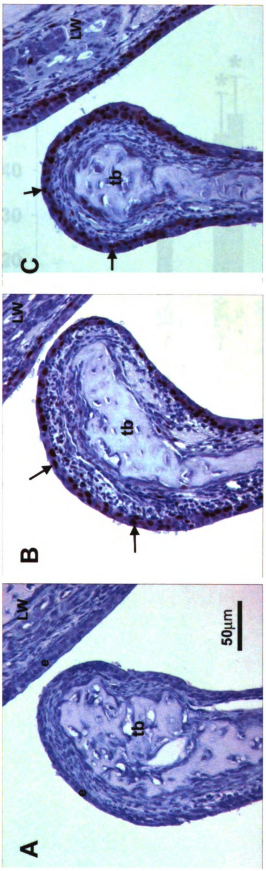

Figure 5-11

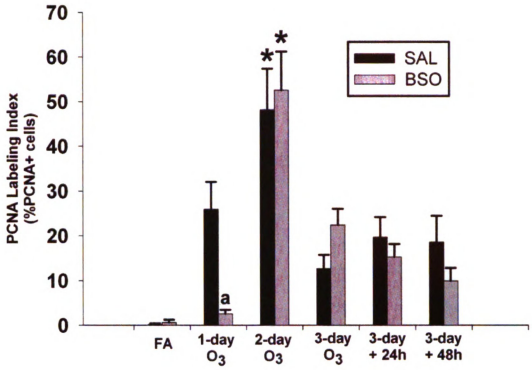

Figure 5-12. Effect of ozone exposure +/- BSO treatment on PCNA labeling index in the NTE lining the anterior maxilloturbinate. Bars represent group mean ± SEM (n = 6/group). * = significantly different from respective FA-exposed rats. a = significantly different from respective saline-treated rats.

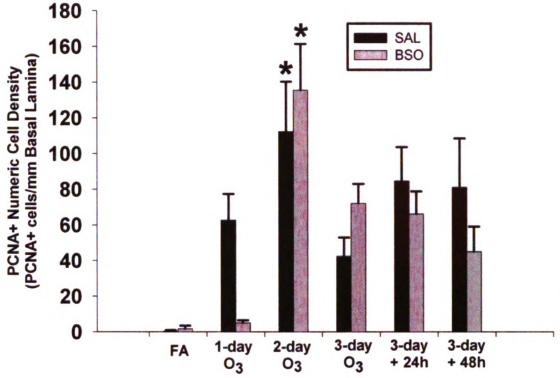

Figure 5-13. Effect of ozone exposure +/- BSO treatment on the numeric cell density of cells expressing PCNA in the NTE lining the anterior maxilloturbinate. Bars represent group mean ± SEM (n = 6/group). * = significantly different from respective FA-exposed rats.

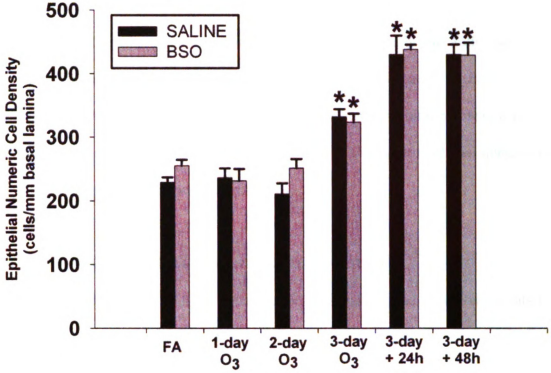

Figure 5-14. Effect of ozone exposure +/- BSO treatment on the numeric cell density of epithelial cells in the NTE lining the anterior maxilloturbinate. Bars represent group mean ± SEM (n = 6/group). * = significantly different from respective FA-exposed rats.

In both saline- and BSO-treated rats, ozone induced a significant increase in the total number of epithelial cells lining the dorsal maxilloturbinate following 3-day exposure (45% and 26% increases, respectively), 3-day exposure + 24 hour recovery (88% and 72% increases, respectively), and 3-day exposure + 48 hour recovery (88% and 68% increases, respectively). BSO treatment had no effect on the epithelial numeric cell density at any exposure time point (Figure 5-14).

Morphometric Quantitation of Neutrophilic Inflammation

After 2-day exposure to 0.8 ppm ozone, both saline- and BSO-treated rats had significantly greater (28-fold and 8-fold, respectively) neutrophil influx into the NTE lining the dorsal maxilloturbinates than similarly treated FA-exposed rats (Figure 5-15). This increase in neutrophilic inflammation was also observed in saline- and BSO-treated rats following 3-day exposure (16-fold and 8-fold, respectively). There was no significant effect of BSO-treatment on neutrophil influx at any exposure time point.

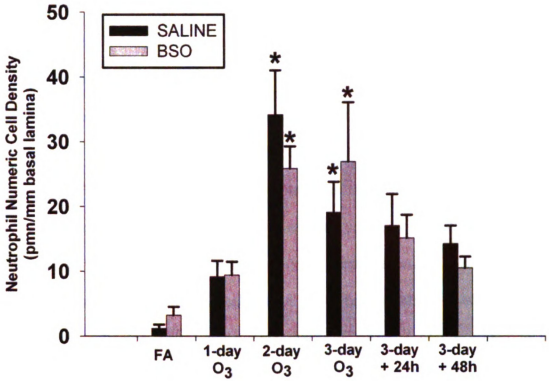

Figure 5-15. Effect of ozone exposure +/- BSO treatment on the numeric cell density of intraepithelial neutrophils in the NTE lining the anterior maxilloturbinate. Bars represent group mean $\pm$ SEM (n = 6/group). * = significantly different from respective FA-exposed rats.

DISCUSSION

The results of the present study indicate that ozone-induced cell proliferation in the nasal airways of immature rats is not dependent upon the local upregulation of intracellular GSH concentration. Daily exposure to 0.8 ppm ozone caused epithelial hyperplasia in the nasal airways of immature rats. Treatment with BSO, a potent inhibitor of GSH synthesis, caused marked depletion of intracellular GSH concentrations prior to and during ozone exposures. There was a conspicuous lack of DNA synthesis observed in BSO-treated animals following day 1 of ozone-exposure. Furthermore, by day 1 of exposure, BSO-treated animals had 57% lower concentrations of intracellular GSH than saline-treated animal undergoing the same ozone exposure. Despite the marked GSH depletion and delayed cell proliferation observed on day 1, the BSO-treated, ozone-exposed animals exhibited levels of cell proliferation similar to those observed in saline-treated, ozone-exposed rats by day 2, the day of peak cell proliferation rates in both groups. This ultimately resulted in similar degrees of epithelial hyperplasia in saline- and BSO-treated rats following ozone exposure.

In the present study, exposure to 0.8 ppm ozone, 8h/day, for 3 consecutive days, caused epithelial hyperplasia and transient neutrophilic inflammation in the anterior nasal airways of immature rats. The time course of cell proliferation and neutrophilic inflammation observed in our study was consistent with results from similarly exposed adult rats (Cho et al. 1999). We did not observe a significant difference in the magnitude or progression of ozone-induced rhinitis between saline- and BSO-treated animals. Previous studies have provided conflicting results regarding the potential role of neutrophilic inflammation in the modulation of ozone-induced cell proliferation. Salmon,

et al., showed that apocynin, an NADPH oxidase inhibitor, and the corticosteroid dexamethasone, were each capable of inhibiting ozone-induced cell proliferation in rat bronchiolar epithelium (Salmon et al. 1998). However, Cho, et al., demonstrated that neutrophil depletion did not inhibit ozone-induced epithelial hyperplasia in rat nasal airways (Cho et al. 2000). While our study demonstrates that GSH depletion does not affect nasal airway inflammation, it neither supports nor refutes the role of neutrophilic inflammation in oxidant-mediated cell proliferation.

We hypothesized that early ozone exposures would cause oxidative stress in the nasal airways of rats, increasing the expression of anti-oxidant, pro-inflammatory, and GSH synthetic genes. Further, we hypothesized that increased expression of GCL subunits would result in increases in GSH synthesis that would re-establish a favorable redox balance, and promote cell proliferation (or prevent cell cycle arrest). We did not observe a significant increase in GSH concentrations in the nasal mucosa of saline-treated rats during the course of ozone exposure, nor did we observe an increase in mRNA for either GCL subunit (***Study 1*** from this chapter). This may be due, in part, to alternative mechanisms maintaining a favorable (reduced) redox balance during ozone exposures. The normal GSH/GSSG redox ratio in cells ranges between 30:1 to 100:1 (Hwang et al. 1992). In our study, the GSH/GSSG redox ratio in nasal mucosa was maintained between ~40:1 to 60:1 following the three days of exposures (see Figures 5-7 and 5-8). In the absence of increased GCL expression, other factors may contribute to the maintenance of favorable redox conditions, including glutathione reductase activity, which can regenerate GSH via GCL-independent mechanisms.

The intracellular concentration of GSH also influences the regulation and synthesis of ascorbate (AH_2), which may also contribute to the overall redox state of a cell. In a manner similar to GSH and GSSG, AH_2 exists in a redox couple with dehydroascorbate (Moison et al. 1997). Dehydroascorbate reductase, the enzyme that catalyzes the two-electron reduction of dehydroascorbate back to AH_2, uses GSH as a reducing agent. Thus, in humans, regulation and maintenance of AH_2 is largely GSH-dependent. Unlike humans (and rhesus monkeys), rats are capable of *de novo* synthesis of ascorbate. Furthermore, results from previous studies show that oxidative stress induced via GSH depletion in mice can be ameliorated by a compensatory increase in AH_2 synthesis (Martensson and Meister 1992). In the present study, BSO treatment caused marked reductions in GSH concentrations that were accompanied by mild increases in the intracellular concentration of AH_2 in the nasal mucosa of rats. It is possible that the potential oxidative stress induced by GSH depletion was reversed by compensatory increases in AH_2, thus promoting cell cycle progression and cell proliferation.

In Chapters 3 and 4, we reported the effects of acute and episodic ozone exposure on intracellular antioxidant concentrations in the nasal mucosa of infant monkeys. Acute ozone exposure (0.5 ppm, 8h/day for 5 days) and 5-cycle episodic ozone exposure (5 bi-weekly cycles of 9 days FA, followed by 0.5 ppm, 8h/day for 5 days) each caused widespread reductions in intracellular GSH concentrations. In contrast, 11 cycle exposure caused widespread GSH upregulation in the nasal mucosa. We hypothesized that ozone-induced epithelial hyperplasia was dependent upon GSH upregulation, and

that GSH upregulation was a response to early GSH consumption. Since ozone-induced epithelial hyperplasia developed more quickly in the rat nasal cavity, we hypothesized that ozone-induced GSH upregulation would occur earlier in the rat than in the monkey. While we did not observe an ozone-related increase in GSH levels in the present study, we also did not observe GSH consumption in saline-treated rats following ozone exposures. Several mechanisms may be involved in this differential response to ozone exposures between infant monkeys and infant rats. As previously discussed, rats are capable of synthesizing AH_2 in response to oxidative stress, which may spare intracellular GSH concentrations during short-term ozone exposure. In contrast, monkeys lack the enzyme L-gulonolactone oxidase, which catalyzes the final step in AH_2 synthesis, and cannot regulate AH_2 levels via *de novo* synthesis (Bánhegyi et al. 1997). It is also possible that the ozone concentration selected for the rat studies (0.8 ppm) was insufficient to decrease GSH concentrations, while the lower concentration selected for the infant monkey exposures (0.5 ppm) was more potent due to the decreased sensitivity to ozone-induced injury exhibited by rodents (Hatch et al. 1994).

In summary, GSH depletion during exposure to ozone does not inhibit the development of epithelial hyperplasia in the rat. Our results do not support a direct role for GSH in regulating cell proliferation. However, our findings suggest that compensatory mechanisms, including AH_2 synthesis and GSH redox recycling, may ameliorate oxidative stress induced by GSH depletion, thus facilitating cell cycle progression and cell proliferation. Further studies examining the complex relationships among AH_2, GSH, and oxidant-mediated cellular injury and proliferation are warranted.

REFERENCES

Bánhegyi, G., L. Braun, M. Csala, F. Puskás and J. Mandl (1997). "Ascorbate Metabolism and Its Regulation in Animals." Free Radical Biology and Medicine **23**(5): 793-803.

Bhalla, D. K., P. G. Reinhart, C. Bai and S. K. Gupta (2002). "Amelioration of ozone-induced lung injury by anti-tumor necrosis factor-alpha." Toxicol Sci **69**(2): 400-408.

Canals, S., M. J. Casarejos, S. de Bernardo, E. Rodriguez-Martin and M. A. Mena (2001). "Glutathione depletion switches nitric oxide neurotrophic effects to cell death in midbrain cultures: implications for Parkinson's disease." J Neurochem **79**(6): 1183-1195.

Cho, H. Y., J. A. Hotchkiss, C. B. Bennett and J. R. Harkema (2000). "Neutrophil-dependent and neutrophil-independent alterations in the nasal epithelium of ozone-exposed rats." American Journal of Respiratory & Critical Care Medicine **162**(2 Pt 1): 629-636.

Cho, H. Y., J. A. Hotchkiss and J. R. Harkema (1999). "Inflammatory and epithelial responses during the development of ozone-induced mucous cell metaplasia in the nasal epithelium of rats." Toxicological Sciences **51**(1): 135-145.

Colombrita, C., G. Lombardo, G. Scapagnini and N. G. Abraham (2003). "Heme oxygenase-1 expression levels are cell cycle dependent." Biochem Biophys Res Commun **308**(4): 1001-1008.

Devlin, R. B. (1993). "Identification of subpopulations that are sensitive to ozone exposure: use of end points currently available and potential use of laboratory-based end points under development." Environmental Health Perspectives **101 Suppl 4**: 225-230.

Devlin, R. B., W. F. McDonnell, R. Mann, S. Becker, D. E. House, D. Schreinemachers and H. S. Koren (1991). "Exposure of humans to ambient levels of ozone for 6.6 hours causes cellular and biochemical changes in the lung." Am J Respir Cell Mol Biol **4**(1): 72-81.

Foucaud, L., A. Bennasroune, D. Klestadt, P. Laval-Gilly and J. Falla (2006). "Oxidative stress induction by short time exposure to ozone on THP-1 cells." Toxicology In Vitro **20**(1): 101-108.

Haddad, J. J. (2001). "L-Buthionine-(S,R)-sulfoximine, an irreversible inhibitor of gamma-glutamylcysteine synthetase, augments LPS-mediated pro-inflammatory cytokine biosynthesis: evidence for the implication of an IkappaB-alpha/NF-kappaB insensitive pathway." Eur Cytokine Netw **12**(4): 614-624.

Harkema, J. R., J. A. Hotchkiss, A. G. Harmsen and R. F. Henderson (1988). "In vivo effects of transient neutrophil influx on nasal respiratory epithelial mucosubstances. Quantitative histochemistry." American Journal of Pathology **130**(3): 605-615.

Hatch, G. E., R. Slade, L. P. Harris, W. F. McDonnell, R. B. Devlin, H. S. Koren, D. L. Costa and J. McKee (1994). "Ozone dose and effect in humans and rats. A comparison using oxygen-18 labeling and bronchoalveolar lavage." Am. J. Respir. Crit. Care Med. **150**(3): 676-683.

Heales, S. J., J. P. Bolanos and J. B. Clark (1996). "Glutathione depletion is accompanied by increased neuronal nitric oxide synthase activity." Neurochem Res **21**(1): 35-39.

Henderson, R. F., J. A. Hotchkiss, I. Y. Chang, B. R. Scott and J. R. Harkema (1993). "Effect of cumulative exposure on nasal response to ozone." Toxicology & Applied Pharmacology **119**(1): 59-65.

Hotchkiss, J. A. and J. R. Harkema (1992). "Endotoxin or cytokines attenuate ozone-induced DNA synthesis in rat nasal transitional epithelium." Toxicol Appl Pharmacol **114**(2): 182-187.

Hotchkiss, J. A., J. R. Harkema and R. F. Henderson (1991). "Effect of cumulative ozone exposure on ozone-induced nasal epithelial hyperplasia and secretory metaplasia in rats." Experimental Lung Research **17**(3): 589-600.

Hotchkiss, J. A., J. R. Harkema and N. F. Johnson (1997). "Kinetics of nasal epithelial cell loss and proliferation in F344 rats following a single exposure to 0.5 ppm ozone." Toxicology & Applied Pharmacology **143**(1): 75-82.

Hwang, C., A. J. Sinskey and H. F. Lodish (1992). "Oxidized redox state of glutathione in the endoplasmic reticulum." Science **257**(5076): 1496-1502.

Hyde, D. M., W. C. Hubbard, V. Wong, R. Wu, K. Pinkerton and C. G. Plopper (1992). "Ozone-induced acute tracheobronchial epithelial injury: relationship to granulocyte emigration in the lung." Am J Respir Cell Mol Biol **6**(5): 481-497.

Iles, K. E. and R. M. Liu (2005). "Mechanisms of glutamate cysteine ligase (GCL) induction by 4-hydroxynonenal." Free Radic Biol Med **38**(5): 547-556.

Jin, Y. and A. M. K. Choi (2005). "Cytoprotection of Heme Oxygenase-1/Carbon Monoxide in Lung Injury." Proc Am Thorac Soc **2**(3): 232-235.

Johnson, N. F., J. A. Hotchkiss, J. R. Harkema and R. F. Henderson (1990). "Proliferative responses of rat nasal epithelia to ozone." Toxicology & Applied Pharmacology **103**(1): 143-155.

Joshi, M., J. Ponthier and J. Lancaster (1999). "Cellular antioxidant and pro-oxidant actions of nitric oxide." Free Radic Biol Med **27**(11-12): 1357-1366.

Kavanagh, T. J., A. Grossmann, E. P. Jaecks, J. C. Jinneman, D. L. Eaton, G. M. Martin and P. S. Rabinovitch (1990). "Proliferative capacity of human peripheral blood lymphocytes sorted on the basis of glutathione content." J Cell Physiol **145**(3): 472-480.

Koren, H. S., R. B. Devlin, D. E. Graham, R. Mann, M. P. McGee, D. H. Horstman, W. J. Kozumbo, S. Becker, D. E. House, W. F. McDonnell and et al. (1989). "Ozone-induced inflammation in the lower airways of human subjects." Am Rev Respir Dis **139**(2): 407-415.

Leikauf, G. D., L. G. Simpson, J. Santrock, Q. Zhao, J. Abbinante-Nissen, S. Zhou and K. E. Driscoll (1995). "Airway Epithelial Cell Responses to Ozone Injury." Environmental Health Perspectives **103**: 91-95.

Lu, Q., F. L. Jourd'Heuil and D. Jourd'Heuil (2007). "Redox control of G(1)/S cell cycle regulators during nitric oxide-mediated cell cycle arrest." J Cell Physiol **212**(3): 827-839.

Lu, S. C. (2008). "Regulation of glutathione synthesis." Mol Aspects Med.

Luppi, F., J. Aarbiou, S. van Wetering, I. Rahman, W. I. de Boer, K. F. Rabe and P. S. Hiemstra (2005). "Effects of cigarette smoke condensate on proliferation and wound closure of bronchial epithelial cells in vitro: role of glutathione." Respiratory Research **6**: 140.

Maples, K. R., K. J. Nikula, B. T. Chen, G. L. Finch, W. C. Griffith and J. R. Harkema (1993). "Effects of Cigarette Smoke on the Glutathione Status of the Upper and Lower Respiratory Tract of Rats." Inhal Toxicol **5**: 389-401.

Martensson, J. and A. Meister (1992). "Glutathione deficiency increases hepatic ascorbic acid synthesis in adult mice." Proceedings of the National Academy of Sciences of the United States of America **89**(23): 11566-11568.

McKinney, W. J., R. H. Jaskot, J. H. Richards, D. L. Costa and K. L. Dreher (1998). "Cytokine mediation of ozone-induced pulmonary adaptation." Am J Respir Cell Mol Biol **18**(5): 696-705.

Moison, R. M., A. J. de Beaufort, A. A. Haasnoot, T. M. Dubbelman, D. van Zoeren-Grobben and H. M. Berger (1997). "Uric acid and ascorbic acid redox ratios in plasma and tracheal aspirate of preterm babies with acute and chronic lung disease." Free Radic Biol Med **23**(2): 226-234.

Morse, D. and A. M. K. Choi (2005). "Heme Oxygenase-1: From Bench to Bedside." Am. J. Respir. Crit. Care Med. %R 10.1164/rccm.200404-465SO **172**(6): 660-670.

Muskhelishvili, L., J. R. Latendresse, R. L. Kodell and E. B. Henderson (2003). "Evaluation of Cell Proliferation in Rat Tissues with BrdU, PCNA, Ki-67(MIB-5) Immunohistochemistry and In Situ Hybridization for Histone mRNA." J. Histochem. Cytochem. **51**(12): 1681-1688.

Pendino, K. J., R. L. Shuler, J. D. Laskin and D. L. Laskin (1994). "Enhanced production of interleukin-1, tumor necrosis factor-alpha, and fibronectin by rat lung phagocytes following inhalation of a pulmonary irritant." Am. J. Respir. Cell Mol. Biol. **11**(3): 279-286.

Plopper, C. G., G. E. Hatch, V. Wong, X. Duan, A. J. Weir, B. K. Tarkington, R. B. Devlin, S. Becker and A. R. Buckpitt (1998). "Relationship of inhaled ozone concentration to acute tracheobronchial epithelial injury, site-specific ozone dose, and glutathione depletion in rhesus monkeys." Am J Respir Cell Mol Biol **19**(3): 387-399.

Rajini, P., T. R. Gelzleichter, J. A. Last and H. Witschi (1993). "Airway epithelial labeling index as an indicator of ozone induced lung injury." Toxicology **83**(1-3): 159-168.

Reddy, N. M., S. R. Kleeberger, M. Yamamoto and S. P. Reddy (2008). "Nrf2-dependent Glutathione-regulated Transcriptional Program Controls Lung Type II Cell Proliferation and Protection against Oxidative Stress." Proc Am Thorac Soc **5**(3): 367-.

Romanska, H. M., J. M. Polak, R. A. Coleman, R. S. James, D. W. Harmer, J. C. Allen and A. E. Bishop (2002). "iNOS gene upregulation is associated with the early proliferative response of human lung fibroblasts to cytokine stimulation." J Pathol **197**(3): 372-379.

Salmon, M., H. Koto, Oonagh T. Lynch, E.-B. Haddad, Nicholas J. Lamb, Gregory J. Quinlan, Peter J. Barnes and K. Fan Chung (1998). "Proliferation of Airway Epithelium After Ozone Exposure . Effect of Apocynin and Dexamethasone." Am. J. Respir. Crit. Care Med. **157**(3): 970-977.

Shaw, J. P. and I. N. Chou (1986). "Elevation of intracellular glutathione content associated with mitogenic stimulation of quiescent fibroblasts." J Cell Physiol **129**(2): 193-198.

Vandesompele, J., K. De Preter, F. Pattyn, B. Poppe, N. Van Roy, A. De Paepe and F. Speleman (2002). "Accurate normalization of real-time quantitative RT-PCR data by geometric averaging of multiple internal control genes." Genome Biology **3**(7): 34.1 - 34.11.

Yu, M., X. Zheng, H. Witschi and K. E. Pinkerton (2002). "The role of interleukin-6 in pulmonary inflammation and injury induced by exposure to environmental air pollutants." Toxicol Sci **68**(2): 488-497.

CHAPTER 6

SUMMARY AND CONCLUSIONS

The inflammatory and epithelial responses to acute and chronic ozone exposure have been well characterized in the nasal airways of monkeys and rats. Acute or chronic exposure to ozone causes epithelial necrosis and acute inflammation, followed by epithelial hyperplasia and mucous cell metaplasia, in the nasal transitional epithelium and ciliated respiratory epithelium of monkeys (Harkema, Plopper et al. 1987; Harkema, Plopper et al. 1987), and in the nasal transitional epithelium of rats (Harkema, Barr et al. 1997; Harkema, Hotchkiss et al. 1999). While the previous studies were designed to describe these nasal epithelial proliferative responses to ozone exposure, subsequent studies from our laboratory using rodent models were designed to investigate the mechanisms behind these epithelial alterations. Hotchkiss et al., demonstrated that pre-treatment with the pro-inflammatory cytokines IL-1 and TNF-α inhibits ozone-induced DNA synthesis and cell proliferation (Hotchkiss and Harkema 1992). Cho et al., demonstrated that while ozone-induced mucous cell metaplasia is neutrophil dependent, ozone-induced epithelial hyperplasia is neutrophil-independent (Cho, Hotchkiss et al. 2000).

Ozone-induced injury and repair exhibits site-specificity in both the nasal and pulmonary airways. Ozone-induced lesions are confined to the anterior nasal cavity, and to the tracheobronchial epithelium and terminal bronchiolar epithelium in the lungs. The site-specificity of ozone-induced injury and repair is correlated to sites of ozone-induced antioxidant alterations in the lungs of rats (Plopper, Duan et al. 1994) and monkeys (Plopper, Hatch et al. 1998). The relationship between local antioxidant status and ozone-induced injury and repair in the nasal airways had not been previously investigated. We designed the current research to examine the relationship between site-

specific ozone-induced epithelial hyperplasia and local glutathione (GSH) status. Our governing hypothesis was that ozone-induced epithelial hyperplasia in the nasal airways of monkeys and rats is a GSH-dependent process.

With our initial investigations in infant rhesus monkeys, we sought to determine the temporal and spatial relationships among ozone-induced nasal airway injury and repair, and local antioxidant regulation. We first identified, quantified, and mapped the nasal epithelial lesions induced by acute (0.5 ppm, 8h/day for 5 days), episodic (0.5 ppm.8h/day for 5 days + 9 days of filtered air, 5 cycles), and chronic, episodic (0.5 ppm.8h/day for 5 days + 9 days of filtered air, 11 cycles) exposure to ozone. We also measured intracellular concentrations of GSH, GSSG, AH2, and UA in site-matched nasal mucosal samples. Acute ozone exposure caused epithelial necrosis and atrophy in the ciliated respiratory epithelium lining the anterior maxilloturbinate, with no epithelial hyperplasia at this site. Cyclic exposure for 2 months (episodic) caused nasal lesions similar in nature, distribution, and magnitude, to those observed following acute exposure. Both acute and episodic exposure regimens caused GSH depletion in samples corresponding to the site of ozone-induced injury. In contrast, cyclic exposure for 5 months (11 cycles) caused epithelial hyperplasia and squamous metaplasia along the same site as the ozone-induced injury following acute and 2-month cyclic exposures. Furthermore, this hyperplastic and metaplastic response was correlated with a 65% increase in the local, intracellular GSH concentration. While these results established a temporal correlation between GSH concentration and epithelial hyperplasia, they did not establish a causal relationship between GSH regulation and cell proliferation.

Based on the results of our studies in rhesus monkeys, we chose to further investigate the possible relationship between GSH and epithelial hyperplasia. Results from several recent reports provide evidence that intracellular redox state in cells can influence cell cycle progression, and that GSH regulation plays an important role in the maintenance of redox state and cellular protection during oxidative stress (Luppi, Aarbiou et al. 2005; Lu, Jourd'Heuil et al. 2007). Using a rodent model of ozone-induced cell proliferation, we tested the hypothesis that ozone exposure causes intracellular oxidative stress, induction of cytoprotective, pro-inflammatory, and GSH-synthetic genes, and GSH upregulation prior to the initiation of ozone-induced cell proliferation. Furthermore, we hypothesized that GSH depletion would diminish this cytoprotective effect, and inhibit ozone-induced cell proliferation. For this purpose, we treated rats with BSO, an inhibitor of GCL, to cause GSH depletion in the nasal mucosa.

The results from this study indicated that ozone exposure induced the expression of the cytoprotective enzymes (HO-1, iNOS), pro-inflammatory cytokines (TNF-α, IL-6), and neutrophil chemokines (MIP-2, CINC) in the nasal mucosa during the first 2 days of ozone exposure, and prior to or concurrent with ozone-induced DNA synthesis (BrdU incorporation). However, ozone exposure did not cause upregulation of GSH concentrations, nor did it induce the expression of GCL-C or GCL-M, the rate-limiting enzymes in *de novo* GSH synthesis, in rat nasal mucosa. Furthermore, we found that GSH depletion did not inhibit the development of ozone-induced epithelial hyperplasia. Interestingly, we also found that BSO-induced depletion of GSH was accompanied by a mild increase in intracellular AH_2 concentrations. We speculate that the potential

increases in oxidative stress caused by GSH depletion may be ameliorated by concurrent increases in AH_2.

The results from these experiments also provide the basis for important comparisons between rodents and monkeys as animal models of human inhalation. In Chapter 2, we reviewed and summarized the scientific literature relevant to the antioxidant profile of the rat nasal cavity. This review highlighted important differences that exist between rats and humans in the relative abundances of specific low molecular weight nasal antioxidants, and their role in protection against inhaled oxidant challenge. In Chapter 3, we detailed the similarities between the nasal airways of humans and monkeys, and the importance of these structural similarities in making accurate extrapolations of risk data from histopathologic, biochemical, and dosimetry studies from monkeys to humans. In Chapter 4, we reported that episodic exposure to ozone causes squamous metaplasia in the nasal airway of infant monkeys. This nasal epithelial response in monkeys is similar to that observed in the nasal airways of children chronically exposed to high ambient concentrations of ozone, and illustrates the importance of the non-human primate studies in the evaluation of human risk. In Chapter 5, we discussed the potential influence of local AH_2 regulation on ozone-induced GSH flux in rat nasal mucosa. These findings bring to light important differences between rats and monkeys, and important similarities between monkeys and humans, in the regulation and synthesis of low molecular weight antioxidants. While the results of these experiments lend significant support for the use of non-human primates in inhalation toxicologic studies, they also bring to light important species differences that must be considered when designing comparative mechanistic studies.

In summary, we determined that ozone exposure causes epithelial hyperplasia and squamous metaplasia in the nasal airways of infant monkeys. The findings in our non-human primate model are consistent with the nasal injury observed in children chronically exposed to high ambient levels of ozone (Calderon-Garciduenas, Valencia-Salazar et al. 2001) (Calderon-Garciduenas, Rodriguez-Alcaraz et al. 2001). Furthermore, we determined that these alterations are temporally correlated with increases in the steady-state intracellular concentrations of GSH in the nasal mucosa following chronic, episodic exposures. Additional studies are needed to fully understand the durability and long-term consequences of nasal epithelial hyperplasia and squamous metaplasia. While this metaplastic change may protect the nasal epithelium from subsequent oxidant exposure, it may also serve to increase toxicant delivery to the pulmonary airways. These studies may help to better evaluate and predict the risks and long-term health effects associated with chronic or repeated childhood exposures to air pollution.

In contrast, while ozone exposure also caused epithelial hyperplasia in the nasal airways of rats, there was not a concurrent upregulation of intracellular GSH. We also found that GSH depletion during ozone exposure does not inhibit the development of nasal epithelial hyperplasia in rats. However, our findings suggest that other antioxidant mechanisms (e.g. AH_2) may also contribute to the maintenance of redox balance during ozone exposures in rats, thus facilitating cell cycle progression and cell proliferation. Future studies are needed to more fully investigate the interactions between GSH and AH_2, and their roles in oxidant-mediated cell proliferation in rats as well as primates, particularly in light of the fact that primates are not capable of *de novo* AH_2 synthesis.

Results of these studies will contribute to our understanding of the specific cellular mechanisms involved in ozone-induced epithelial hyperplasia, and contribute to our general understanding of the role of antioxidants in oxidant-mediated cell proliferation in these two laboratory species used to predict the risk of ozone toxicity in humans.

REFERENCES

Calderon-Garciduenas, L., A. Rodriguez-Alcaraz, et al. (2001). "Nasal biopsies of children exposed to air pollutants." Toxicol Pathol **29**(5): 558-64.

Calderon-Garciduenas, L., G. Valencia-Salazar, et al. (2001). "Ultrastructural nasal pathology in children chronically and sequentially exposed to air pollutants." American Journal of Respiratory Cell & Molecular Biology **24**(2): 132-8.

Cho, H. Y., J. A. Hotchkiss, et al. (2000). "Neutrophil-dependent and neutrophil-independent alterations in the nasal epithelium of ozone-exposed rats." American Journal of Respiratory & Critical Care Medicine **162**(2 Pt 1): 629-36.

Harkema, J. R., E. B. Barr, et al. (1997). "Responses of rat nasal epithelium to short- and long-term exposures of ozone: image analysis of epithelial injury, adaptation and repair." Microsc Res Tech **36**(4): 276-86.

Harkema, J. R., J. A. Hotchkiss, et al. (1999). "Long-lasting effects of chronic ozone exposure on rat nasal epithelium." Am J Respir Cell Mol Biol **20**(3): 517-29.

Harkema, J. R., C. G. Plopper, et al. (1987). "Effects of an ambient level of ozone on primate nasal epithelial mucosubstances. Quantitative histochemistry." American Journal of Pathology **127**(1): 90-6.

Harkema, J. R., C. G. Plopper, et al. (1987). "Response of the macaque nasal epithelium to ambient levels of ozone. A morphologic and morphometric study of the transitional and respiratory epithelium." American Journal of Pathology **128**(1): 29-44.

Hotchkiss, J. A. and J. R. Harkema (1992). "Endotoxin or cytokines attenuate ozone-induced DNA synthesis in rat nasal transitional epithelium." Toxicol Appl Pharmacol **114**(2): 182-7.

Lu, Q., F. L. Jourd'Heuil, et al. (2007). "Redox control of G(1)/S cell cycle regulators during nitric oxide-mediated cell cycle arrest." J Cell Physiol **212**(3): 827-39.

Luppi, F., J. Aarbiou, et al. (2005). "Effects of cigarette smoke condensate on proliferation and wound closure of bronchial epithelial cells in vitro: role of glutathione." Respiratory Research **6**: 140.

Plopper, C. G., X. Duan, et al. (1994). "Dose-dependent tolerance to ozone. IV. Site-specific elevation in antioxidant enzymes in the lungs of rats exposed for 90 days or 20 months." Toxicology & Applied Pharmacology **127**(1): 124-31.

Plopper, C. G., G. E. Hatch, et al. (1998). "Relationship of inhaled ozone concentration to acute tracheobronchial epithelial injury, site-specific ozone dose, and glutathione depletion in rhesus monkeys." Am J Respir Cell Mol Biol **19**(3): 387-99.